

University of Alberta

**Development and Evaluation of a Close-Proximity, Real Time
Thermoacoustic Ultrasound Sensor**

by

Michael Choi

A thesis submitted to the Faculty of Graduate Studies and Research
in partial fulfillment of the requirements for the degree of

Master of Science

in

Biomedical Engineering

Department of Electrical and Computer Engineering

©Michael Choi

Spring 2012

Edmonton, Alberta

Permission is hereby granted to the University of Alberta Libraries to reproduce single copies of this thesis and to lend or sell such copies for private, scholarly or scientific research purposes only. Where the thesis is converted to, or otherwise made available in digital form, the University of Alberta will advise potential users of the thesis of these terms.

The author reserves all other publication and other rights in association with the copyright in the thesis and, except as herein before provided, neither the thesis nor any substantial portion thereof may be printed or otherwise reproduced in any material form whatsoever without the author's prior written permission.

Abstract

A close proximity, real time thermoacoustic sensor was designed, tested, and implemented in the SonaCell™ ultrasound generator. When placed in contact with the SonaCell™ ultrasound transducer, a copper backed plexiglass absorber converted ultrasound energy into heat, where it was measured by a thermistor on the back face of the absorber. A transient model was used to calculate ultrasound intensity from temperature data by fitting the curve $T_{ave} = C \left(1 - e^{-\frac{t}{\tau}}\right) + T_0$ to the measured data using a least squares method and relating the coefficient C to the applied ultrasound intensity. Over an ultrasound intensity range of 30 mW/cm² to 100 mW/cm² the thermoacoustic sensor was able to calculate ultrasound intensities with an average error of 8.38% and a maximum observed standard deviation of 5.00 mW/cm² when compared to measurements made with a radiation force balance. Analysis of the model and a full evaluation of the designed sensor was carried out.

Acknowledgements

I would like to thank Dr. Jie Chen for providing me the opportunity to work in his research group and carry out this project. The work has been both challenging and rewarding. I would like to express my appreciation to the members of my thesis committee: Dr. Albert Cook, and Dr. Roger Zemp. I would also like to recognize my project mentor Woon Ang, the employees of IntelligentNano Inc., and the members of the BINARY lab group, thank you for all your guidance and support. Finally, I would like to gratefully acknowledge the financial support from the NSERC IPS award.

Table of Contents

1.0.	Introduction	1
1.1.	What is Ultrasound	1
1.1.1.	The History of Ultrasound	1
1.1.2.	The Application of Ultrasound	2
1.1.3.	Ultrasound Generation	4
1.2.	Ultrasound Theory	5
1.2.1.	Ultrasound Transmission and Reflection	5
1.2.2.	Ultrasound Attenuation	7
1.2.3.	Ultrasound Standing Waves	7
1.2.4.	Ultrasound Focal Points	8
1.3.	Ultrasound and Biology	10
1.4.	Ultrasound Calibration	12
1.4.1.	Methods and Associated Theory	13
1.4.2.	Thermoacoustic Sensors	16
1.5.	Motivation	18
2.0.	The Thermoacoustic Sensor	19
2.1.	Thermoacoustic Sensor Designs and Characteristics	19
2.1.1.	Physical Design	19
2.1.2.	Relationship Between Acoustic Intensity and Measured Temperature	21
2.1.3.	General Measurement Procedure	23
2.2.	Design Goals	24
2.3.	A Close Proximity Thermoacoustic Sensor	24

2.4.	Evaluating the Methods of Relating Measured Temperature to the Incident Ultrasound Intensity	25
2.4.1.	Evaluating the Equilibrium Temperature Model	25
2.4.2.	Evaluating the Initial Rate of Change Model	30
2.4.3.	Evaluating the Transient Temperature Model	32
2.5.	The Physical Sensor	33
2.5.1.	Physical Design	33
2.5.2.	Sensor Material Choice	34
2.5.3.	Acoustic Evaluation	36
2.5.4.	Evaluation of Alternative Materials	37
2.6.	Thermoacoustic Sensor Hardware	40
2.6.1.	Thermistor	40
2.6.2.	Analog to Digital Converter	41
2.6.3.	MAX6682 – Thermistor to Digital Converter	42
2.6.4.	Atmel ATmega324P Microcontroller	43
2.7.	Data Sampling: Measuring the Temperature	45
2.7.1.	Data Sampling	45
2.7.2.	Oversampling and Decimation	47
2.8.	Thermistor Calibration	53
2.9.	Curve Fitting: The Least Squares Model	55
3.0.	Evaluation of the Transient Model	57
3.1.	Evaluation of the Transient Model: Long Periods of Time	57
3.2.	Evaluation of the Transient Model: Short Periods of Time	69

4.0.	Thermoacoustic Sensor Evaluation	72
4.1.	Thermoacoustic Sensor Calibration: Substitution Calibration	72
4.2.	Thermoacoustic Sensor Evaluation	75
4.2.1.	The Influence of Ambient Temperature	78
4.2.2.	Response to Duty Cycle	81
4.2.3.	Assessment of the Copper Backed Sensor vs. a Sensor with No Copper	82
4.2.4.	Evaluation of the Number of Data Points Required For Accurate Readings	86
4.2.5.	Thermoacoustic Sensor Error	87
5.0.	Implementing the Thermoacoustic Sensor in an Embedded System	90
5.1.	Programming the Least Squares Method	90
5.2.	The Real Time Clock	92
5.3.	Communication with the SonaCell™ Ultrasound System	93
6.0.	Future Study	95
7.0.	Conclusion	99
	References	102
	Appendix A: Thermoacoustic Sensor ATmega324P Code	105
	Appendix B: MATLAB lsqcurvefit function	115

List of Tables

Table I: Linear slopes fit to temperature vs. time plots (p. 31)

Table II: Evaluation of the methods used to relate temperature change to applied ultrasound intensity (p. 32)

Table III: Thermal properties of the thermoacoustic sensor (p. 36)

Table IV: Acoustic properties of the thermoacoustic sensor (p. 37)

Table V: Acoustic properties of rubber and aluminum (p. 38)

Table VI: Thermal properties of rubber and aluminum (p. 38)

Table VII: Comparison of alternative materials (p. 39)

Table VIII: Coefficients of the transient model for an applied ultrasound intensity of 30 mW/cm² at 22 °C (p. 60)

Table IX: Goodness of fit analysis for an applied ultrasound intensity of 30 mW/cm² at 22 °C (p. 60)

Table X: Coefficients of the transient model for an applied ultrasound intensity of 30 mW/cm², 60 mW/cm², 100 mW/cm² at 22 °C (p. 65)

Table XI: Goodness of fit analysis for an applied ultrasound intensity of 30 mW/cm², 60 mW/cm², 100 mW/cm² at 22 °C (p. 67)

Table XII: Coefficients of the transient model for an applied ultrasound intensity of 30 mW/cm² at 22 °C for 30 seconds (p. 70)

Table XIII: Goodness of fit analysis for an applied ultrasound intensity of 30 mW/cm² at 22 °C for 30 seconds (p. 70)

Table XIV: Acoustic calibration using a radiation force balance (p. 73)

Table XV: Acoustic calibration for the thermoacoustic sensor (p. 74)

Table XVI: Thermoacoustic sensor evaluation: thermoacoustic sensor measurements at 22 °C (p. 77)

Table XVII: Comparison between measurements made using a radiation force balance and measurements made using a thermoacoustic sensor (p. 77)

Table XVIII: Calculated C coefficients with regards to ambient temperature (p. 78)

Table XIX: Calibration line for the relationship between ultrasound intensity and C values at ambient temperatures between 22 °C and 26 °C (p. 80)

Table XX: Error between thermoacoustic sensor measurements and radiation force balance measurements at various ambient temperatures (p. 80)

Table XXI: The impact of sensor-transducer orientation on the thermoacoustic sensor operation (p. 84)

List of Figures

Figure 1-1: Applications of ultrasound sorted by frequency (p. 3)

Figure 1-2: Ultrasound wave at the boundary between two materials (p. 5)

Figure 1-3: The creation of standing waves after ultrasound is reflected off a surface (p. 8)

Figure 1-4: Unfocused transducer's near field, far field, and divergence angle (p. 9)

Figure 1-5: Block diagram of SonaCellTM ultrasound system (p. 12)

Figure 1-6: Diagram of a membrane hydrophone, and diagram of the front of a needle hydrophone (p. 14)

Figure 1-7: Schematic of a radiation force balance with a reflecting cone target (p. 15)

Figure 2-1: Various thermoacoustic sensor designs (p. 20)

Figure 2-2: Comparison between typical thermoacoustic sensor operation and close proximity thermoacoustic sensor operation (p. 25)

Figure 2-3: Temperature vs. Time curve of the temperature outputted by an ultrasound transducer operating at 60 mW/cm^2 (p. 26)

Figure 2-4: Measured peak voltage, and peak current (p. 27)

Figure 2-5: Diagram of phase shift between AC voltage and current (p. 28)

Figure 2-6: Measured phase shift between the applied current and voltage, and the signal's period (p. 29)

Figure 2-7: Temperature vs. Time data showing the linear slope model (p. 30)

Figure 2-8: Relationship between the applied ultrasound intensity and the linear slope of the temperature vs. time curve (p. 31)

Figure 2-9: Thermoacoustic sensor design with dimensions (p. 34)

Figure 2-10: Incident ultrasound wave striking thermoacoustic sensor (p. 37)

Figure 2-11: Thermoacoustic sensor hardware block diagram (p. 44)

Figure 2-12: Thermoacoustic sensor schematic (p. 44)

Figure 2-13: Thermoacoustic sensor printed circuit board layout (p. 45)

Figure 2-14: ADC Input vs. Time using the ATmega324P 10-bit ADC with the voltage change across a heated thermistor as the input (p. 46)

Figure 2-15: How enhancing the ADC's resolution can increase the precision of converted digital signal (p. 47)

Figure 2-16: Thermistor calibration, 10-bit ADC with no oversampling (p. 49)

Figure 2-17: Thermistor calibration, 14-bit ADC with oversampling (p. 49)

Figure 2-18: The increase in temperature due to an applied ultrasound intensity of 80 mW/cm² with no oversampling (p. 50)

Figure 2-19: The increase in temperature due to an applied ultrasound intensity of 80 mW/cm² with oversampling (p. 50)

Figure 2-20: Oversampling computation period, and the time the thermistor has an applied current (p. 52)

Figure 2-21: Start of each thermoacoustic sensor computation (p. 52)

Figure 2-22: Thermistor calibration experiment setup (p. 53)

Figure 2-23: Thermistor temperature vs. ADC reading for thermistor calibration line (p. 54)

Figure 3-1: Temperature vs. time curve measured using the thermoacoustic sensor for an applied ultrasound intensity of 30 mW/cm² (p. 58)

Figure 3-2: Temperature vs. time curve measured using the thermoacoustic sensor for an applied ultrasound intensity of 30 mW/cm². Data was fit with equation (33) using the least squares model with prediction bounds with 95% certainty, ambient temperature of 22 °C (p. 59)

Figure 3-3: Residual plots for temperature vs. time data with the fitted transient model. Ultrasound intensity of 30 mW/cm², ambient temperature of 22 °C (p. 59)

Figure 3-4: Temperature vs. time data measured using the thermoacoustic sensor. Applied ultrasound intensities of 30 mW/cm², 60 mW/cm², and 100 mW/cm² (p. 62)

Figure 3-5: (Top) Temperature vs. time data measured using the thermoacoustic sensor with the fitted model, and 95% certainty prediction bounds for an ultrasound intensity of 60 mW/cm². (Bottom) Residual plot for fitted data (p. 63)

Figure 3-6: (Top) Temperature vs. time data measured using the thermoacoustic sensor with the fitted model, and 95% certainty prediction bounds for an ultrasound intensity of 100 mW/cm². (Bottom) Residual plot for fitted data (p. 64)

Figure 3-7: Temperature vs. time data measured for 30 seconds for an ultrasound intensity of 30 mW/cm² fit was the transient model with 95% confidence prediction bounds (p. 69)

Figure 3-8: Residual plots for temperature vs. time data with the fitted transient model. Ultrasound intensity of 30 mW/cm² (p. 70)

Figure 3-9: Linear relationship between applied ultrasound and the calculated C coefficient. Ambient temperature of 22 °C (p. 71)

Figure 4-1: Substitution calibration results using a radiated force balance to calibrate the thermoacoustic sensor (p. 75)

Figure 4-2: Evaluation of the thermoacoustic sensor by comparing measurements made with the thermoacoustic sensor with measurements taken using a radiation force balance (p. 76)

Figure 4-3: Ultrasound intensity vs. C coefficients calculated from data collected at different ambient temperatures (p. 79)

Figure 4-4: Influence of duty cycle on thermoacoustic sensor measurements (p. 82)

Figure 4-5: Orientation of the transducer (dotted line) and the thermoacoustic sensor (solid line). To evaluate the influence of orientation, the sensor was placed on four of the sensor's edges (left), and in the middle of the sensor (right) and readings were taken (p. 83)

Figure 4-6: Ultrasound intensity vs. C values using a sensor with no copper back. 3 sets of readings are taken and compared (p. 85)

Figure 4-7: Ultrasound intensity vs. C values using a sensor with a copper back. 3 sets of readings are taken and compared (p. 85)

Figure 4-8: The number of data points needed to take an accurate reading using the thermoacoustic sensor (p. 86)

Figure 5-1: Least squares algorithm flow chart (p. 91)

Figure 5-2: Communication flow chart between the thermoacoustic sensor and the SonaCellTM system (p. 94)

Chapter 1: Introduction

1.1. What is Ultrasound

1.1.1. The History of Ultrasound

The birth of ultrasound as a specific branch of science can be attributed to its applications underwater. Ultrasound, a form of acoustic energy, is a subsection of acoustic science that is characterized by frequencies greater than 20 kHz and below 1 GHz, or in other terms above the human hearing range and lower than the hypersonic regime [1]. Used in nature as a form of echolocation, humans have harnessed ultrasonic energy for numerous applications in a wide range of fields.

Numerous historic events have culminated in the development of ultrasound, as we know it today. The study and development of acoustic science by physicians and mathematicians in the 17th and 18th centuries laid the groundwork for the science of ultrasound. The discovery of piezoelectricity by the Curie brothers in 1880 was a major development in the history of ultrasound. But it was not until World War I, for the purpose of underwater detection, did serious interest into ultrasound begin [1]. The concept of transmitting acoustic energy through water had already been primitively demonstrated when submerged bells were rung to warn ships of dangerous objects, or when Morse code was transmitted underwater between ships at 500 – 1000 Hz frequencies. However, during World War I, with the threat of submarines to the Allies, ultrasonics was used for the first time to detect an underwater vessel [2]. Ultrasound, as a detection modality, grew to a noteworthy proportion during World War II with the advent of the sonar and the radar. Since then, the interest in underwater

ultrasound has only increased, and ultrasound systems have been developed for domestic, industrial, and military use.

1.1.2. The Application of Ultrasound

There are now numerous applications of ultrasound in many industries other than underwater detection, and communication. In ultrasonics, the application generally determines the generated ultrasound intensity. If the primary purpose of the ultrasound wave is to transmit the energy through the medium without producing an effect on the medium, it is considered low intensity ultrasound [2]. The objective of low intensity ultrasound is typically to learn something about the medium the ultrasound is passed through or to transmit information through the medium. Applications of low intensity ultrasound include non-destructive testing, measurement of the elastic properties of materials, medical diagnosis, and underwater applications such as sound generation, depth sounding, echo ranging, communication, and detection [2]. Presently, non-destructive testing using ultrasound is a very important industry, possibly the largest application of low-intensity ultrasound today.

In contrast, high intensity ultrasound is used to produce an effect on a medium or its contents. Applications may include medical therapy, atomization of liquids, machining, cleaning, disrupting biological cells, welding, or the homogenization or mixing of materials [2]. Ultrasound cleaning provides one of the largest markets for high intensity ultrasound equipment. This classification method is not without error; for example, depending on the medium and desired

distance an echo ranging device may operate at a higher intensity than a therapeutic ultrasound generator.

Arguably, the most well known application of ultrasound is in the medical field. Medical applications of ultrasound include both high and low intensity ultrasound; for example, low intensity ultrasound is used for diagnostic purposes incorporating many principals of non-destructive testing. While high intensity ultrasound is typically used for therapeutic purposes to treat soreness or for surgical purposes [2]. Alternatively, ultrasound can also be divided by its operational frequency [1]. Cavitation, the creation of microbubbles in a liquid is done at a lower frequency. Applications of ultrasound at increasing frequencies include guide waves for ultrasonic testing, non-destructive testing, and medical imaging. Finally, the higher frequency range of ultrasound is used for acoustic sensors and acoustic microscopy. A list of applications with regards to frequency is shown in figure 1-1.

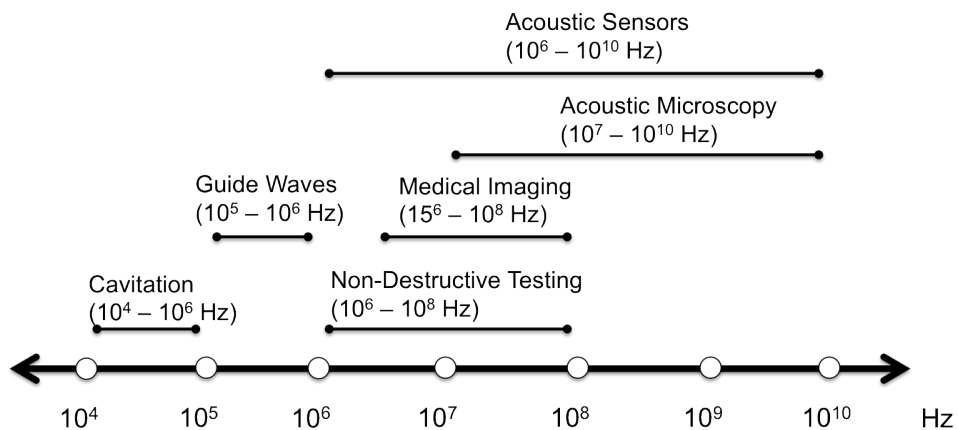


Figure 1-1: Applications of ultrasound sorted by frequency [1]

1.1.3. Ultrasound Generation

Ultrasound generation can be accomplished with simple electronics: a frequency generator, an amplifier, and a transducer. A transducer is a device that converts one form of energy into another; in the case of ultrasound this is typically electrical energy into mechanical energy. There are two main types of ultrasound transducers used: piezoelectric transducers, and magnetostrictive transducers [1].

Ultrasound transducers based on the piezoelectric effect can be used throughout a wide range of frequencies by converting electrical pulses into mechanical vibrations. The piezoelectric effect states that when an electric field is applied across a piezoelectric material, the polarized molecules will align themselves with the electric field. This will result in induced dipoles within the molecular or crystal structure, and cause the material to change dimensions. In the field of ultrasound, alternating voltage pulses can be applied to a piezoelectric ceramic to rapidly change its shape and produce ultrasound waves [3].

Magnetostrictive transducers are used in applications requiring high ultrasound intensities, but are only effective in a frequency range up to 50 kHz [4]. These transducers utilize the changing dimensions of a magnetic material, typically a ferromagnetic material, under the influence of a magnetic field to generate ultrasound. Both of these processes can be reversed and a transducer can receive an ultrasound wave and convert it into another form of energy.

Piezoelectric transducers are commonly used for diagnostic applications,

employing computer algorithms to interpret the electric signals produced by the transducer when it receives the ultrasound waves.

1.2. Ultrasound Theory

Ultrasound theory is associated with the basic principles of wave propagation. Similar to light, ultrasound is reflected from surfaces, transmitted through matter, refracted when going from one medium to another, and diffracted at the edges of surfaces or around obstacles. Obeying a general wave equation, ultrasound travels through homogenous materials at a velocity that is dependent on the properties of the medium [5].

1.2.1. Ultrasound Transmission and Reflection

The interaction between the ultrasound wave and material at any boundary is one of the fundamental principles dictating the operation of the thermoacoustic sensor. When an ultrasound wave reaches the boundary between two materials, the wave is either transmitted through the material or reflected away from the material. The properties of the material and the ultrasound wave parameters will dictate the interplay between the incident acoustic wave and material.

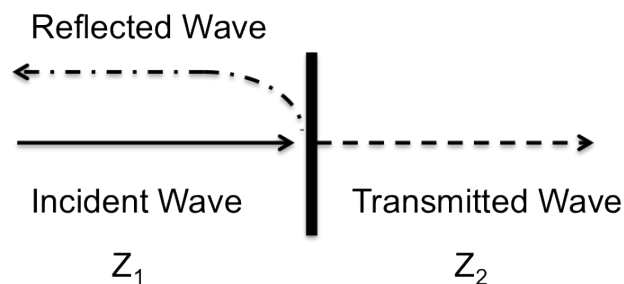


Figure 1-2: Ultrasound wave at the boundary between two materials

When an ultrasonic wave encounters an interface between two media, the energy of the wave is partitioned in a manner depending on the type of incident wave, how the wave approaches the interface, and the acoustic properties of the two media. At a normal incidence, the percentage of the incident ultrasound wave that is transmitted through a material is related to the two materials' properties [1].

Reflections occur at interfaces with two dissimilar materials. The reflection of an acoustic wave is related to the acoustic impedance of the two materials on either side of the boundary. Acoustic impedance (Z) is dependent on a material's density (ρ), and elastic properties, which in turn will dictate the acoustic velocity of the wave (v) through the material [6]. Ultrasound waves are reflected at boundaries where there is a difference in acoustic impedance on each side of the boundary; this is referred to as an impedance mismatch. The greater the mismatch is, the greater the percentage of energy that will be reflected at the interface is. The reflection coefficient (R) can be calculated if the acoustic impedance of both materials is known. Multiplying the reflection coefficient by 100 yields the amount of energy reflected as a percentage of the original energy.

$$Z = \rho v \quad (1)$$

$$\%R = \left(\frac{Z_2 - Z_1}{Z_2 + Z_1} \right)^2 \times 100\% \quad (2)$$

In order to satisfy the law of conservation of energy, the portion of the ultrasound wave that is not reflected at the boundary is transmitted through the material.

1.2.2. *Ultrasound Attenuation*

Attenuation is the diminishing intensity of a wave as it progresses through a medium. As a wave propagates through a medium, it is constantly losing energy due to the spreading of the wave front, the changing of the acoustic energy into thermal energy, and the scattering of the wave from irregular surfaces. Ultrasound attenuation is dependent on two factors: (i) the material through which the wave passes, and (ii) the frequency of the ultrasound [2]. A common cause of attenuation is the scattering of the wave. Scattering may affect the attenuation in two ways. Single scattering occurs when energy is deflected once by an obstacle in the path of the beam and is lost to the main beam. Multiple scattering is when a ray is scattered many times, the result may be one of three cases: all the energy may be lost from the main beam, part of the energy may be lost and part returned, all of the energy may be returned to the main beam. Attenuation due to the conversion of acoustic energy into thermal energy is another prominent cause of attenuation. The ultrasound intensity after attenuation at a distance z can be calculated using equation (3), where I_0 is the initial ultrasound intensity, and μ is the absorption coefficient.

$$I(z) = I_0 e^{-\mu z} \quad (3)$$

1.2.3. *Ultrasound Standing Waves*

Standing waves occur when two traveling waves with the same frequency and mode, but travelling in two opposite directions, are combined. Standing waves are characterized by a static pattern of nodes and antinodes, areas where there is no propagation of energy [1]. When an ultrasound wave encounters a surface that

is parallel to the transducer front, part of the energy is reflected. This reflected pressure is the negative of the incident pressure. If the entire wave is reflected, with no shift in phase, this will lead to a node, an area where the sum of the amplitude of the incident wave and reflected wave is zero.

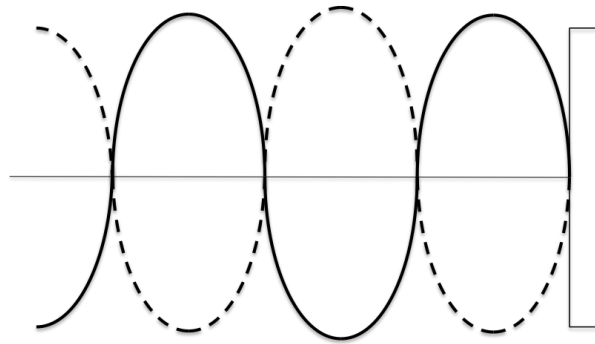


Figure 1-3: The creation of standing waves after transmitted ultrasound (solid line) is reflected off a surface (dashed line) [1].

However, very often the reflection coefficient is not unity, and the standing wave pattern is not complete. In this case, the amplitude at the nodes is no longer zero and the wave field is regarded as being part standing wave and part travelling wave. This is commonly described by the standing wave ratio (SWR), where R_p represented the reflection coefficient, 0 denotes full transmission, and 1 stands for full reflection [1].

$$SWR = \frac{1+R_p}{1-R_p} \quad (4)$$

1.2.4. Ultrasound Focal Points

An unfocused transducer produces a beam with two distinct zones: the near field (Fresnel zone), and the far field (Fraunhofer zone), figure 1-4 [5]. In the near field, ultrasound pulses maintain a relatively constant diameter, which is determined by the diameter of the transducer. However, the intensity along the

beam axis is not constant, and oscillates between maximum and zero several times in the area between the transducer and the near/far field boundary. This is due to the interference patterns created by the sound waves emitted from the transducer's surface [5]. The length of the near field (N) is related to the diameter of the transducer (D), and the beam's wavelength (λ).

$$N = \frac{D^2}{4\lambda} \quad (5)$$

In the far field, the beam begins to diverge causing the ultrasound pulses to be larger in diameter, but have less intensity along the central axis. The divergence angle (θ) is expressed in equation (6).

$$\theta = \frac{70\lambda}{D} \quad (6)$$

Ultrasonic energy can be focused. Sound, because of its longer wavelengths, focuses in a region rather than at a point. The smallest practical focal region is a sphere one wavelength in diameter [1]. The best focus can be obtained when the focal length is the distance to the final pressure peak in the near field.

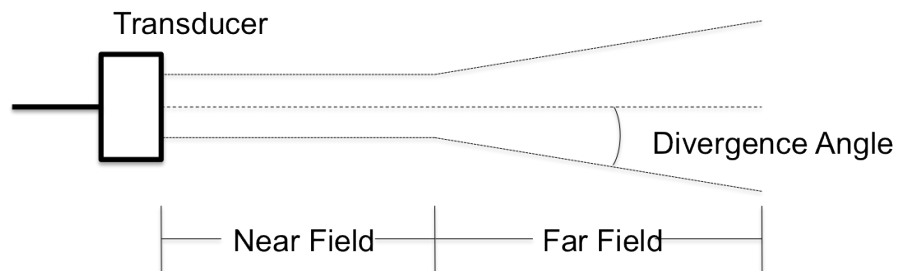


Figure 1-4: Unfocused transducer's near field, far field and divergence angle [7]

1.3. Ultrasound and Biology

In biology, medical diagnostics is a widely known implementation of ultrasound. One of the most celebrated applications of ultrasound imaging is fetal imaging because of the tremendous detail and clarity available compared to other imaging modalities [2]. Other medical applications for diagnostic ultrasound include imaging areas in order to locate defects. Therapeutic ultrasound is another common medical application of ultrasound [8]. Therapeutic ultrasound is typically used to manage ligament, muscle, and tendon injuries using higher intensities to produce a heating effect.

The chemical and physical effects induced by ultrasound can also be utilized in a biological laboratory setting. The application of ultrasound in chemistry took off in 1945 with the understanding of cavitation, the phenomenon of producing microbubbles in a liquid due to a large negative pressure [9]. Cavitation is the largest non-thermal effect generated by ultrasound and can cause a chemical reaction and/or a physical effect in a given medium [9]. Chemical reactions can include the generation of free radicals, while an example of a physical effect is microstreaming, which may cause sheer stress or enhanced movement and mass transfer [10]. It is both the physical and chemical effects that have led researches to apply ultrasound to enhance their biological processes.

Low Intensity Pulsed Ultrasound (LIPUS) is a category of ultrasound that is widely used for biological experiments because of the reduced thermal component that is found at higher intensities. The term pulsed ultrasound refers to the non-continuous ultrasound wave. A pulsed ultrasound wave has periods where it is on

and periods where it is off. The application of LIPUS in cell experiments has been documented in literature and includes ultrasound enhanced cell proliferation [11-12], increased biological function such as protein synthesis, and enzyme production [10, 13-14], ultrasound accelerated healing [8, 15], and ultrasound induced sonoporation [16-17]. Sonoporation refers to the utilization of ultrasound to deliver material, typically a protein or a gene, into a cell. Sonoporation is a non-chemical, non-viral, non-invasive delivery method that relies on a physical effect. It is hypothesized that sonoporation is caused by the physical side effects of acoustic cavitation, specifically that the creation and oscillation of the bubbles generated in the liquid due to ultrasound waves generate shear forces that lead to acoustic microstreaming, moving material towards the cell.

A majority of LIPUS experiments carried out in a research setting use commercially built ultrasound devices that were designed for other purposes, typically therapeutic systems [11]. These systems provide a limited amount of parameter control, normally only allowing the intensity, pulse repetition frequency, and duty cycle to be adjusted [11]. An alternative to a commercially built ultrasound generator is to build an in-house ultrasound generator for the experiment.

The system I had the opportunity to work with was a commercially developed ultrasound system for biological labs called the SonaCell™, developed by IntelligentNano Inc. (Edmonton, Alberta). The SonaCell™ system has four major components: the power supply, the control system, the ultrasound generator, and the amplifier stage, shown in figure 1-5.

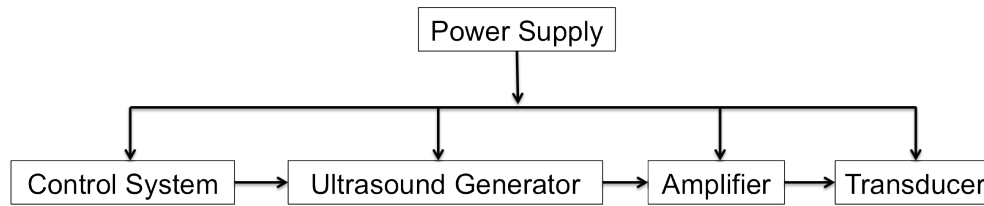


Figure 1-5: Block diagram of the SonaCell™ ultrasound system.

The power supply, as its name implies, provides power to the motherboard, which distributes it to the other systems. An AC to DC converter inputs 15 volts to the system, which is then divided into a 15 V, 8 V, and 5 V supply for various purposes. The control system is the brains of the device. It communicates to the entire system using the RS485 protocol and displays the current status of the ultrasound system on an intelligent graphical LCD display. The ultrasound board generates the 1.5 MHz waveform using a 6 MHz crystal oscillator divided twice. Additionally, this board controls the signal's duty cycle and pulse repetition frequency. Finally, the driver board amplifies the generated 1.5 MHz waveform using a series of MOSFETs and BJTs, producing an adjustable peak-to-peak voltage to drive a piezoelectric transducer. The thermoacoustic sensor was designed specifically for this system, and the transducers used by this system.

1.4. Ultrasound Calibration

For every application of ultrasound, it is important to regulate the acoustic output. Specifically for biological experiments, calibration is imperative in order to ensure the quality and consistency of each trial. If not monitored, the under application of ultrasound can lead to an incomplete treatment that may not produce the desired results, and the over application can lead to cell death [18]. In

a research setting, being able to accurately calibrate the ultrasound device is imperative to repeat experimental conditions. Unfortunately, ultrasound calibration is not a process that is only required once in a lifetime of an ultrasound generator. In a study conducted in the UK investigating 85 therapeutic ultrasound generators, 81% of the machines had power outputs in error of more than +/- 20% of the displayed output power [19]. It can be concluded that ultrasound calibration is periodically required in order to ensure that the displayed output power and the actual output power are in line.

1.4.1. Ultrasound Calibration Methods and Associated Theory

There are two widely used instruments for ultrasound calibration: the hydrophone, and the radiation force balance. A hydrophone is considered the universal instrument to characterize the acoustic output of medical diagnostic ultrasound devices. It operates on the piezoelectric effect, generating an electric output when subjected to an acoustic pressure, with the voltage directly proportional to the acceleration of the acoustic pressure. Most commercial ultrasound hydrophone probes are constructed with a piezoelectric material, such as polyvinylidene fluoride (PVDF), as the sensitive element [20].

Hydrophones can be split into two categories: membrane hydrophones, and needle hydrophones [20]. Membrane hydrophones are characterized by a laminated structure comprising of two layers of PVDF stretched over a hoop, figure 1-3 (left). During operation, the acoustic beam passes through the aperture exciting the active PVDF element. PVDF exhibits strong piezoelectric properties, and therefore, when the ultrasound passes through the aperture, the vibrated

PVDF generates electric signals. Alternatively, needle type hydrophones consist of a circular PVDF film backed by a material with high acoustic impedance. The physical shape is needle like with a tapered active end, figure 1-3 (right).

Similarly, the vibrations due to ultrasound cause the PVDF film to generate an electric signal.

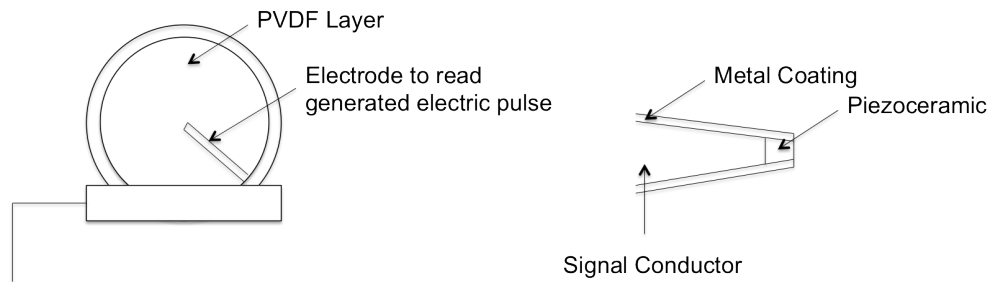


Figure 1-6: (left) Diagram of a membrane hydrophone, (right) diagram of the front of a needle hydrophone [21].

For determining ultrasound output power, the accepted technique is the use of a radiation force balance, figure 1-7. As its name implies, a radiation force balance measures the radiation force applied by an ultrasound transducer and calculates the corresponding ultrasound output power. The main component of a radiation force balance is the target. A target is placed in the path of an acoustic beam and will experience a force due to the momentum associated with the beam. There are a wide range of commercially available radiation force balances, which can be placed into one of two distinct categories depending on their target: absorbing or reflecting. An absorbing target is made from a material with a high acoustic absorbance, typically polyurethane rubbers, and must be large enough to intercept the whole acoustic beam [18]. The target is connected to a force-measuring device that measure the change in force experienced by the target when

struck by the acoustic beam. The measured force is proportional to the acoustic power contained in the beam. The radiation force balance is dependent on the propagation speed of the ultrasound wave in the coupling material, which is usually water [18].

The second type of radiation force balance is one with a reflecting target. Reflecting targets are typically conical in shape formed from air backed thin metal membranes. They simulate a close acoustical approximation to an ideal water-air interface, reflecting close to one hundred percent of transmitted acoustic waves. Similar to their absorbing counterpart, reflecting targets are placed so they intercept the whole acoustic beam and measure the change in force due to the ultrasonic wave. Radiation force balances with a reflecting target typically have measurement vessels lined with an absorbing material to prevent secondary reflections. Radiation force balances are capable of measuring ultrasound in the low MHz frequency ranges with output powers around 100 mW [18].

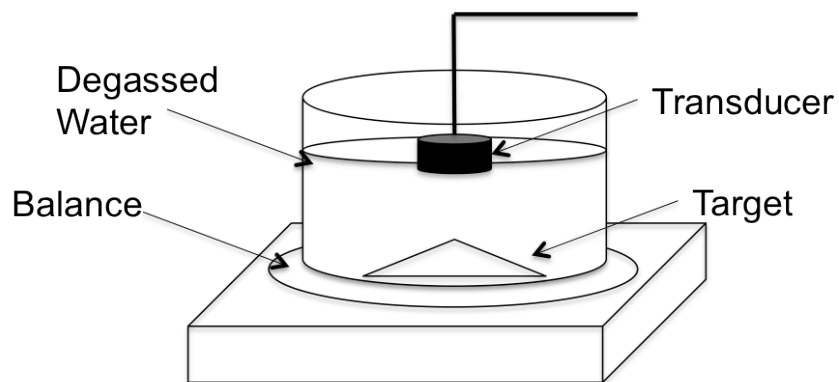


Figure 1-7: Schematic of a radiation force balance with a reflecting cone target

A third type of more experimental sensor under development is a pyroelectric sensor. Pyroelectric sensors rely on the pyroelectric effect experienced by a thin membrane bonded to an acoustical absorber with a very high attenuation

coefficient [22]. During operation, a majority of the ultrasonic energy is passed through the membrane and absorbed by the acoustic absorber producing a rapid increase in temperature. This change in temperature causes a change in voltage due to the pyroelectric effect of the membrane, which is proportional to the delivered ultrasonic power when the ultrasound generator is initially turned on. Pyroelectric sensors require cross calibration using another calibration modality, and will not replace the hydrophone or radiation force balance, but instead will provide a complimentary measurement method [22].

1.4.2. Thermoacoustic Sensors

Even though the radiation force balance and hydrophone are two of the most widely used calibration apparatuses employed in the industry, they both have drawbacks. The necessary procedures required to operate a hydrophone can be technically difficult, time consuming, and expensive. Specific insight into the operation of the ultrasound generator may be required in order to interpret the recorded waveforms, and it is quite possible that the common user will be unable to use a hydrophone to easily characterize the output ultrasound [23-24]. The radiation force balance is limited by its strong dependence on the ultrasound waves' geometry. If the target does not completely intercept the wave, for example an ultrasound generator with a strongly divergent transducer, significant uncertainty in readings can occur [22]. Related to this, the radiation force balance is constrained by the setup apparatus required. The ultrasound transducer needs to be placed directly inline with the target so that the whole wave is intercepted, and the wave must be transmitted through a coupling medium. This is inconvenient

for an array of transducer or a transducer fixed to a specific location that cannot be placed in the radiation force balance's measurement vessel. Finally, like a balance the radiation force balance is susceptible to background vibrations, introducing uncertainty into low-intensity measurements [22].

These constraints provide an opening for another sensor technique to compliment the hydrophone, and radiation force balance. Sensors using the pyroelectric effect are an example of a sensor that utilizes substitution calibration techniques to supplement the already existing ultrasound sensors. The disadvantages of pyroelectric sensors are they require a thin membrane of piezoelectric polymer PVDF, typically in the micrometer range, which requires a complicated manufacturing process [22]. Additionally, these sensors read the change in temperature due to the ultrasound generator being toggled on and off, limiting their functionality as an ultrasound sensor for readings that span a long duration. However, using the relationship between the ultrasound's output power and the local heat production can be done using a different method. These sensors are typically called thermoacoustic sensors. Calibration techniques employing thermoacoustic sensors have the potential to be simple, inexpensive methods of determining the acoustic power radiated by ultrasound transducers [25].

The concept of using temperature to determine absolute sound levels dates back to 1954 [26]. The close correlation between ultrasound output intensity and the heat production make thermal sensors an attractive solution for quick transducer measurements and even calibration. Various iterations of thermoacoustic sensors have been designed; however, in general they all are

based on the transformation of the incident ultrasonic energy into heat inside a small cylindrical absorber, and the detection of the temperature on the rear side of the absorber. Using easy materials to work with, these sensors can be quickly made at a low cost and give an accurate measurement.

1.5. Motivation

At the beginning of my program I had the opportunity to work with the biology group in our lab. The project I was involved in was the stimulation of cells using ultrasound waves. Specifically, we were trying to demonstrate that ultrasound could be used to increase the proliferation, and function of *T. ressei*; fungi that can be used to break down lignocellulose material, an application useful in the biofuel industry. It was extremely important that before every experiment the SonaCell™ ultrasound generators were calibrated to ensure that the precise amount of ultrasound intensity was applied to the system. Additionally, one reoccurring unknown in our experiments was the amount of incident ultrasound energy that was able to pass through the flask and transmit into the system. A solution was to design a sensor that could do ultrasound intensity measurements before an experiment to check if the ultrasound generator needed to be calibrated, and also be incorporated into the biological system in order to measure the ultrasound energy throughout the experiment. This led to the design, and implementation of the thermoacoustic sensor.

Chapter 2: The Thermoacoustic Sensor

2.1. Thermoacoustic Sensor Designs and Characteristics

All thermoacoustic sensors rely on the measured temperature, which depends on the characteristics of the absorber and the power of the incident ultrasonic wave [9]. While simple in concept, this approach has been done numerous different ways, many of which have been demonstrated in literature. The following section will review several of the different thermoacoustic sensor designs and their performance, and reveal the optimal design of a thermoacoustic sensor.

2.1.1. *Physical Design*

The ideal material for a thermoacoustic sensor would combine perfect acoustic impedance matching with strong acoustic absorption. Acoustic impedance matching would minimize the reflections that occur at the two materials' boundary, allowing a high percentage of acoustic waves to transmit through the second material, attenuate, and produce measurable thermal energy. A common material used in the construction of thermoacoustic sensors is plexiglass [9, 23-24 27-28]. Its acoustic properties make it a functional choice for an acoustic absorber; furthermore, it is a readily available material that is easy to process.

The physical shape of the thermoacoustic sensor has gone through various iterations and improvements over the years. One of the first groups to analyze the relationship between acoustic absorption and temperature change used a simple thermocouple wire surrounded by a cylinder of acoustic absorbent material, figure

2-1 (left) [26]. In this set up, acoustic waves were propagated in a direction perpendicular to the axis of the wire. A more sophisticated design involved a thermocouple sandwiched between an acoustic absorbent plexiglass front layer and a highly absorbent back layer, figure 2-1 (middle) [28]. The front plate's main purpose is to thermally isolate the temperature measuring device. The acoustic wave is directed towards the plexiglass layer, and is transmitted through the material to the absorbing back layer. This layer absorbs the ultrasound and transforms the ultrasonic power into heat. However, the most commonly used design is a cylindrical absorber figure 2-1 (right) [9, 18, 25, 27-29]. The sensor comprises of a hollow cylinder with a second solid cylinder inside of it that absorbs the incident wave, attenuates the wave, and transports the heat to the back face of the cylinder where the temperature is measured. This setup isolates the area where the temperature reading is taken, removing the influence of the ambient temperature. The typical size of a thermoacoustic sensor is between 0.5 mm to 3 mm in diameter, and 2 mm to 4 mm in absorber length [23-24].

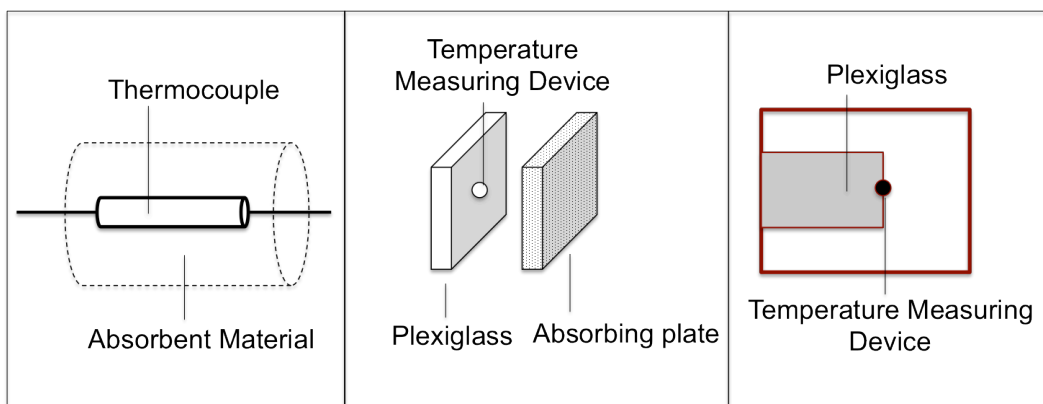


Figure 2-1: Various thermoacoustic sensor designs: (left) Thermocouple wire surrounded by a cylinder of imbedding medium [26], (middle) temperature measuring device sandwiched between a plexiglass layer and an absorbing back layer [28], (right) isolating double cylinder design [23].

2.1.2. *The Relationship Between Acoustic Intensity and Measured Temperature*

When a material having an acoustic intensity absorption coefficient μ per unit path length is subject to a beam of acoustic radiation with intensity I , the initial rate of change of temperature is,

$$\frac{\partial T}{\partial t} = \frac{\mu I}{\rho c_p} \quad (7)$$

If the absorption coefficient, the material's density (ρ), and heat capacity (C_p) are known, and the rate of change of temperature can be measured, the absolute sound intensity can be calculated at any given location [26]. As the temperature rises, heat conduction processes contribute to the change in temperature over time. However, the initial change in temperature, the equilibrium temperature reached, and the change in temperature over time are all influenced by the absorbed acoustic wave; using this relationship, the measured temperature caused by the ultrasound wave can be used to calculate the initial incident ultrasound intensity.

Equilibrium Temperature Method

One way of equating the relationship between the applied ultrasound intensity and the measured temperature is evaluating the temperature at equilibrium. This method is commonly used when the thermoacoustic sensor is placed in a water bath with the transducer, at a fixed distance apart [23]. The contact with the water causes the front face of the sensor to approach the same temperature as the water bath. During sonication, the temperature at the rear side of the sensor begins to rise. Due to heat conduction, part of the heat produced inside the absorber permanently flows through the front face to the water. After a certain period of constant intensity, a thermal equilibrium will appear between the heat produced

by the absorption of the ultrasound waves, and the heat lost to the surrounding water. A relationship between the applied ultrasound intensity (I) and the equilibrium temperature ($T_{equilibrium}$) reached at the rear side of the absorber can be found.

$$I \propto T_{equilibrium} \quad (8)$$

Initial Rate of Change Method

A second method to calculate ultrasound intensity from measured temperature is an initial rate of change method. A pyroelectric material that measures the initial change in temperature when the ultrasound generator is switched on, and then immediately switched off has been demonstrated [22]. A linear relationship between the peak pyroelectric voltage measured when the ultrasound was switched on and then switched off and the applied power was observed [22]. With the proper physical sensor, it is possible to generate a temperature increase of 12 °C within 2 seconds of the ultrasound being switched on [22].

Transient Method

The middle ground between an equilibrium temperature method and an initial rate of change method is a transient measurement method that calculates the ultrasound intensity after a certain duration of time. M.R. Myers and B.A. Herman investigated the transient temperature evaluation in a theoretical assessment done in [25]. In their work, they followed the single reflection theory and described a steady state solution and a transient solution to the temperature rise averaged over the absorber's cross-section.

Myers and Herman suggested that measured temperatures over time data could be fit with a curve with the form,

$$T_{ave}(t) = \sum_{n=0}^{\infty} C_n \left(1 - e^{-\frac{t}{\tau}}\right)$$

where $C_n = \frac{I_0}{\mu k} \frac{16(1+e^{-2\mu l})}{\pi(2n+1)(\mu^2 l^2 + (2n+1)^2 \pi^2)}$, and $\tau = \frac{4l^2 \rho C_p}{\pi^2 k}$ (9)

In equation (9), $T_{ave}(t)$ is the average temperature measured in the sensor in relationship to the temperature of the water bath, I_0 is the incident ultrasound intensity, μ is the absorption coefficient, l is the length of the absorber, k is the thermal conductivity of the absorber material, C_p is the heat capacity of the material, and ρ is the density of the material. Using this model, the ultrasound intensity can be inferred from the parameter C_n .

2.1.3. General Measurement Procedure

The thermoacoustic sensor is a cross-calibration device. It requires another ultrasound measuring modality to measure the output of a transducer before calibration. This is called substitution calibration. In general, substitution calibrations require two steps. In the first step, a transducer is calibrated using a hydrophone or a radiation force balance. In the second step, the hydrophone or radiation force balance is replaced with the thermoacoustic sensor and a reading is taken. This allows a direct one to one correlation between ultrasound intensity and the measured temperature. For convenience sake, measurements are always taken at the back face of the sensor.

2.2. Design Goals

After a literature search was performed in the area of thermoacoustic sensors, a set of design goals were drafted to guide the project. The goal was to design an accurate, easy to use thermoacoustic sensor that would benefit scientists performing experiments using ultrasound for cell stimulation. Therefore, the design goals of this project were to build a thermoacoustic sensor that is,

1. Simple to use
2. Able to perform quick calibration checks
3. Capable of measuring ultrasound for a long duration of time

2.3. A Close Proximity Thermoacoustic Sensor

The advantage of a thermoacoustic sensor is its simplicity: it does not require any complicated setup procedures, or calculations. Previous thermoacoustic sensor operation [9, 23-24, 27-29] required the sensor and transducer to be placed in a water tank, similar to hydrophone or radiation force balance measurements, figure 2-2 (left). To further simplify the thermoacoustic sensor operation, I have designed and tested a close-proximity thermoacoustic sensor that can determine radiated ultrasound intensities when placed in contact with an ultrasound transducer. The sensor can be coupled directly to the transducer using ultrasound gel (Sonic Relief, Miami, Florida, USA), as shown in figure 2-2 (right) and when ultrasound is applied a reading can be obtained.

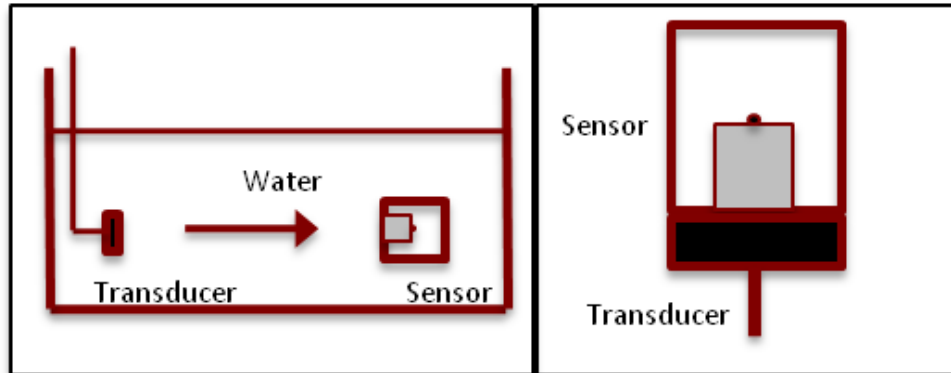


Figure 2-2: Comparison between typical thermoacoustic sensor operation (left), and close-proximity thermoacoustic sensor operation (right)

2.4. Evaluating the Methods of Relating Measured Temperature to the Incident Ultrasound Intensity

2.4.1. Evaluating the Equilibrium Temperature Model

After choosing to do a close proximity sensor, the method of relating measured temperature to incident ultrasound intensity had to be determined. Previously developed thermoacoustic sensors [20-21, 24, 29-30] have mostly used the relationship between the equilibrium temperature reached by the thermoacoustic sensor and the incident ultrasound intensity to indirectly measure the ultrasound intensity. One requirement of the equilibrium temperature model is that the sensor must be placed in a water bath. Therefore, any heat generated by the transducer is dispersed throughout the water and does not influence the thermoacoustic sensor's readings. As well, a portion of the heat produced in the sensor is conducted into the water. In a close-proximity setup, this model requires an impractical amount of time for each reading due to the heat contributed by the vibrating transducer.

To measure the heat produced by the transducer during typical operation, temperature readings were taken by attaching a temperature probe directly to the

operating transducer. At time $t = 0$ seconds, the ultrasound generator was turned on with an output intensity of 60 mW/cm^2 , and remained on throughout the whole process. Temperature readings were taken every second for 1200 seconds. The temperature vs. time curve is shown in Figure 2-3. The largest increase in temperature occurred between $t = 0$ seconds and $t = 200$ seconds, and an equilibrium temperature of approximately $32 \text{ }^\circ\text{C}$ was reached at $t = 800$ seconds.

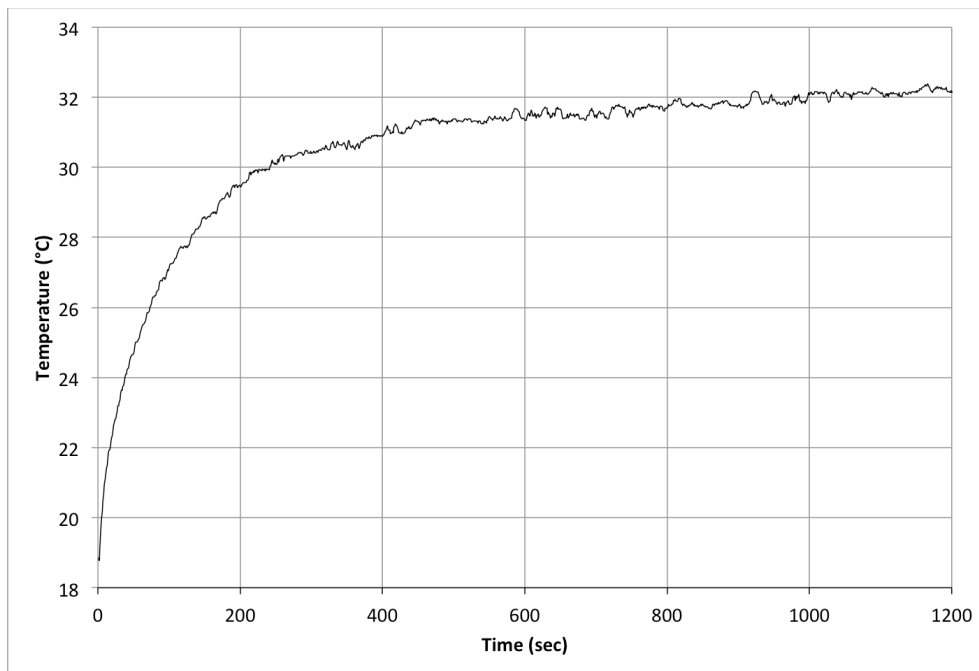


Figure 2-3: Temperature vs. Time curve of the temperature outputted by an ultrasound transducer operating at 60 mW/cm^2

The heat generated by the transducer is due to the energy lost during the conversion of electrical energy to mechanical energy. A portion of the energy is lost because of the internal friction in the transducer, which results in thermal energy. To evaluate the amount of energy lost, the input power into the ultrasound transducer was calculated using equation (10), and the output ultrasound power using a radiation force balance was measured.

$$P_{avg} = V_{rms}I_{rms}\cos\varphi \quad (10)$$

The root mean squared voltage (rms) and current are computed using the peak voltage and peak current measured with a digital phosphor oscilloscope (Tektronix, Beaverton, OR, USA) shown in figure 2-4. The phase difference between the voltage and the current is represented by φ , as shown in figure 2-5.

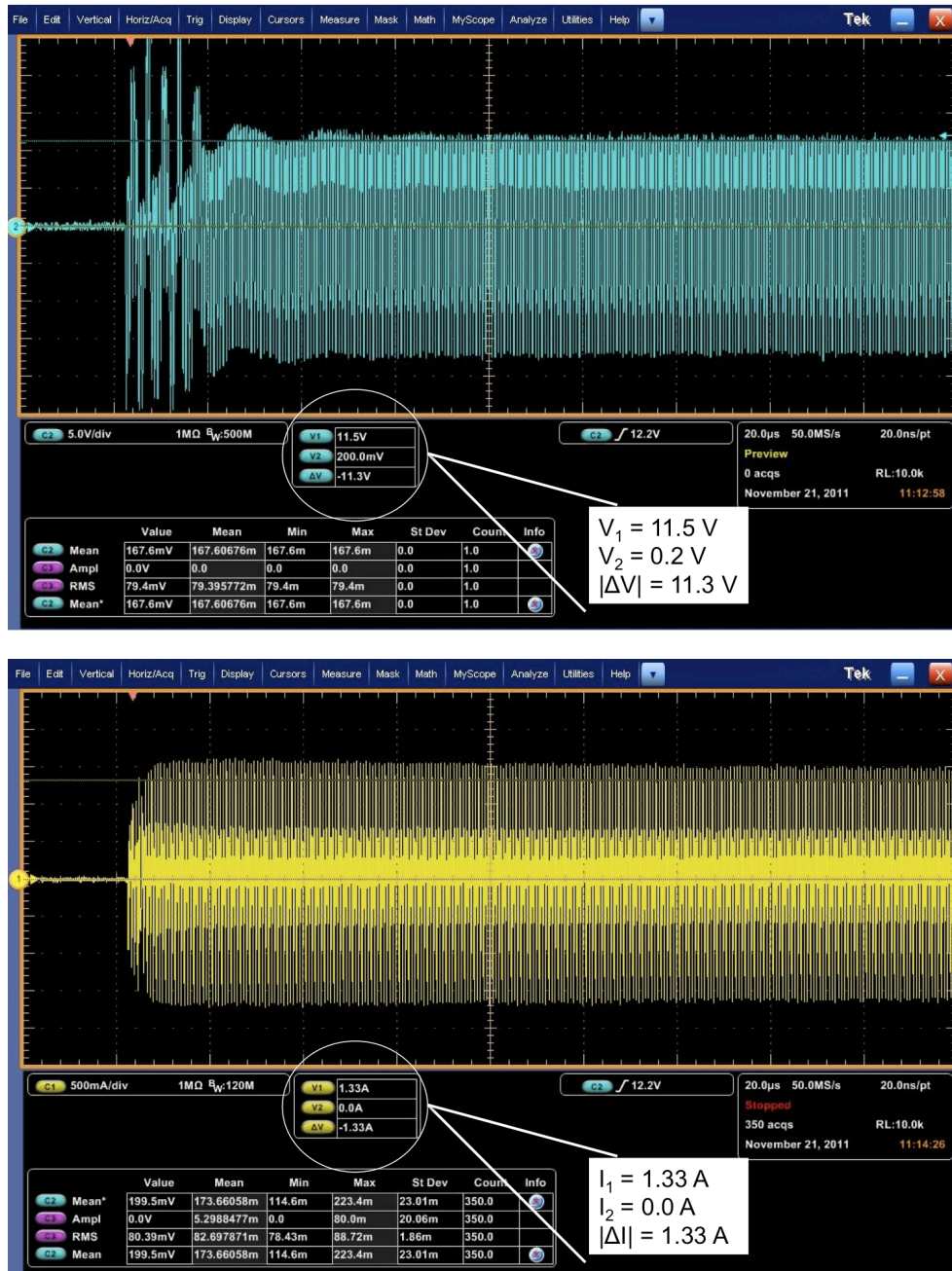


Figure 2-4: Measured peak voltage (top), and peak current (bottom)

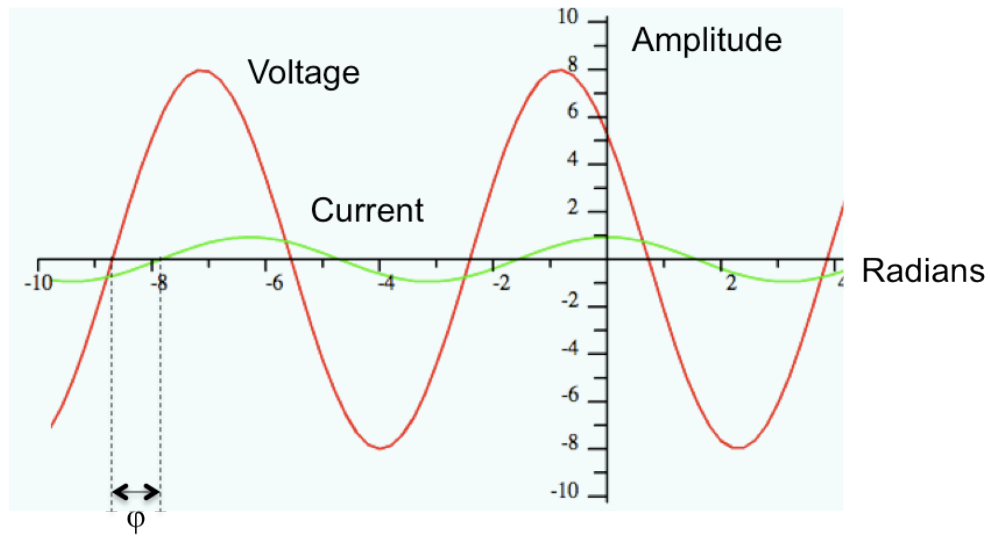
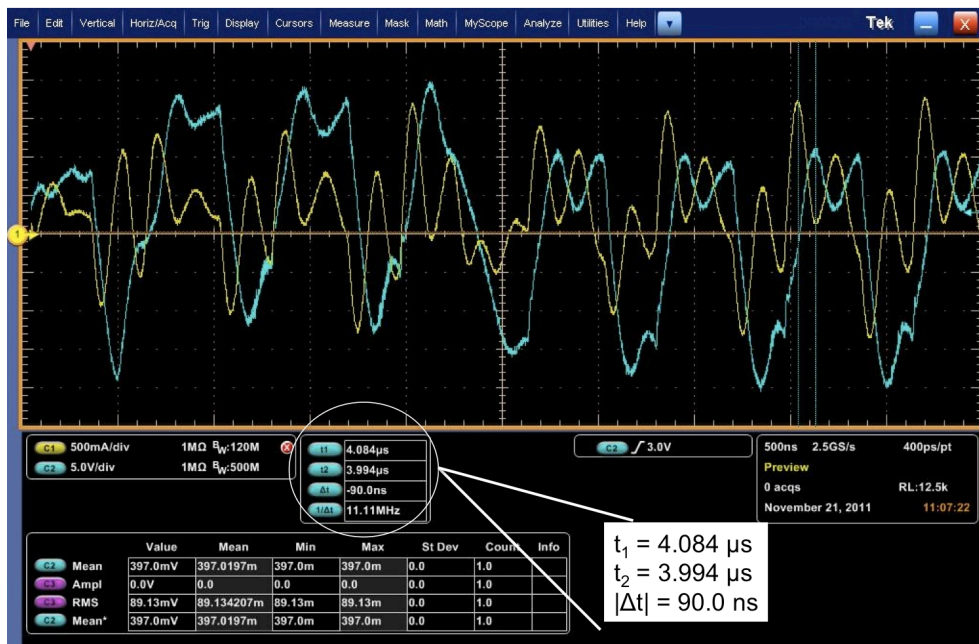


Figure 2-5: Diagram of phase shift between AC voltage and current [53]

The phase shift, ϕ , is calculated in equation (11) using the measured time difference between voltage peaks and current peaks (d), and the overall period (t), figure 2-6.

$$\phi = \frac{d}{t} \times 2\pi \quad (11)$$



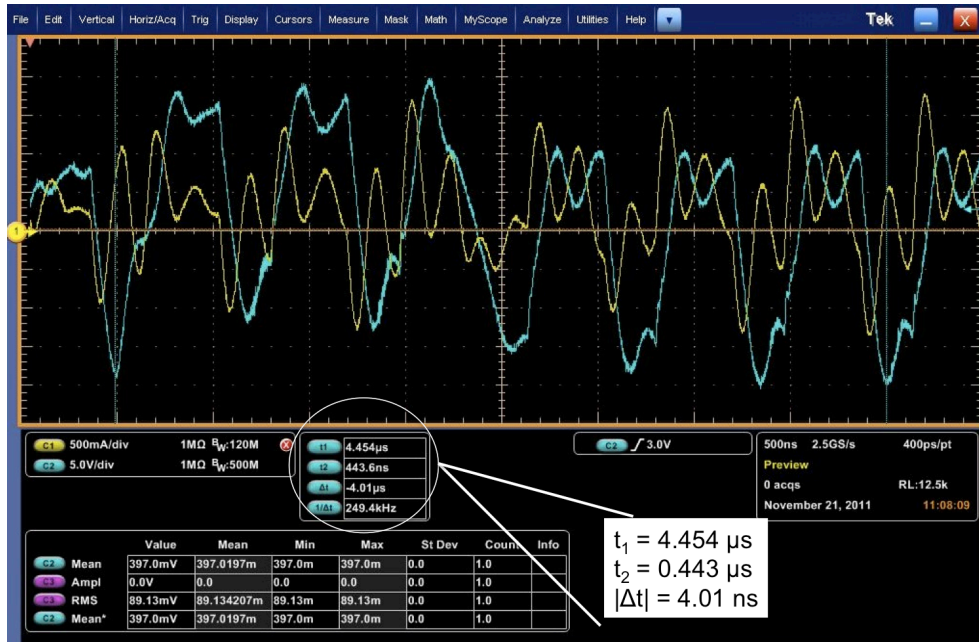


Figure 2-6: Measured phase shift between the applied current and voltage (top), and the signal's period (bottom)

Equation (12) shows the calculated power into the transducer.

$$\varphi = \frac{90 \times 10^{-9} \text{ s}}{668 \times 10^{-9} \text{ s}} \times 2\pi = 0.8465$$

$$V_{rms} = \frac{V_p}{\sqrt{2}} = \frac{11.3}{\sqrt{2}} = 7.99 \text{ V}$$

$$I_{rms} = \frac{I_p}{\sqrt{2}} = \frac{1.33}{\sqrt{2}} = 0.94 \text{ A}$$

$$P_{in} = (7.99)(0.94) \cos(0.8465) = 4.9792 \text{ W} \quad (12)$$

The output power was measured using a radiation force balance, and the power lost was calculated, shown in equation (13)

$$P_{out} = 2.25 \text{ W}$$

$$\frac{P_{out}}{P_{in}} = 0.4519 \quad (13)$$

Approximately 55% of the input energy is lost during the conversion of electrical energy to mechanical energy. In the close proximity setup, the heat produced by the transducer will contribute to the temperature readings collected. If the thermoacoustic sensor algorithm requires the sensor's equilibrium temperature, the sensor's response time will be longer than 800 seconds, which does not fit the design rules.

2.4.2. Evaluating the Initial Rate of Change Model

The initial rate of change method describes using a pyroelectric material to measure the change in temperature when the ultrasound generator is turned on and then immediately turned off. A similar method was tried using a thermoacoustic sensor. For a short duration of time the measured temperature vs. time curve is linear, I evaluated the relationship between the linear slope and the applied incident ultrasound. Measured temperature data was collected for 100 seconds, as shown in figure 2-7.

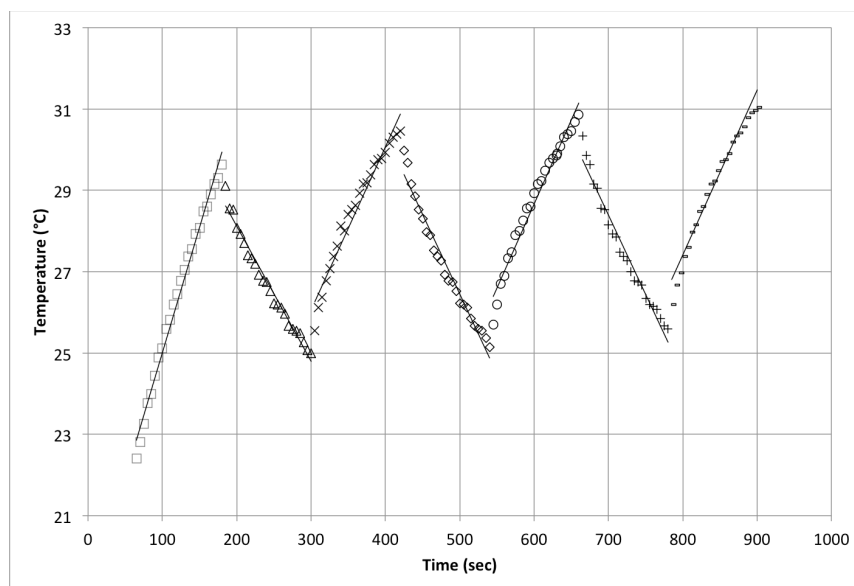


Figure 2-7: Temperature vs. Time data showing the linear slope method. Data was collected for 100 seconds when an ultrasound intensity of 30 mW/cm^2 was applied to the sensor

Table XII outlines the slopes of each line, omitting the slope from set 1, the standard deviation between slopes is 0.000611 °C/sec.

TABLE I
LINEAR SLOPES FIT TO TEMPERATURE VS. TIME PLOTS
ULTRASOUND INTENSITY OF 30 mW/cm²

	SLOPE
ON – Set 1	0.0616
ON – Set 2	0.0387
ON – Set 3	0.0387
ON – Set 4	0.0397

The relationship between applied incident ultrasound intensities and the measured linear slope is depicted in figure 2-8, ultrasound intensities of 30 mW/cm², 45 mW/cm², 60 mW/cm², and 82 mW/cm² where measured.

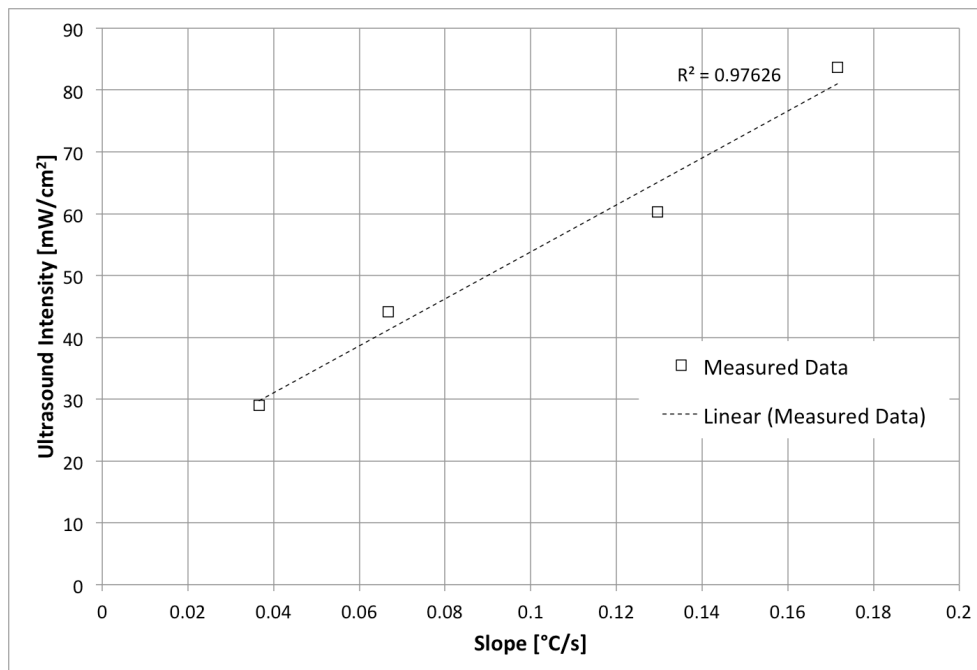


Figure 2-8: The relationship between the applied ultrasound intensity, and the linear slope of the temperature vs. time curve

A correlation between the applied ultrasound intensity and the measured linear slope is seen. The main disadvantage of the linear model is it is not

capable of measuring past the time where the temperature vs. time graph is linear, approximately 100 seconds. This breaks the design rule of the project stating that the sensor can be used for long-term measurements.

2.4.3. *Evaluating the Transient Temperature Model*

Due to the heat produced by the transducer, in a close proximity set up, the equilibrium temperature method is not desirable. As well, because the sensor is required to perform quick measurements, as well as long-term measurements, the initial rate of change method cannot be used. Table II recaps the advantages and disadvantages of the equilibrium and initial rate of change methods.

TABLE II
EVALUATION OF THE METHODS USED TO RELATE TEMPERATURE CHANGE TO
APPLIED ULTRASOUND INTENSITY

	Advantage	Disadvantage
Equilibrium Method	Simple measurement algorithm	Set up must take place in water
Initial Rate of Change Method	Simple measurement algorithm	Can not measure past linear section of the Temperature vs. Time curve

The third method is the transient temperature method suggested by Myers and Herman in [25]. They claimed that as the average temperature is measured across the absorber's back face, a curve can be fit to the measured data and the ultrasound power can be inferred. Taking a closer look at equation (9) on page 23, we can see that the relationship between measured temperature and the applied ultrasound can be seen in the coefficient C_n . The transient method should allow the sensor to take quick measurements for a calibration check, or longer measurements to evaluate the ultrasound inputted into a system throughout an

experiment, meeting the project's design goals.

This thesis will explore the implementation of the transient temperature model in a thermoacoustic sensor that can operate in contact with an ultrasound transducer. It will show that the transient method can accurately measure ultrasound intensity at different times throughout the application. Additionally, it will also improve on the work done in [25] by showing that adding a thin copper layer to increase the heat conduction across the back face of the sensor's absorber reduces the error of the thermoacoustic sensor. The parameters related to the fitting procedure, such as the number of samples needed to accurately measure the coefficient C , and the impact of the initial starting parameters for the fitting method will also be examined.

2.5. The Physical Sensor

2.5.1. Physical Design

There are numerous ways to implement a thermoacoustic sensor. The essential components are an acoustic absorbent material and a temperature-sensing device. The cylindrical absorber design is a commonly used design in literature [6, 15, 22, 28 – 30]. Its main advantage is that the area where temperature readings are taken is thermally isolated, eliminating the influence of the ambient temperature. This is the design that I chose to implement. The cylindrical absorber design comprises of a solid cylinder within a hollow cylinder, figure 2-9. The sensor was built in two parts. The front face, 1.30 mm thick, is a threaded, solid plexiglass cylinder 38 mm in diameter. The front face and the solid interior cylinder are one piece. The absorbing cylinder is centered on the

front face with a diameter of 20 mm and a length of 2 mm. The total absorbing component, front face plus the inner cylinder, is 3.30 mm long. The threads allow the front face to be screwed into the hollow cylinder. The second component is the body of the sensor, a hollow cylinder 38 mm in length. The main purpose of the body is to isolate the absorbing component from the surrounding environmental temperature. The hollow cylinder is designed with an O-ring to seal the junction where the front face screws into the body of the sensor. There is also a hole at the back of the hollow cylinder for wires to connect the thermistor to the electronic components. This hole was later sealed with a waterproof silicone sealant.

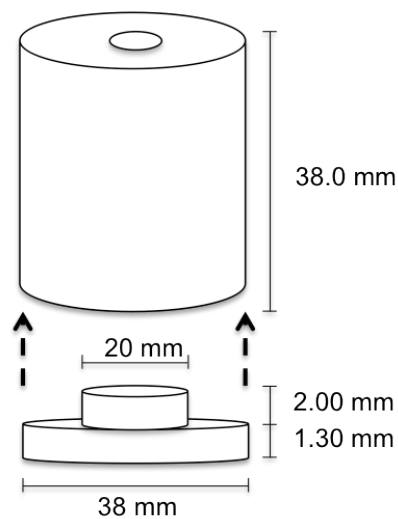


Figure 2-9: Thermoacoustic sensor design with dimensions

2.5.2. *Sensor Material Choice*

The ideal material for a thermoacoustic sensor would combine perfect acoustic impedance matching with strong acoustic absorbance. Plexiglass has been successfully used in previous investigations, and is an available material that can be easily processed and quickly assembled in house, for these reasons plexiglass was the material chosen for my thermoacoustic sensor.

The thermal properties of the material will be important when considering the propagation of heat through the sensor. In solid materials, heat is conducted due to vibrations of the molecules in a lattice or phonons with the energy transferred by free electrons [18]. The thermal diffusivity (α) expresses the rate a material transfers heat from one point to another and is related to the thermal conductivity (k), density (ρ) and specific heat capacity (C_p) of the material.

$$\alpha = \frac{k}{\rho C_p} \quad (14)$$

We are interested in the heat diffusivity on the back face, where the thermistor is located. In the transient temperature model we are implementing, the relationship between temperature and applied ultrasound intensity uses the averaged temperature rise across the back face [25]. To improve the heat diffusivity on the back face of the sensor, a thin copper sheet was attached to the plexiglass absorber. The purpose of the copper sheet is to equally distribute the temperature across the whole surface faster than the plexiglass material could alone. Table III outlines the thermal properties of the plexiglass material and the copper metal [30]. Plexiglass has a thermal diffusivity of $1.09 \times 10^{-7} \text{ m}^2/\text{s}$. Copper, a material with a high thermal conductivity, has a thermal diffusivity of $1.18 \times 10^{-4} \text{ m}^2/\text{s}$, 3-orders of magnitude greater than plexiglass. The copper should conduct heat at a much faster rate than plexiglass. The temperature sensing thermistor is placed on top of the copper layer. Care was taken to ensure that the copper did not short the thermistor leads.

TABLE III
THERMAL PROPERTIES OF THE THERMOACOUSTIC SENSOR

Material	Thermal Conductivity (k) [W/(m*K)]	Density (ρ) [kg/m ³]	Heat Capacity (C_p) [J/(kg*K)]	Thermal Diffusivity (α) [m ² /s]
Plexiglass	0.167	1180	1300	1.09×10^{-7}
Copper	401	8790	385	1.185×10^{-4}

2.5.3. Acoustic Evaluation

After the materials for the thermoacoustic sensor were chosen, an acoustic evaluation of the sensor was carried out. The main focus was on calculating the percent of the incident wave that would be reflected and transmitted at the boundaries between different materials. Table IV depicts the acoustic properties of plexiglass, the ultrasound gel used, copper, and air [31]. At the gel-plexiglass interface, approximately 13% of the ultrasound wave will be reflected back towards the ultrasound transducer (15). Ignoring scattering effects, 87% of the ultrasound intensity will be transmitted into the plexiglass absorber, figure 2-10. A thin copper sheet was added to the back face of the absorber to increase the thermal diffusivity. Ignoring the thermal paste, at the boundary between the plexiglass and copper 69% of the ultrasound wave will be reflected back towards the front of the sensor (16). The insulating material, air, has a low acoustic impedance value compared to the copper material. When the ultrasound wave reaches the back of the sensor, 100% of the wave will be reflected (17).

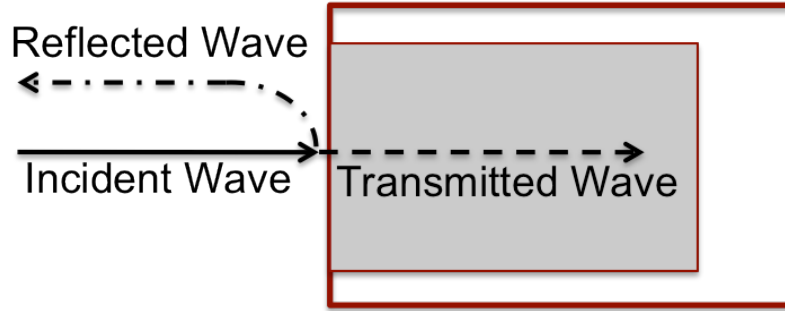


Figure 2-10: Incident ultrasound wave striking thermoacoustic sensor

TABLE IV
ACOUSTIC PROPERTIES OF THE THERMOACOUSTIC SENSOR

Material	Density (ρ) [kg/m ³]	Acoustic Velocity (v) [m/s]	Acoustic Impedance (Z) [kg*m ² /s]
Plexiglass	1180	2700	3.186×10^6
Ultrasound Gel	1003.2	1480	1.485×10^6
Copper	8940	3810	34.06×10^6
Air	1.2041	343.26	413.3

$$\%R_{Gel-Plexiglass} = \left(\frac{3.186 \times 10^6 - 1.485 \times 10^6}{3.186 \times 10^6 + 1.485 \times 10^6} \right)^2 \times 100\% = 13.26\% \quad (15)$$

$$\%R_{Plexiglass-Copper} = \left(\frac{3.186 \times 10^6 - 34.06 \times 10^6}{3.186 \times 10^6 + 34.06 \times 10^6} \right)^2 \times 100\% = 68.71\% \quad (16)$$

$$\%R_{Plexiglass-Air} = \left(\frac{413.3 - 34.06 \times 10^6}{413.3 + 34.06 \times 10^6} \right)^2 \times 100\% = 100\% \quad (17)$$

The impact of the reflected waves within the plexiglass sensor is discussed as a source of error.

2.5.4. Evaluation of Alternative Materials

For a thermoacoustic sensor design, plexiglass has been used multiple times in literature. Two materials were chosen and compared to plexiglass, rubber with a high acoustic absorbance, and aluminum with a high thermal

diffusivity. Their respective properties that influence the operation of the thermoacoustic sensor are outlined in table V, and table VI [31].

TABLE V
ACOUSTIC PROPERTIES OF RUBBER AND ALUMINUM

Material	Density (ρ) [kg/m ³]	Acoustic Velocity (v)[m/s]	Acoustic Impedance (Z) [kg*m ² /s]
Rubber	1110	1660	1.843x10 ⁶
Aluminum	2700	6320	17.10x10 ⁶

TABLE VI
THERMAL PROPERTIES OF RUBBER AND ALUMINUM

Material	Absorption Coefficient (μ) [dB/cm*MHz]	Thermal Conductivity (k)[W/(m*K)]	Density (ρ) [kg/m ³]	Specific Heat Capacity (C) [J/(kg*K)]	Thickness of Material (z) [m]
Plexiglass	0.554	0.167	1180	1300	0.0033
Rubber	7.7	0.09	1110	1940	0.0033
Aluminum	0.0521	237	2700	910	0.0033

$$\%R_{Gel-Rubber} = \left(\frac{1.843 \times 10^6 - 4.86 \times 10^6}{1.843 \times 10^6 + 4.86 \times 10^6} \right)^2 \times 100\% = 1.15\% \quad (18)$$

$$\%R_{Gel-Al} = \left(\frac{17.10 \times 10^6 - 4.86 \times 10^6}{17.10 \times 10^6 + 4.86 \times 10^6} \right)^2 \times 100\% = 70.6\% \quad (19)$$

$$I_{Plexiglass} = I_0 e^{-(0.554)(1.5)(0.033)} = (0.973)I_0 \quad (20)$$

$$I_{Rubber} = I_0 e^{-(7.7)(1.5)(0.033)} = (0.683)I_0 \quad (21)$$

$$I_{Al} = I_0 e^{-(0.0521)(1.5)(0.033)} = (0.997)I_0 \quad (22)$$

$$\alpha_{Rubber} = \frac{0.09}{1100 \times 1940} = 4.217 \times 10^{-8} \text{ m}^2/\text{s} \quad (23)$$

$$\alpha_{al} = \frac{237}{2700 \times 910} = 9.646 \times 10^{-5} \text{ m}^2/\text{s} \quad (24)$$

TABLE V
COMPARISON OF ALTERNATIVE MATERIALS

Material	% Reflection at gel-material boundary	% Absorption through 0.0033 m of material	Thermal Diffusivity
Plexiglass	13.26%	2.70%	$1.185 \times 10^{-7} \text{ m}^2/\text{s}$
Rubber	1.15%	31.7%	$4.217 \times 10^{-8} \text{ m}^2/\text{s}$
Aluminum	70.6%	0.30%	$9.646 \times 10^{-5} \text{ m}^2/\text{s}$

Rubber has an acoustic impedance much closer to the water based gel, reducing the percent of the ultrasound wave that is reflected at the gel-sensor boundary. Additionally, it has a higher acoustic attenuation, attenuating 31.7% of the initial transmitted wave after 0.033 cm. The thermal diffusivity of rubber is lower than plexiglass. The acoustic properties of rubber make it a good choice for a thermoacoustic sensor. The performance of a thermoacoustic sensor made from rubber was evaluated in [23], and it was determined that it showed considerable instability over time when the equilibrium temperature was evaluated. The author hypothesized that these results may be due to the non-uniform, rough surface of the rubber material. Additionally, there is a trade off between the high acoustic attenuation, and the lower thermal diffusivity. The heat may not be able to conduct towards the temperature-sensing device as quickly as the plexiglass sensor. A metal, such as aluminum, has a higher thermal diffusivity than a non-metal such as plexiglass or rubber. However, its acoustic properties make it an unlikely choice for thermoacoustic sensor design. The work done in this thesis focuses on the design of a thermoacoustic sensor using plexiglass; however, alternative materials other than plexiglass should be explored to improve the

operation of the thermoacoustic sensor. This will be further discussed in the *Future Studies* section of the thesis.

2.6. Thermoacoustic Sensor Hardware

The hardware of the thermoacoustic sensor consists of three main modules: temperature sensing, processing, and communication. In the following sections, each of these components will be discussed in detail.

2.6.1. Thermistor

A thermistor is a type of resistor. The main property of a thermistor is its resistance varies significantly with its temperature. There are two types of thermistors: positive temperature coefficient (PTC) thermistors, and negative temperature coefficient (NTC) thermistors. These classifications depend on the sign of the temperature coefficient (k_T) in the linear approximation equation that describes the operation of a thermistor,

$$\Delta R = k_T \Delta T \quad (25)$$

Where ΔR is the change in resistance, and ΔT is change in temperature. In contrast, resistors are designed to have a temperature coefficient as close to zero as possible in order to not be effected by the surrounding temperature [32].

Thermistors differ from resistance temperature detectors (RTD) with regards to the materials used for construction, and performance. RTDs are generally constructed from pure metal, while thermistors are normally made from a ceramic or polymer. Thermistors typically achieve a higher precision within a limited temperature range, while RTDs have the ability to measure greater spans of temperatures [33].

The drawbacks of using a thermistor include its limited operational range, and self-heating effects. The linear approximation equation is only true over a small temperature range. Additionally, depending on the circuit designed, thermistors can suffer from self-heating effects. If a thermistor is used to calculate a change in temperature by measuring the voltage drop across itself, the current that must be run through the thermistor will generate heat that will raise the temperature of the thermistor above the actual ambient temperature. Low power circuit design is implemented to prevent this.

For the thermoacoustic sensor, a thermistor was implemented to measure the changes in temperature due to absorbed ultrasonic energy. A Honeywell discrete thermistor was chosen. This glass bead thermistor has a rapid response time of 0.5 seconds in still air, is micro sized measuring only 0.36 mm in diameter, is sensitive to changes to temperature and has excellent long term stability. The thermistor was secured firmly to the back face of the thermoacoustic absorber using a small piece of electrical tape and the leads were soldered onto longer wires that connected back into the thermoacoustic sensor printed circuit board. At room temperature, the thermistor measured 2000 Ohms [34].

2.6.2. *Analog to Digital Converter*

An analog to digital converter (ADC) is used to convert input analog voltage to a digital number proportional to the magnitude of the voltage. The opposite device is a digital to analog converter (DAC), which performs the same function but in reverse. An ADC allows the analog information measured to be

manipulated by digital equipment, such as a microcontroller. In this case, the ADC value is calculated using the following equation,

$$ADC = \frac{V_{IN} \times 2^n}{V_{REF}} \quad (26)$$

where n is the number of bits of resolution [35]. In this design, the supply voltage (3.3 V) is inputted to the reference voltage pin (V_{REF}), the voltage drop across the thermistor is the input voltage (V_{IN}), and 14 bits of resolution (n) are calculated.

2.6.3. *MAX6682 – Thermistor to Digital Converter*

An integrated circuit made by MAXIM is used to supply the current to measure the voltage drop across the thermistor. The MAX6682, a thermistor to digital converter, was implemented in the circuit [36]. While the MAX6682 is capable of calculating the resistance to temperature relationship and communicate with a microcontroller using a serial peripheral interface (SPI), the precision, accuracy, and flexibility of the microcontroller's ADC was preferred. Using the ADC, resolution to the millionth decimal point could be reached, compared to thousandth obtainable using the MAX6682. However, the MAX6682 was still used to provide a minute current across the thermistor for the ADC to measure the voltage drop. The power management circuitry built into the MAX6682 reduced the average thermistor current, thus minimizing thermistor self-heating. A 220 μA current is issued across the thermistor during a reading, between conversions the supply current is reduced to 21 μA .

2.6.4. *Atmel ATmega324P Microcontroller*

The ATmega324P, a high performance, low power Atmel AVR 8-bit microcontroller, is the processing unit for the thermoacoustic sensor [37]. Capable of twenty million instructions per second, with 32 kilobytes of in-system self-programmable flash memory, the ATmega324P was able to carry out the computations required. The main features of the ATmega324P include, the real time counter, the analog to digital converter, the programmable serial universal asynchronous receiver/transmitter port, and the internal interrupts. The 44-pin TQFP package was chosen, and programming was carried out using an AVR JTAGICE mkII. The microcontroller was operated at 3.3 V and a processing speed of 12 MHz.

Communication was carried out using a MAX448 RS-485 transceiver (MAXIM). The MAX448 is a low-power, slew rate limited transceiver capable of RS-485 communication [38]. This integrated circuit features a reduced slew rate driver that minimizes electromagnetic interference (EMI) and reduces reflections caused by improperly terminated cables. The MAX448 is capable of error free data transmission up to 250 kbps, and draws between 120 μ A and 500 μ A of supply current during operation. The RS-485 standard is a communication standard that specifies the electrical characteristics of the driver and receiver. It is used throughout the SonaCellTM system in a master-slave orientation.

The thermoacoustic sensor's hardware block diagram, schematic, and PCB layout are shown in figure 2-11, 2-12, and 2-13, respectively.

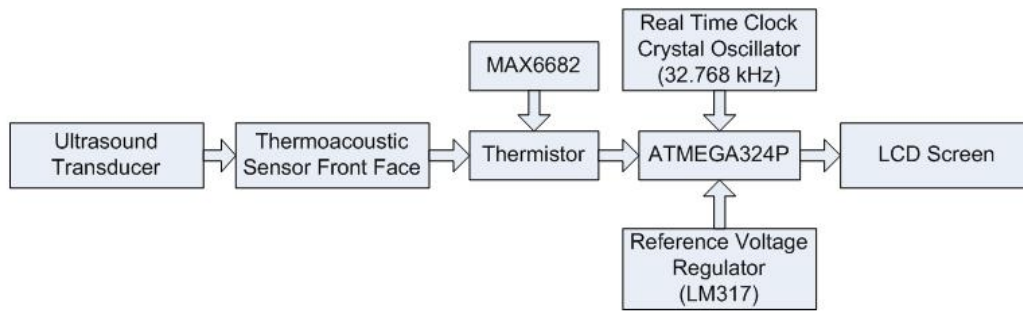


Figure 2-11: Thermoacoustic sensor hardware block diagram

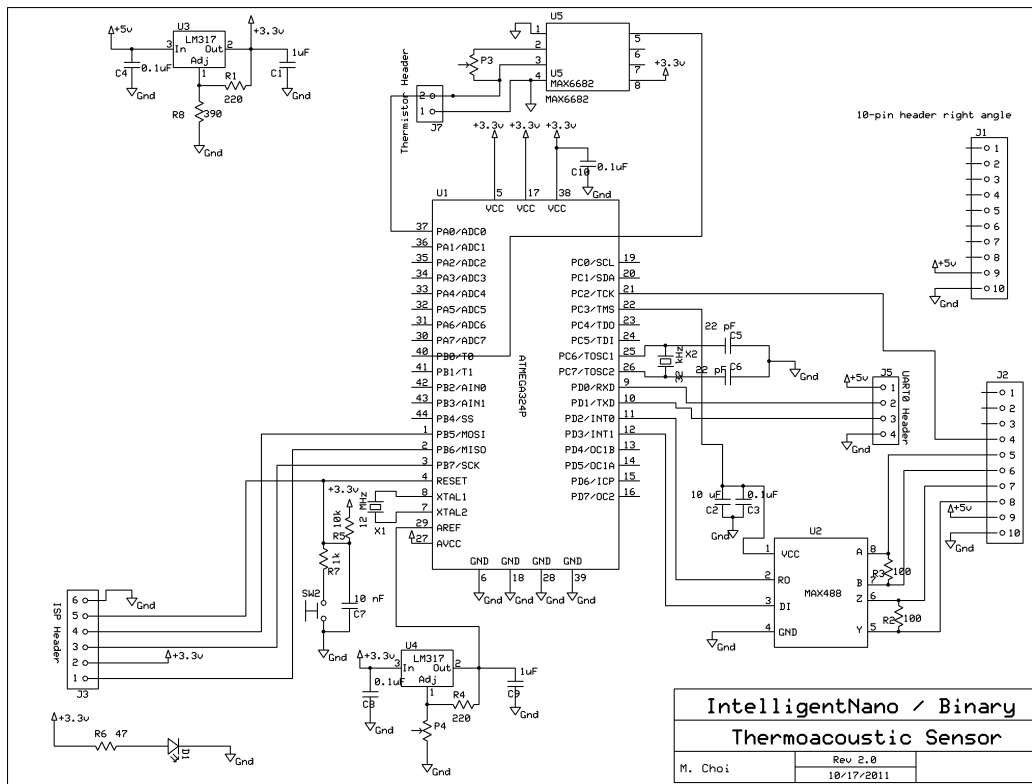


Figure 2-12: Thermoacoustic sensor schematic

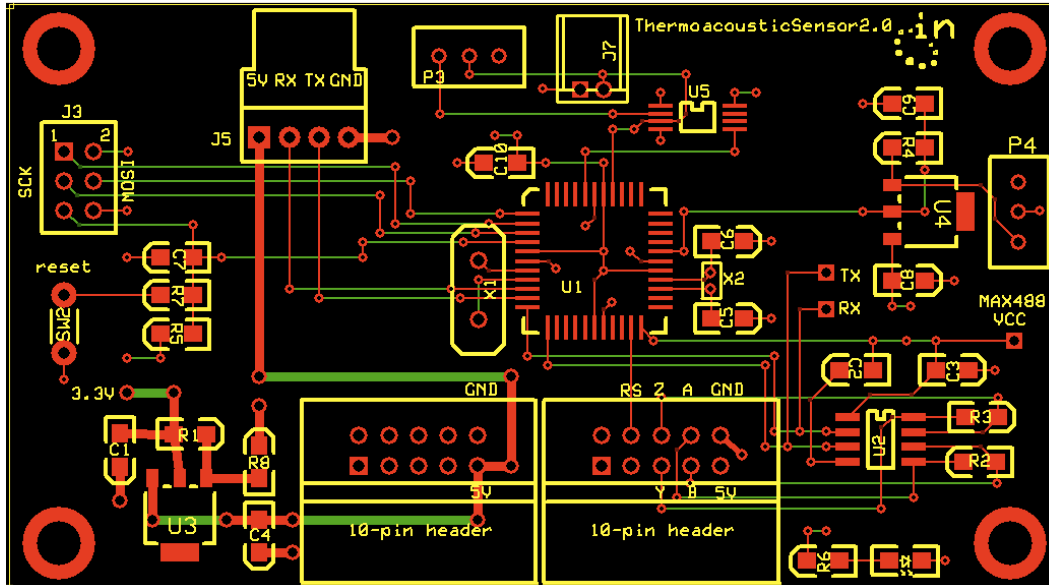


Figure 2-13: Thermoacoustic sensor printed circuit board layout

2.7. Data Sampling: Measuring the Temperature

After the thermoacoustic sensor's hardware was implemented and tested, the sensor's firmware was designed. This section will focus on data sampling, how the thermoacoustic sensor measured temperature.

2.7.1. Data Sampling

As discussed in the hardware section, a thermistor was implemented to monitor the thermoacoustic sensor's temperature, by measuring the change in voltage across the thermistor as the temperature changed using an analog to digital converter (ADC). ADC's are characterized by their reference voltage, conversion rate, and resolution. The ADC's reference voltage of 3.3 V, and conversion time of 260 μ s [37] were sufficient for the thermoacoustic sensor; however, the ADC's built in resolution was examined further.

The ATmega324P ADC has a built in resolution of 10 bits. For a 10-bit analog to digital converter with a voltage reference of 3.3 V, the least significant digit is,

$$LSB = \frac{V_{REF}}{2^n} \quad (27)$$

$$LSB = \frac{3.3 V}{2^{10}} = 0.0032 V \quad (28)$$

Using the 10-bit built in ADC, the change in measured ADC values when the thermistor was heated up over time is shown in figure 2-14. Even though the thermistor is being heated by a constant heat source, the scatter plot has a “step-like” profile (dashed line), instead of the linear line expected (solid line).

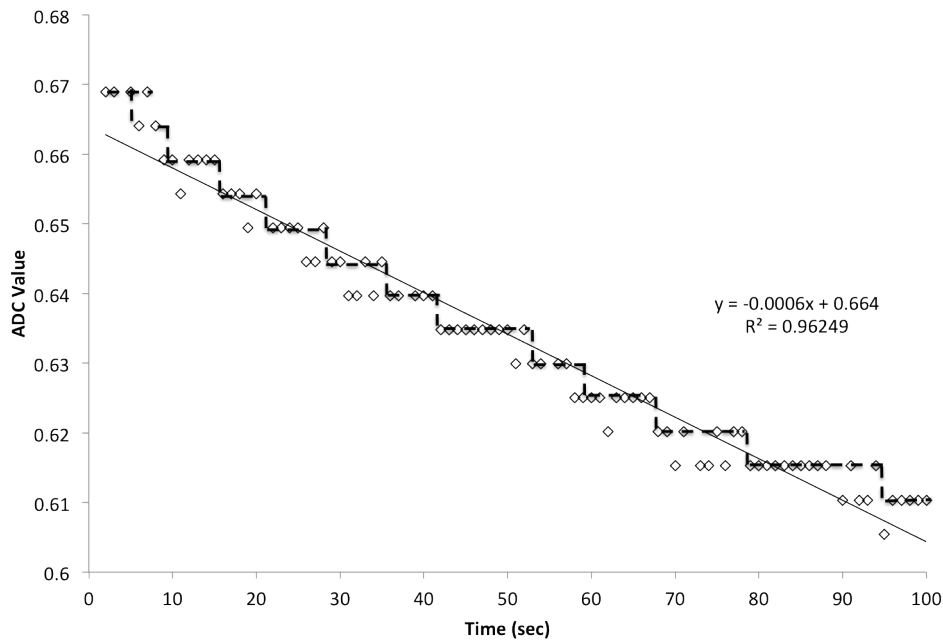


Figure 2-14: ADC input vs. time using the ATmega324P 10-bit ADC with the voltage change across a heated thermistor as the input. ADC displays a “step like” profile (dashed line) instead of the expected linear profile (solid line)

This is a result of the ADC's resolution. Enhancing the resolution of the ADC can be used to smooth out the linear measured data by enabling the ADC to resolve the small differences in a measurement, figure 2-15. Oversampling and decimation techniques were used to enhance the analog to digital converter's resolution.

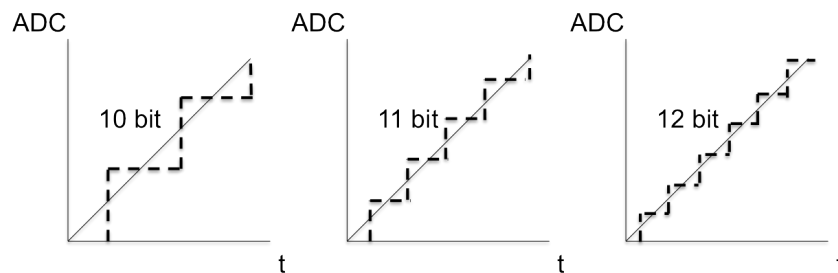


Figure 2-15: Example of how enhancing the ADC's resolution can increase the accurate approximation of the sampled signal [35]

2.7.2. *Oversampling and Decimation*

Oversampling is a technique that can be used to increase the resolution of the ADC, and reduce the noise measured by the ADC. While oversampling does not directly improve the ADC's resolution, it does provide more samples, which allows the ADC to more accurately track the input signal by better utilizing its dynamic range. The process of decimation uses the oversampled signal to increase the effective resolution of the analog to digital converter. Decimation involves oversampling the input signal so that a number of samples can be used to compute a virtual result with a greater accuracy than a single real sample can provide. Overall, the oversampling and decimation process yields a more accurate approximation of the sampled signal. Additionally, this procedure can improve the signal to noise ratio by spreading the effect of random noise across multiple samples.

The first step is to oversample the signal 4^n times, where n is the number of virtual bits desired in the result. The oversampled signals are added, like in normal averaging, but instead of dividing the signal by the number of readings, the result is right shifted by n . Right shifting a binary number n times is equal to dividing the binary number by a factor of 2^n . This yields a result with a resolution increased by n bits. In this system, the ADC was oversampled to yield an additional 4-bits of resolution, bring the total to 14-bits [35]. The C code used to program the oversampling function is displayed in *Appendix A*.

One requirement for the oversampling and decimation procedure is the sampled signal has to vary when it is sampled. This variation should be the noise-component of the signal. Ideally, the noise in the input signals should have amplitudes greater than 1 LSB of the ADC, have a mean value of zero, and be randomly distributed. The other constraint of the system is the oversampling process will increase the sample time of the system. Instead of sampling once per second, the system must now sample 4^n times per second. Care must be taken to ensure that the sampling time does not exceed the one-second window allocated to collecting and processing the measured data.

Measured results using an oversampled 14-bit analog to digital converter were compared to the ATmega324P's 10-bit ADC. The first measurements were taken by placing the thermoacoustic sensor in a heated water bath and measuring the change in input voltage into the ADC as the voltage drop across the thermistor changed. This was the same setup used for the thermistor calibration process. A thermometer was placed in the water bath beside the thermoacoustic sensor, and

every incremental increase in temperature the corresponding ADC reading was recorded. Using the thermometer, the thermistor and ADC were calibrated.

The second measurements were taken after the thermistor – ADC slope was programmed into the microcontroller. An ultrasound beam with an output intensity of 80 mW/cm^2 was applied to the thermoacoustic sensor, and the increase in temperature over time was measured.

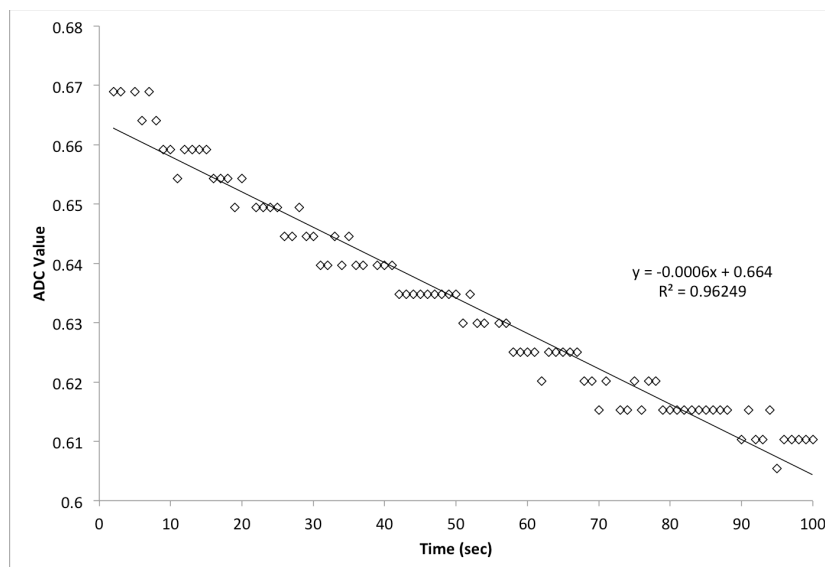


Figure 2-16: Thermistor calibration using a constant heat source, 10-bit ADC with no oversampling

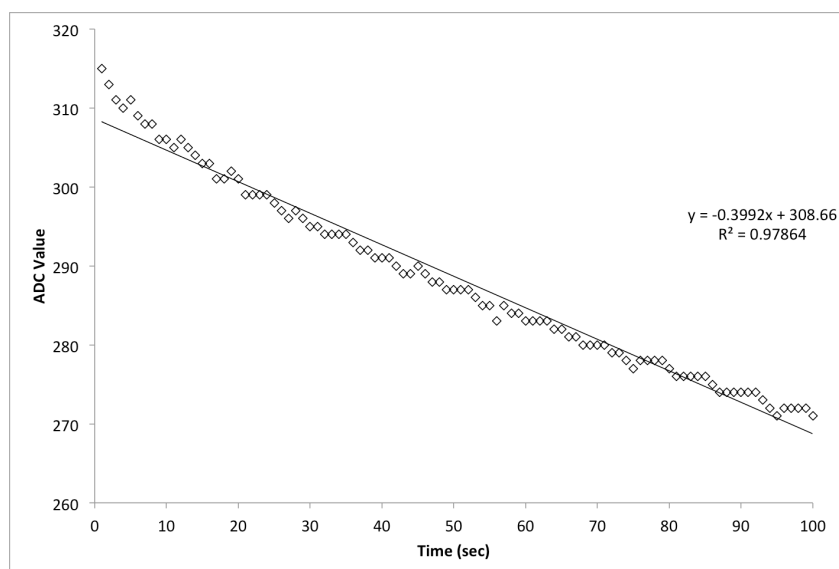


Figure 2-17: Thermistor calibration using a constant heat source, 14-bit ADC with oversampling

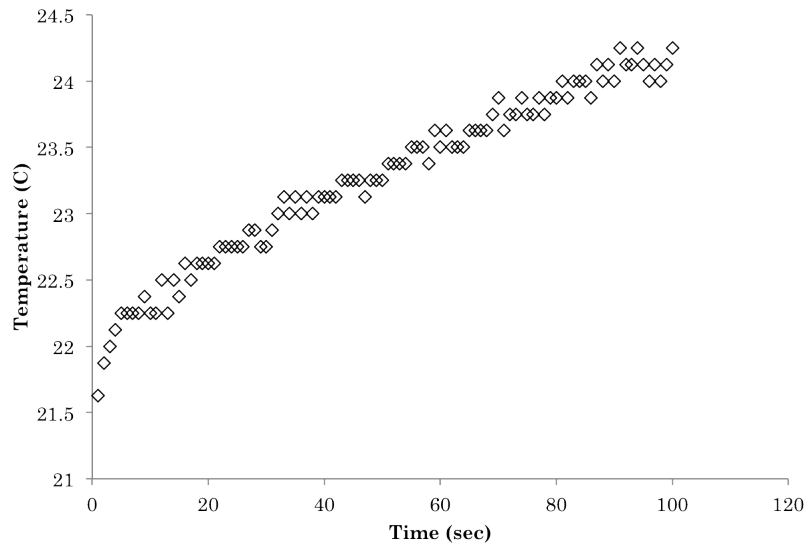


Figure 2-18: The increase in temperature due to an applied ultrasound intensity of 80 mW/cm^2 , 10-bit ADC with no oversampling

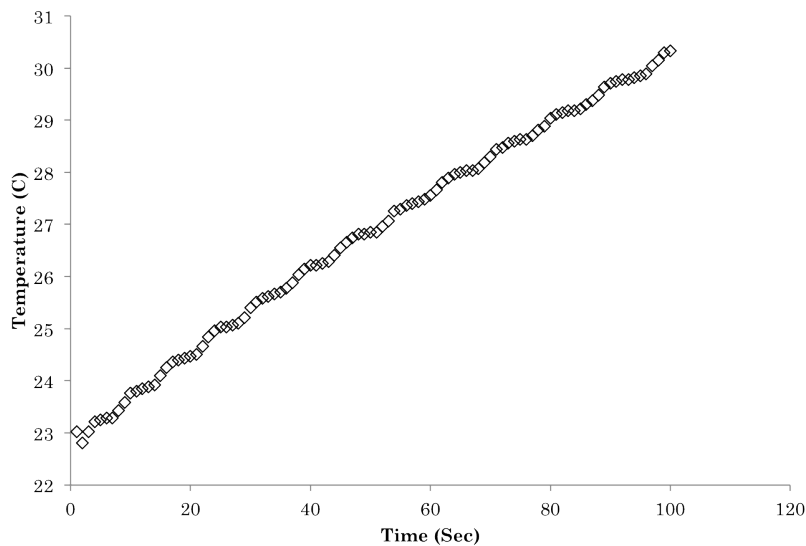


Figure 2-19: The increase in temperature due to an applied ultrasound intensity of 80 mW/cm^2 , 14-bit ADC with oversampling

The measurements taken using a non-oversampled ADC during thermistor calibration using a constant heat source yielded a linear regression of 0.96249, compared to a linear regression of 0.97864 when oversampling was used, figures 2-16, and 2-17, respectively. Using the linear regression value is one measure to

evaluate how well the ADC reconstructed the input analog data; a linear regression value closer to 1 is desired. Compared to the data collected using the 10-bit ADC, the 14-bit ADC had less of a step-like profile. Using a calibrated ADC, the measured increase in temperature due to an applied ultrasound beam was recorded. Again, the data collected using the 10-bit ADC had a large number of repeated values, which led to the step-like profile, figure 2-18, while the 14-bit ADC was able to record the minute changes in temperature and the collected data had less repeated values, figure 2-19. The oversampled system was able to reconstruct the measured analog signal better than the non-oversampled signal, whether it was a linear increase due to a constant heat source or a non-linear curve due to an absorbed ultrasound beam. The 14-bit ADC had a least significant bit of 0.0002014 V. After thermistor calibration, the thermoacoustic sensor was able to measure temperature with a resolution of 0.018505 °C. This increased resolution will allow the thermoacoustic system to measure changes in temperature more accurately, and calculate the small changes in absorbed ultrasound energy more quickly.

The oversampled ADC must take readings while current is being applied to the thermistor. Figure 2-20 shows the oversampled process, orange line, occurring within the timeframe the MAX6682 is applying a current to the thermistor, green line. One drawback of oversampling an ADC is the increased sampling time required. The least-squares method that the thermoacoustic sensor employs needs temperature readings to be taken every second. The start time of each thermoacoustic sensor computation was recorded on the oscilloscope, figure

2-21. The difference in time (Δt) between each reading is 1.04 seconds, confirming that a reading is taken every second.

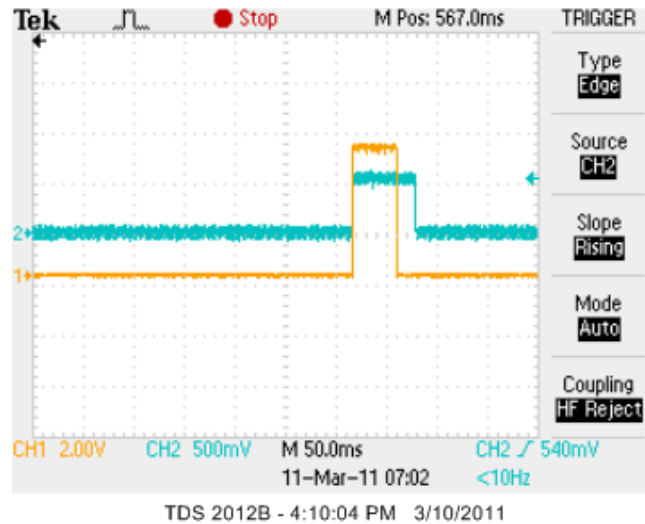


Figure 2-20: Oversampling computation period (orange), and time the thermistor has an applied current (green)

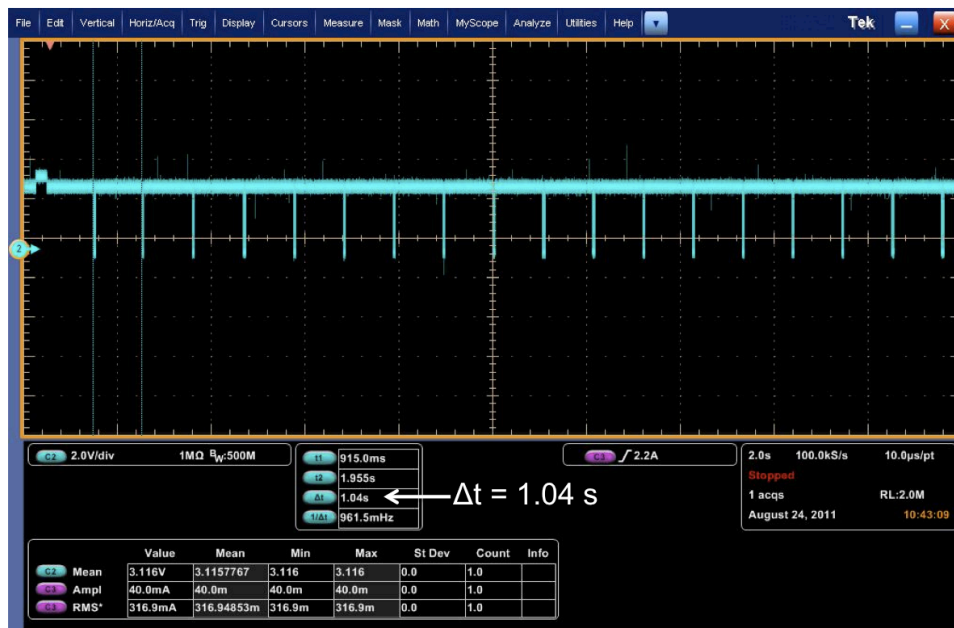


Figure 2-21: Start of each thermoacoustic sensor computation

2.8. Thermistor Calibration

Once the oversampled analog to digital converter was implemented, the thermistor was characterized. This involved finding the relationship between the change in the thermistor's resistance and the change in temperature. Using the microcontroller's ADC, the voltage drop across the thermistor at different temperatures was found. Over the thermoacoustic sensor's operational temperature, the resistance to temperature relationship is expected to be linear; therefore, the slope of the line can be used to extrapolate the temperature.

The thermistor calibration was carried out by placing the thermoacoustic sensor in a temperature monitored water bath on top of a hot plate set to 100 °C, seen in figure 2-22. As the water temperature increased, the thermoacoustic sensor temperature increased, and the resistance of the thermistor changed. Using a thermometer, every degree increase in temperature was measured from 22 °C to 37 °C, and the corresponding ADC value was recorded. This was repeated three times.

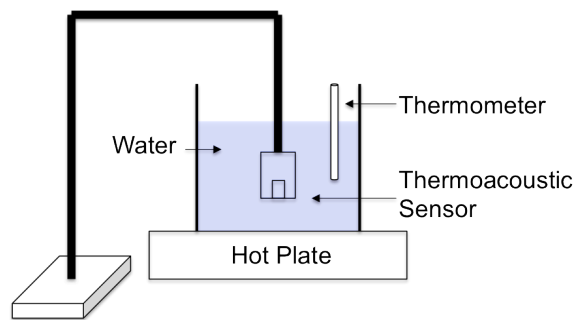


Figure 2-22: Thermistor Calibration Experiment Setup

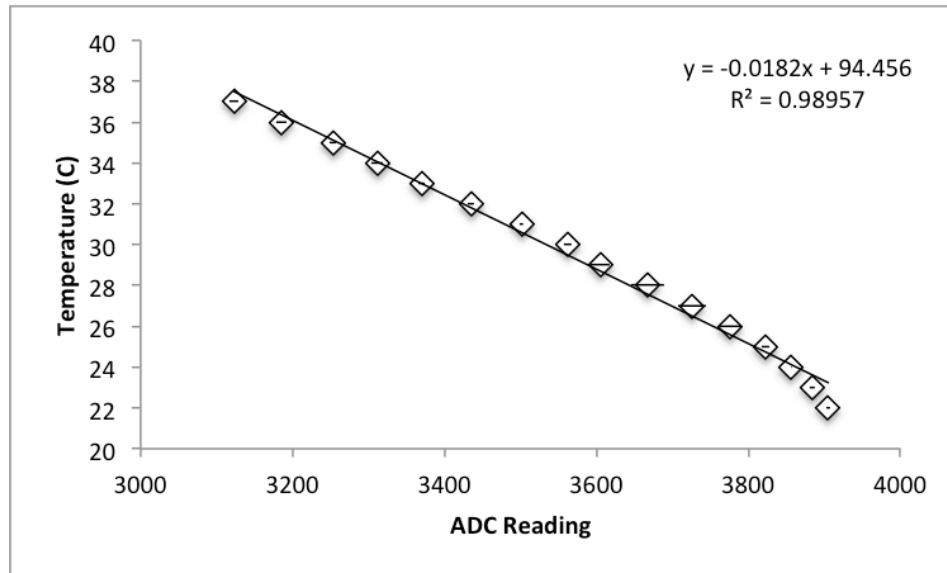


Figure 2-23: Thermistor temperature vs. ADC reading for thermistor for thermistor calibration line

The temperature vs. ADC value plot is displayed in figure 2-23. Over the desired temperature range, there was a linear correlation between the change in resistance and the change in temperature, with a linear regression of 0.98957. The slope of the line, where y is the temperature and x is the ADC value is,

$$y = -0.0182x + 94.456 \quad (29)$$

Horizontal error bars are added to represent the standard deviation between readings. The maximum standard deviation observed using the ADC was 22.37.

In accordance to the operation of a negative temperature coefficient thermistor, the resistance decreased as the temperature increased. The points on the graph that do not fall on the linear line are due to the initial heat diffusion through the thermoacoustic sensor. When the water bath is heated, the thermometer reading the water temperature will initially change before the heat is transferred to the back face of the thermoacoustic sensor where the temperature measuring component is placed. This initial delay is seen for the 22 °C and 23 °C

data points. The relationship shown in equation (29) is programmed into the microcontroller operating the thermoacoustic sensor, allowing the sensor's temperature to be extrapolated in real time.

2.9. Curve Fitting: The Least Squares Model

The transient method implemented relates the measured temperature to the incident ultrasound intensity by fitting a curve to the measured data and inferring the ultrasound intensity from the coefficients of this curve. Therefore, a curve fitting procedure is required. For the thermoacoustic sensor, the least squares curve fitting method was chosen.

The least squares fitting method is a procedure for finding the best fitting curve to a given set of data points by minimizing the sum of squared vertical offsets, where the vertical offset is the distance in the vertical direction the measured data point is from the fitted curve. This process solves a system of equations in an approximation sense, but instead of solving the equations only the sum of squares is minimized [39-40]. In a non-linear, least squares fitting procedure the coefficients (a_1, a_2, \dots, a_n) are approximated before the procedure and iteratively optimized until the resulting residual (R^2) is minimized. R^2 is the sum of the squared difference between the measured data (y_i), and the function ($f(x_i, a_1, a_2, \dots, a_n)$) representing the curve, this is shown in equation (30).

$$R^2 = \sum [y_i - f(x_i, a_1, a_2, \dots, a_n)]^2 \quad (30)$$

Non-linear least squares fitting methods can produce good estimates of the unknown parameters in a model with relatively small data sets; however, it requires an iterative optimization procedure that can be processor intensive, and

requires approximations of the starting parameters that are reasonably close to the unknown parameters.

Initial analysis was carried out using the *lsqcurvefit* function in MATLAB.

The MATLAB *lsqcurvefit* function can be used to solve nonlinear curve-fitting problems using a least squares process. Given input data $xdata$, and observed output data $ydata$, the function finds the coefficients x that solves the problem,

$$\min_x \|F(x, xdata) - ydata\|_2^2 = \min_x \sum_i (F(x, xdata_i) - ydata_i)^2 \quad (31)$$

In this equation, $F(x, xdata)$ is a function of the same size as $ydata$. The implementation of the *lsqcurvefit* function is as follows,

$$x = \text{lsqcurvefit}(\text{fun}, x_0, xdata, ydata) \quad (32)$$

The function will start using the conditions x_0 and will proceed to find the coefficients x that best fit the nonlinear function $\text{fun}(x, xdata)$ to the data given, $ydata$ [41]. This is carried using a least squares process. The MATLAB code used to run the *lsqcurvefit* function is outlined in Appendix B.

Chapter 3: Evaluation of the Transient Model

Chapter 2 described the construction of the thermoacoustic sensor, and the implementation of the data sampling firmware to accurately measure the sensor's temperature. It discussed how the sensor's thermistor was calibrated, and introduced the least squares curve fitting model. This chapter will study how the transient model was implemented, and evaluate how well it can relate measured temperature data to the incident ultrasound intensity.

3.1. Evaluation of the Transient Model: Long Periods of Time

The transient method relates the measured temperature to the incident ultrasound intensity by fitting a curve to the measured data. The curve, equation (9) page 23, proposed in [25] is,

$$T_{ave}(t) = \sum_{n=0}^{\infty} C_n \left(1 - e^{-\frac{t}{\tau}}\right)$$

$$\text{where } C_n = \frac{I_0}{\mu k} \frac{16(1+e^{-2\mu l})}{\pi(2n+1)(\mu^2 l^2 + (2n+1)^2 \pi^2)}, \text{ and } \tau = \frac{4l^2 \rho C_p}{\pi^2 k}$$

To evaluate the transient model with a thermoacoustic sensor implemented in a close proximity setup, measured data was collected and the least squares model was used to fit the curve, equation (33), to the data.

$$T_{ave}(t) = C \left(1 - e^{-\frac{t}{\tau}}\right) + T_0 \quad (33)$$

The value T_{ave} is the measured temperature averaged across the absorber's back face, and T_0 is the starting temperature. The thermoacoustic sensor was coupled directly in contact with the SonaCell™ ultrasound transducer. When the ultrasound generator was turned on, the thermoacoustic sensor began measuring the change in temperature at the absorber's back face. The

measured temperature vs. time curve for ultrasound with an incident ultrasound intensity of 30 mW/cm^2 is shown in figure 3-1.

Using the least squares method and MATLAB's curve fitting toolbox, the transient model was evaluated. The curve described in equation (33) was fit to the measured data with prediction bounds with 95% certainty, and is shown in figure 3-2. Figure 3-3 displays the residuals plot associated with the fitted curve. The residual (r) is the difference between the measured data (y) and the predicted value (\hat{y}) [42],

$$r = y - \hat{y} \quad (34)$$

The residual plot does appear to behave randomly and has r values close to 0, which is an indication that the model fits the data [42].

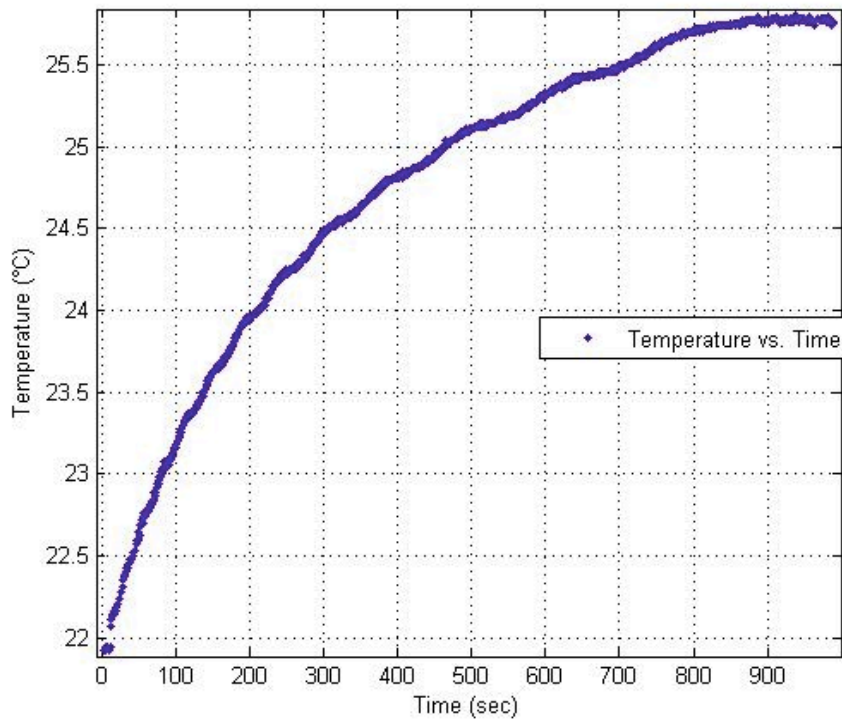


Figure 3-1: Temperature vs. time data measured using the thermoacoustic sensor for an applied ultrasound intensity of 30 mW/cm^2 , ambient temperature of $22 \text{ }^\circ\text{C}$

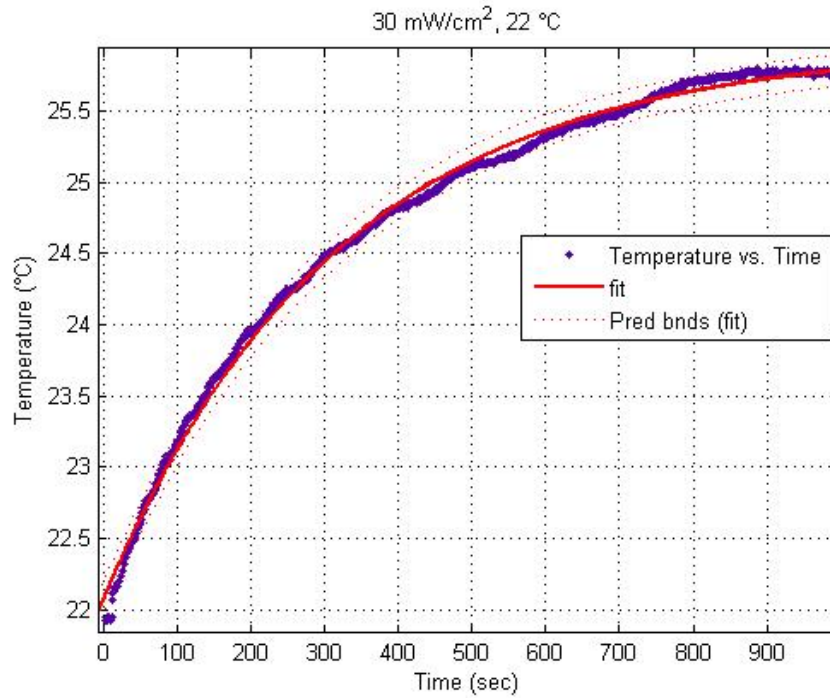


Figure 3-2: Temperature vs. time data measured using the thermoacoustic sensor for an applied ultrasound intensity of 30 mW/cm². Data was fit with equation (33) using the least squares model with prediction bounds with 95% certainty, ambient temperature of 22 °C

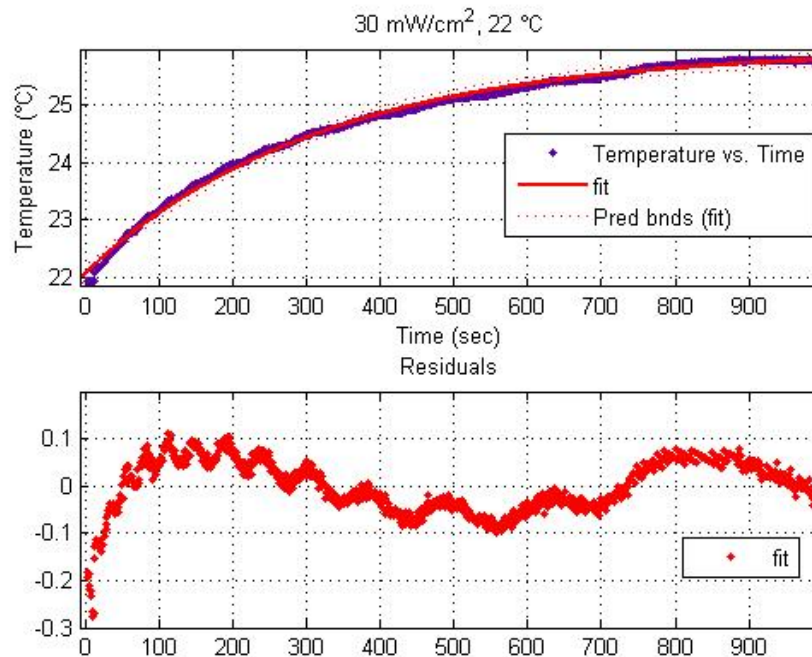


Figure 3-3: Residual plots for a temperature vs. time data with the fitted model curve. Ultrasound intensity of 30 mW/cm², ambient temperature of 22 °C

TABLE VIII
COEFFICIENTS OF THE TRANSIENT MODEL FOR AN APPLIED ULTRASOUND
INTENSITY OF 30 mW/cm² AT 22 °C

Ultrasound Intensity [mW/cm ²]	Coefficient C (95% Confidence Bounds) [kΩ]	Coefficient τ (95% Confidence Bounds) [sec]	Coefficient T ₀ (95% Confidence Bounds) [°C]
30	3.863 (3.849, 3.877)	319.9 (316.4, 323.3)	22.09 (22.08, 22.11)

The coefficients of the transient model are displayed in Table VIII. The 95% confidence bound indicates that the model is 95% confident that the mean value will fall in between the upper and lower bounds. A smaller interval width is desirable because it indicates that in subsequent trials the calculated coefficient values will be near the mean value determined by this curve fitting session.

TABLE IX
GOODNESS OF FIT ANALYSIS FOR DATA FOR AN APPLIED ULTRASOUND
INTENSITY OF 30 mW/cm² AT 22 °C

Ultrasound Intensity	Sum of Squares	R-Squared Value	Root Mean Squared Error
30 mW/cm ²	3.142	0.9968	0.05642

The goodness of fit analysis calculated by the MATLAB curve fitting toolbox is outlined in Table IX. The sum of squares of residuals (SSE) value measures the total deviation between the measured data (y) and the predicted data (\hat{y}) calculated by the fitted curve [43].

$$SSE = \sum_{i=1}^n r_i^2 = \sum_{i=1}^n (y_i - \hat{y}_i)^2 \quad (35)$$

An SSE value closer to 0 indicates that the model has a smaller random error, and it is a better fit. The R-squared value is the square of the correlation between the measured data and the predicted value [43].

$$SST = \sum_{i=1}^n (y_i - \bar{y})^2$$

$$R_{square} = 1 - \frac{SSE}{SST} \quad (36)$$

SST is the sum of squares about the mean, where (\bar{y}) is the overall mean. An R-squared value closer to 1 indicates that a greater proportion of variance is accounted for by the model [43]. Finally, the root mean squared error (RMSE) is an estimate of the standard deviation of the random component of the data. The RMSE calculation is shown in the equation below, where (n) is the number of terms.

$$MSE = \frac{SSE}{n}$$

$$RMSE = \sqrt{MSE} \quad (37)$$

An RMSE value closer to 0 indicates that the model is more useful for prediction [43].

After using the MATLAB curve fitting toolbox to analyze the goodness of fit of equation (33) to the measured temperature vs. time data collected when a 30 mW/cm² ultrasound intensity was applied to the thermoacoustic sensor, we can conclude that the least squares method does fit the curve to the measured data. The sum of squares value is 3.142, the R-squared value is 0.9968, and the root mean squared error value is 0.05642.

A second analysis was done to verify that the model fits data collected at different ultrasound intensities, and to look for any trends between the curves fit to the measured data generated at different ultrasound intensities. The intensity range of the SonaCell™ is 30 mW/cm² to 100 mW/cm²; therefore, equation (33) was also fit to data collected when ultrasound was applied to the sensor at 60 mW/cm² and 100 mW/cm². Figure 3-4 shows the measured temperature vs. time curve when ultrasound was measured by the sensor with ultrasound intensities of 30 mW/cm², 60 mW/cm², and 100 mW/cm². Readings were taken until the temperature stopped increase, approximately 1000 seconds.

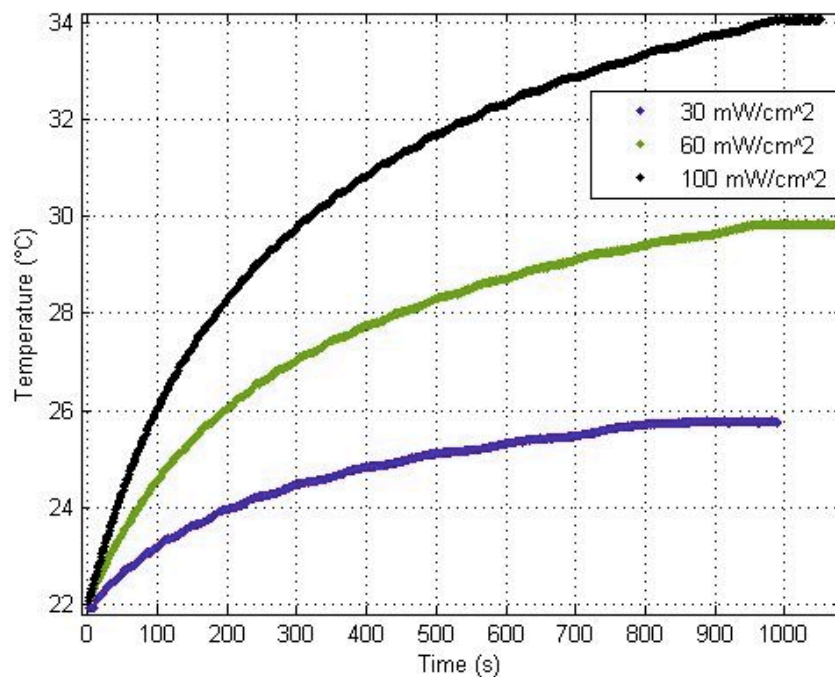


Figure 3-4: Temperature vs. time data measured using the thermoacoustic sensor. Applied ultrasound intensities of 30 mW/cm², 60 mW/cm², and 100 mW/cm².

Curve fitting analysis was again done using MATLAB's curve fitting toolbox.

The measured data and the fitted curve for the 60 mW/cm^2 and the 100 mW/cm^2 ultrasound intensity are shown in figure 3-5, and figure 3-6, respectively.

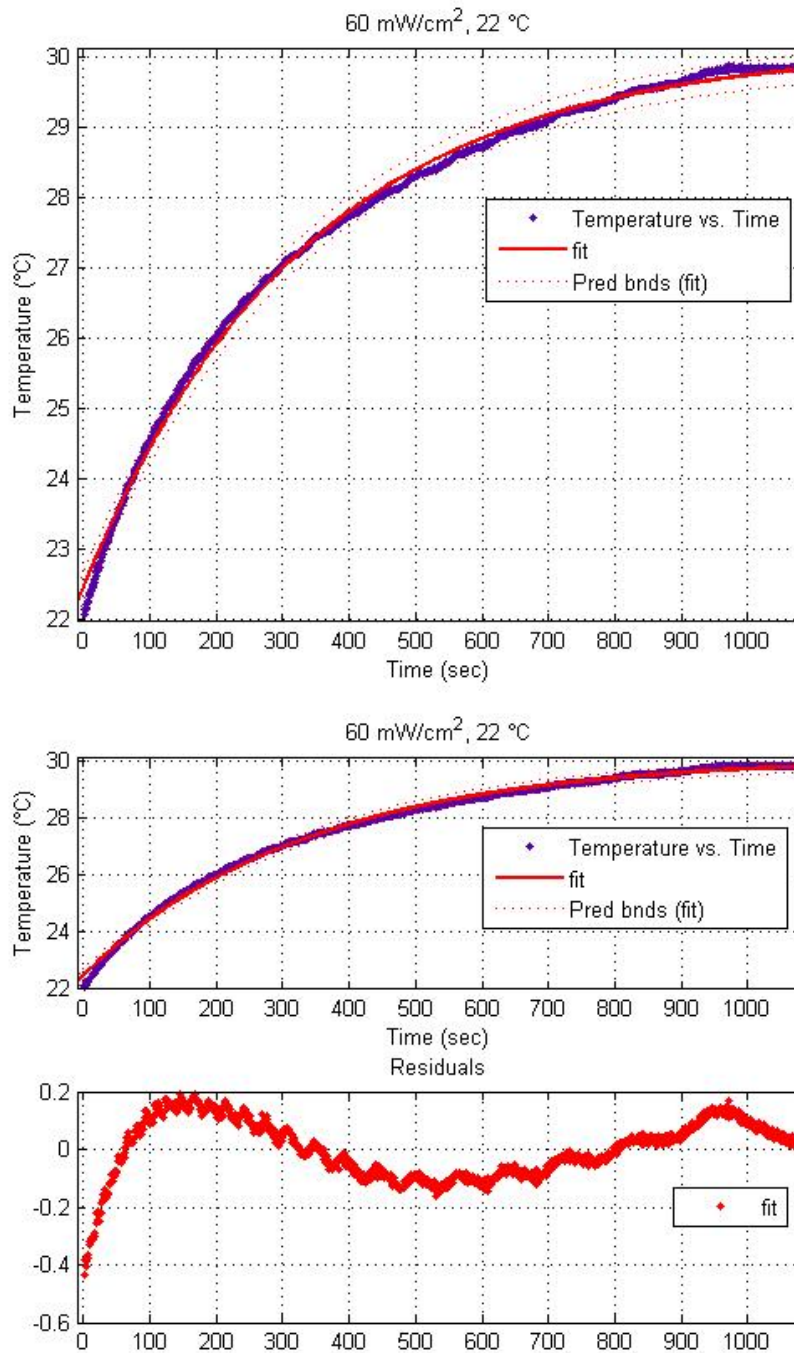


Figure 3-5: (Top) Temperature vs. time data measured using the thermoacoustic sensor with the fitted model, and 95% certainty prediction bounds for an ultrasound intensity of 60 mW/cm^2 .
(Bottom) Residual plot for fitted data

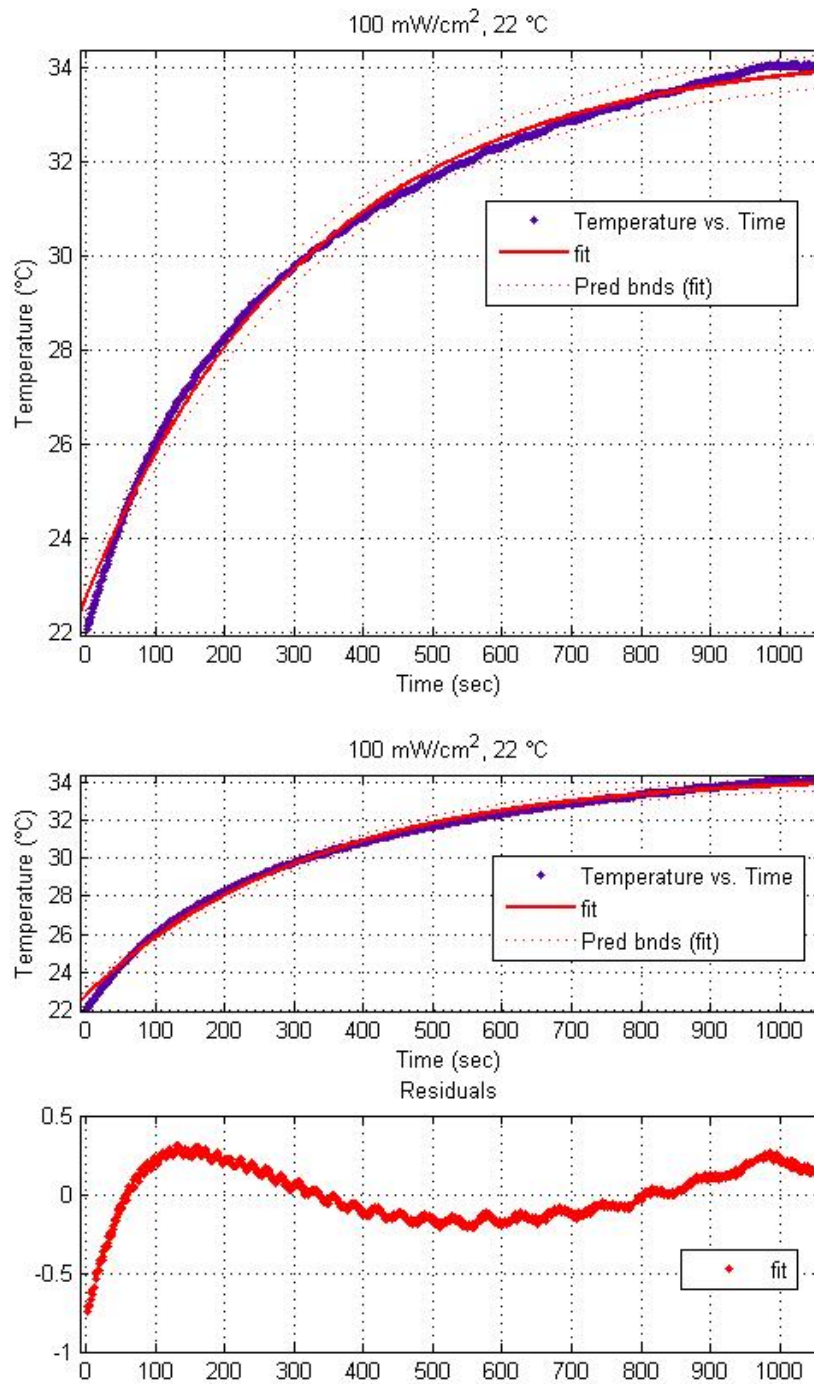


Figure 3-6: (Top) Temperature vs. time data measured using the thermoacoustic sensor with the fitted model, and 95% certainty prediction bounds for an ultrasound intensity of 100 mW/cm².
(Bottom) Residual plot for fitted data

TABLE X
COEFFICIENTS OF THE TRANSIENT MODEL FOR AN APPLIED ULTRASOUND
INTENSITY OF 30 mW/cm², 60 mW/cm², 100 mW/cm² AT 22 °C

Ultrasound Intensity [mW/cm ²]	Coefficient C (95% Confidence Bounds) [kΩ]	Coefficient τ (95% Confidence Bounds) [sec]	Coefficient T ₀ (95% Confidence Bounds) [°C]
30	3.863 (3.849, 3.877)	319.9 (316.4, 323.3)	22.09 (22.08, 22.11)
60	7.636 (7.612, 7.66)	336.1 (332.9, 339.3)	22.48 (22.46, 22.51)
100	11.59 (11.55, 11.63)	328.7 (325.2, 332.2)	22.79 (22.74, 22.83)

Table X outlines the calculated coefficient values of equation (33) for the three ultrasound values measured. We observe that the C coefficient is changing with ultrasound intensity. This is expected because the C coefficient is dependent on the initial ultrasound intensity applied to the sensor. The τ value is ultrasound intensity independent and should not change with changes in ultrasound. The SonaCellTM ultrasound generator is capable of outputting ultrasound at intensities from 30 mW/cm² to 100 mW/cm². Temperature vs. time curves were measured at both extremes and in the middle until equilibrium was reached. The calculated τ value had a mean value of 328.23 and a standard deviation of 2.47. It can be concluded that the τ value is not changing with respect to changes in applied ultrasound intensity. Similarly, as expected the starting temperature (T_0) does not change across the different measured ultrasound intensities.

Taking a closer look at the τ values calculated by the curve fitting toolbox, we noticed that the measured value is not equal to the value calculated by the equation described in [25]. Using the thermal and acoustic properties of the sensor outlined in Table III and Table IV, the τ value described by equation (9) is,

$$\tau = \frac{4l^2 \rho C_p}{\pi^2 k} = \frac{(4)(0.0033 \text{ m})^2 (1180 \frac{\text{kg}}{\text{m}^3}) (1300 \frac{\text{J}}{\text{kg} \cdot \text{K}})}{(\pi^2)(0.167 \frac{\text{W}}{\text{m} \cdot \text{K}})} = 40.54 \text{ s} \quad (38)$$

Wilkins [27] suggested that the validity of the model suggested in [25] is restricted by some simplifying assumptions: the single reflection approximation, lateral homogeneity, and neglect of impedance mismatch at the front face of the sensor. The single reflection approximation used to formulate the transient model assumes that the beam propagates through the absorber, is reflected once at the back face of the absorber, propagates back towards the absorber's front face, and is transmitted out of the sensor. Any subsequent reflections back into the absorber are ignored. Further analysis into validity of the single reflection approximation reveals that this is not the case using this design. Ignoring the copper layer, if the thermoacoustic sensor is used to measure an incident ultrasound beam with an intensity of 100 mW/cm^2 the intensity of the beam that is transmitted into the plexiglass layer at the gel – plexiglass boundary is,

$$I_{Transmitted} = 100 \times (1 - 0.1326) = 86.74 \text{ mW/cm}^2 \quad (39)$$

The beam will then travel through the plexiglass absorber, ignoring scattering the ultrasound intensity at the back face of the sensor after it has traveled through 0.033 cm of plexiglass is,

$$I(0.033) = 86.74 \times e^{-(0.554)(1.5)(0.033)} = 84.39 \text{ mW/cm}^2 \quad (40)$$

Corresponding with the single reflection theory, 99.94% of the ultrasound wave will be reflected at the plexiglass – air boundary, the intensity of the reflected ultrasound wave is,

$$I_{Reflected} = 84.39 \times 0.9994 = 84.34 \text{ mW/cm}^2 \quad (41)$$

The ultrasound wave travels back to the front of the sensor. After being attenuated through another 0.033 cm of plexiglass, the intensity of the reflected ultrasound wave at the front face of the sensor is,

$$I(0.033) = 84.34 \times e^{-(0.554)(1.5)(0.033)} = 82.06 \text{ mW/cm}^2 \quad (42)$$

At the plexiglass – gel boundary 13.26% of the ultrasound wave will be reflected back into the sensor. The ultrasound intensity that will be reflected back into the sensor and is outside the boundaries of the single reflection theory is,

$$I_{\text{Reflected}} = 82.06 \times 0.1326 = 10.88 \text{ mW/cm}^2 \quad (43)$$

In this design, 10.88% of the incident ultrasound intensity will be reflected back into the sensor after the single reflection approximation.

With this in mind, similar to the work done by Wilkens [27] the coefficient τ for the transient model used was calculated from the fitting procedure of the three ultrasound intensities shown in figure 3-4 and outlined in Table X, instead of from the parameters of the absorber.

TABLE XI
GOODNESS OF FIT ANALYSIS FOR AN APPLIED ULTRASOUND INTENSITY OF 30
MW/CM², 60 MW/CM², 100 MW/CM² AT 22 °C

Ultrasound Intensity	Sum of Squares	R-Squared Value	Root Mean Squared Error
30 mW/cm ²	3.142	0.9968	0.05642
60 mW/cm ²	11.36	0.9973	0.103
100 mW/cm ²	32.31	0.9965	0.1756

In Table XI we observe that the curve's goodness of fit decreases as the ultrasound intensity increases. One possible reason for this is the heat generated by the ultrasound transducer due to the energy lost during the conversion of electrical energy to mechanical energy in the transducer. This model does not account for the heat produced by the transducer. As the output ultrasound intensity increases, the heat generated by the transducer will also increase, which will contribute to the goodness of fit values deviating from their target values. This is a source of error in our model that will be discussed in the *Thermoacoustic Sensor Error* section of the thesis.

We have evaluated how our model fits to three different ultrasound intensities over long durations of time. Using the MATLAB curve fitting toolbox and the calculated goodness of fit values we can conclude that the model fits to the measured data at each of the measured ultrasound intensities. We observed that, as expected, the C coefficient changes with respect to the applied ultrasound intensities, and the τ and T_0 do not vary with different ultrasound intensities. Therefore, the average τ value from the data in Table X ($\tau = 324.23$) was used throughout the remainder of the thermoacoustic sensor's evaluation, and the ambient temperature T_0 was measured before sensor readings began.

3.2. Evaluation of the Transient Model: Short Periods of Time

In order to make quick measurements with the thermoacoustic sensor, the transient model's ability to fit data to small sets of data was evaluated.

Ultrasound was applied to the thermoacoustic sensor for 30 seconds and the measured temperature vs. time curves were plotted. Using the MATLAB curve fitting toolbox, the curve described by equation (33), page 57, was fit to the data. Figure 3-7 shows measured temperature vs. time data when ultrasound was applied at 30 mW/cm^2 , and the fitted curve with 95% confidence prediction bounds. The residual plots are shown in figure 3-8, and the calculated coefficients with 95% confidence bounds, and the goodness of fit parameters are outlined in Table XII, and Table XIII, respectively.

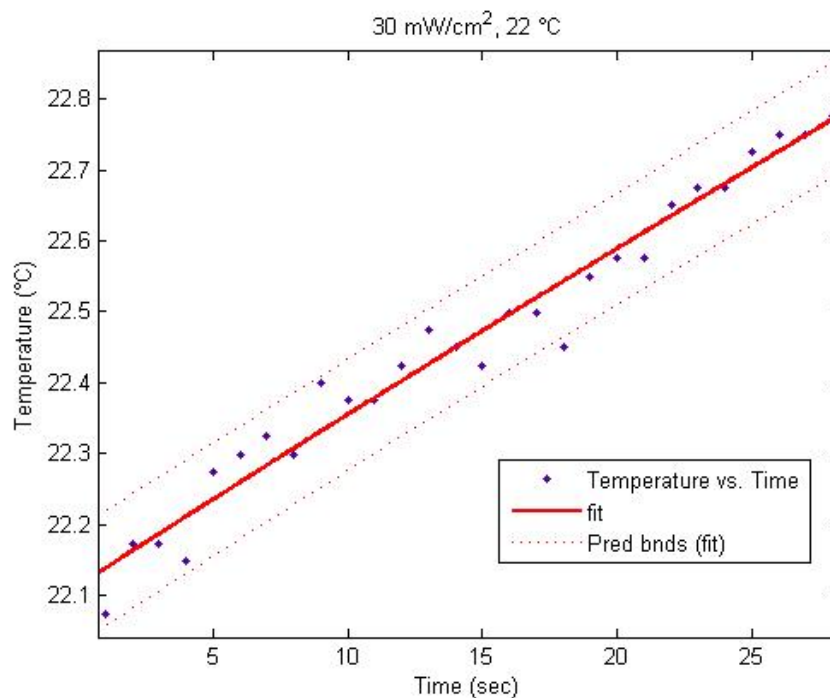


Figure 3-7: Temperature vs. time data measured for 30 seconds for an ultrasound intensity of 30 mW/cm^2 fit was the transient model with 95% confidence prediction bounds.

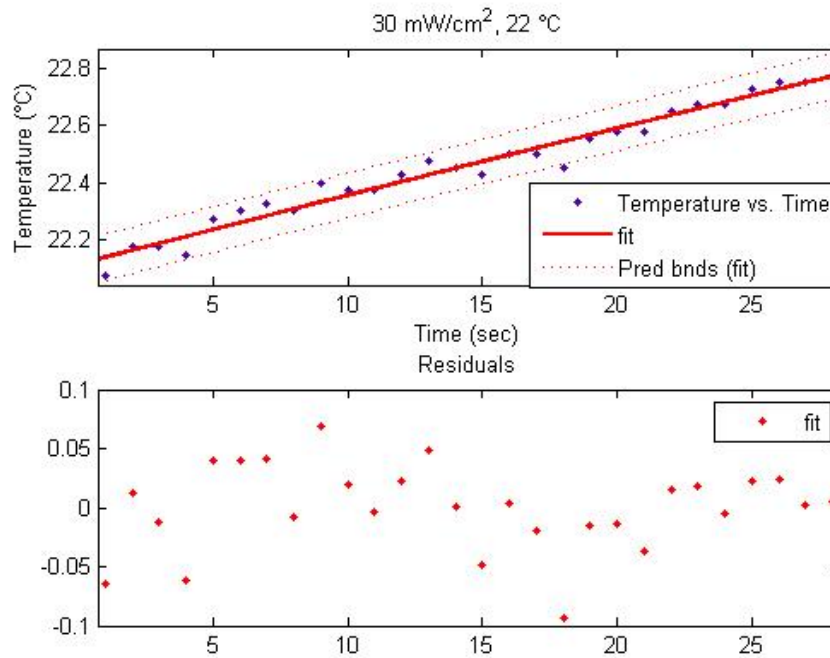


Figure 3-8: Residual plots for temperature vs. time data with the fitted transient model. Ultrasound intensity of 30 mW/cm².

TABLE XII
COEFFICIENTS OF THE TRANSIENT MODEL FOR AN APPLIED ULTRASOUND
INTENSITY OF 30 MW/CM² AT 22 °C FOR 30 SECONDS

Ultrasound Intensity [mW/cm ²]	Coefficient C (95% Confidence Bounds) [kΩ]	Coefficient τ (95% Confidence Bounds) [sec]	Coefficient T ₀ (95% Confidence Bounds) [°C]
30	8.054 (7.439, 8.669)	328.23	22.11 (22.08, 22.14)

TABLE XIII
GOODNESS OF FIT ANALYSIS FOR AN APPLIED ULTRASOUND INTENSITY OF
30 MW/CM² AT 22 °C FOR 30 SECONDS

Ultrasound Intensity	Sum of Squares	R-Squared Value	Root Mean Squared Error
30 mW/cm ²	0.03612	0.9654	0.03727

According to the residual plot, and the goodness of fit parameters, the model still fits the data when only a small time set of data is measured. The model was next evaluated at different ultrasound intensities. Similar to fitting done for long durations of time, it is expected that the coefficient C will change with respect to ultrasound intensity. Figure 3-9 depicts the calculated C coefficient using the least squares method to fit the curve described in equation (33), to temperature data measured over time at different ultrasound intensities. A constant τ value ($\tau=328.23$) was used, and the ambient temperature T_0 was measured before readings were taken.

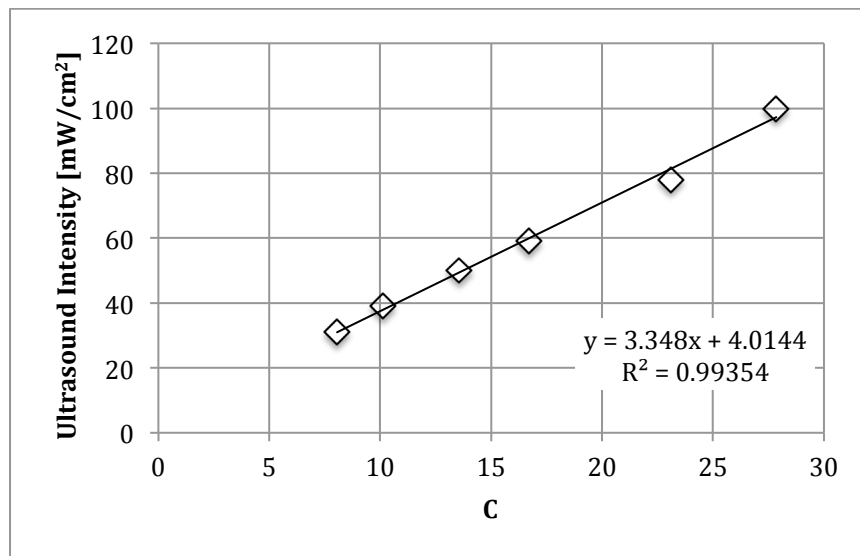


Figure 3-9: Linear relationship between applied ultrasound and the calculated C coefficient. Ambient temperature of 22 °C

The data outlined in figure 3-9 shows that there is a linear relationship between the calculated C coefficient, and the applied ultrasound intensity, as suggested by equation (9), page 23, from [25]. This relationship will be further analyzed and used to evaluate the thermoacoustic sensor's ability to relate applied ultrasound intensity to measure temperature after 30 seconds.

Chapter 4: Thermoacoustic Sensor Evaluation

The evaluation of the transient model showed that there is a relationship between the calculated C coefficients from equation (33), page 57, taken from measured temperature data over time, and the applied ultrasound intensity. This chapter will evaluate the thermoacoustic sensor's operation as a method to measure ultrasound intensity after only 30 seconds of data collection.

4.1. Thermoacoustic Sensor Calibration: Substitution Calibration

A substitution calibration technique was used to find the relationship between the coefficient C calculated by fitting equation (33), page 57, to the temperature vs. time data, and the applied ultrasound intensity. Substitution calibration involves calibrating the ultrasound generator using a known calibration modality, in this case a radiation force balance, and then using the calibrated ultrasound generator to find a relationship between the thermoacoustic sensor and the applied ultrasound.

The ultrasound generator was calibrated using a radiation force balance. Six ultrasound transducers, surface area of 3.5 cm^2 , operated at 1.5 MHz with a 20% duty cycle and a 1 kHz pulse repetition frequency were driven by the SonaCell™ system and initially calibrated to 30, 40, 50, 60, 80, and 100 mW/cm^2 , respectively. The radiation force balance was operated on a level surface away from any sources of vibrations, drafts, or magnetic fields, as advised by the operations manual [44]. Following the directions outlined in the radiation force balance's manual, the tank was filled with degassed water at room temperature and the transducer was placed in the tank so that the radiated face was

approximately 0.5 cm below the water level facing the reflecting cone [44]. To obtain degassed water, distilled water was boiled for 20 minutes; it was then covered and allowed to cool before using. After the balance stabilized, the accuracy was tested using a standardized 1-gram weight. The radiation force balance was then re-zeroed and the ultrasound power was measured. The ultrasound remained on until the reading stabilized, approximately 15 seconds. The output power was displayed in watts, to the thousandth decimal point. To calculate the output intensity (I) in watts per cm-squared, the measured power (P) was divided by the surface area of the transducer ($A_{surface}$).

$$I = \frac{P}{A_{surface}} \quad (43)$$

Three readings were taken and the average was taken as the final ultrasound intensity value. The acoustic calibration results using the radiation force balance to calibrate the SonaCell™ ultrasound generator are outlined in Table XIV.

TABLE XIV
ACOUSTIC CALIBRATION – RADIATION FORCE BALANCE

Transducer	Target [mW/cm ²]	Measurement			Average [mW/cm ²]
		#1 [mW/cm ²]	#2 [mW/cm ²]	#3 [mW/cm ²]	
1	30	29.71	30.29	30.86	30.28
2	40	40.57	40.00	40.57	40.38
3	50	49.14	49.71	48.57	49.14
4	60	58.56	60.00	59.43	59.42
5	80	80	80.57	81.71	80.76
6	100	100.57	100.57	101	100.71

The second component of the substitution calibration procedure was carried out using the designed thermoacoustic sensor. The sensor was coupled directly to the ultrasound transducer using a water based ultrasound gel and ultrasound was applied for 30 seconds. This setup is unique compared to other experimental setups using a thermoacoustic sensor where the sensor and transducer are operated in a degassed water bath.

The calculated coefficients C and the corresponding 95% confidence bounds values for each ultrasound intensity are displayed in Table XV. The applied ultrasound intensity vs. calculated C coefficients plot is shown in figure 4-1. The horizontal error bars signify the interval width of the 95% confidence bounds calculated by the curve fitting process. The largest interval is at the C coefficient calculated at 100 mW/cm^2 , $C_{100} = 27.85 \pm 1.28$; therefore, using this calibration line, with 95% certainty the thermoacoustic sensor can calculate ultrasound intensities within $\pm 7.56 \text{ mW/cm}^2$. Linearity between the applied ultrasound and the C coefficients is observed, R-squared value of 0.99585.

TABLE XV
ACOUSTIC CALIBRATION – THERMOACOUSTIC SENSOR

Ultrasound Intensity	Coefficient C (95% Confidence Bounds)
30.28 mW/cm^2	8.054 (7.439, 8.669)
40.38 mW/cm^2	10.1415 (9.372, 10.912)
49.14 mW/cm^2	13.5733 (12.973, 14.173)
59.42 mW/cm^2	16.699 (15.739, 17.659)
80.76 mW/cm^2	23.1173 (21.957, 24.278)
100.71 mW/cm^2	27.8516 (26.572, 29.132)

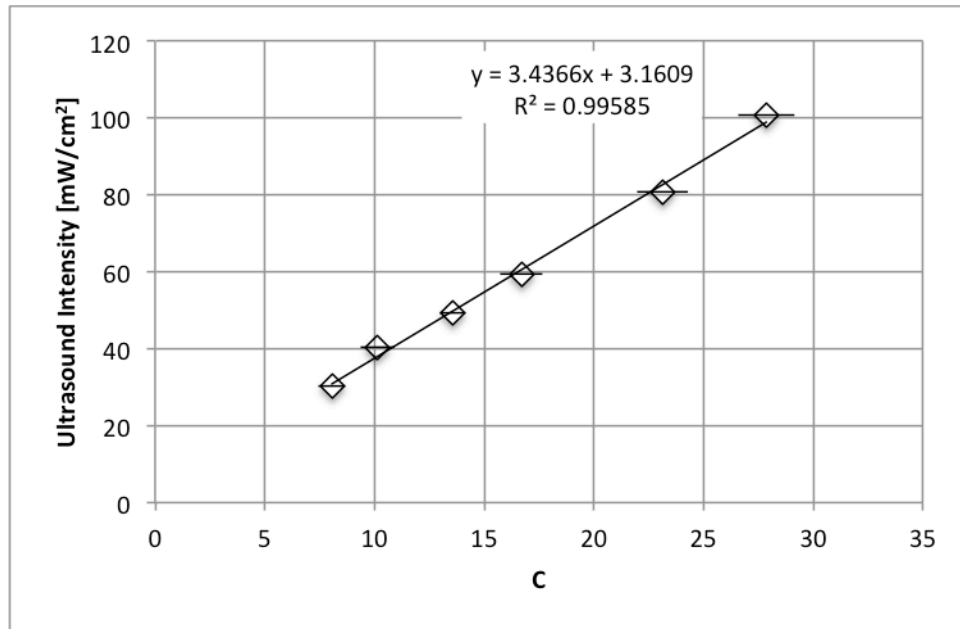


Figure 4-1: Substitution calibration results using a radiated force balance to calibrate the thermoacoustic sensor

The linear relationship between the applied ultrasound intensity (I) and the calculated C coefficient is,

$$I = 3.4366 \times C + 3.1609 \quad (43)$$

After substitution calibration is carried out the sensor is ready to use.

4.2. Thermoacoustic Sensor Evaluation

After calibration, the thermoacoustic sensor's operation was evaluated.

The sensor's ability to measure ultrasound intensity was tested against measurements made using a radiation force balance. The functionality at different starting temperatures was measured, and its response to various duty cycles. Finally, the copper layer was further evaluated compared to a sensor designed with no copper sheet.

The thermoacoustic sensor's functionality was evaluated by comparing readings taken by a calibrated radiation force balance to readings taken using the

calibrated thermoacoustic sensor. Ideally, both measurement techniques will measure similar output intensities. Using equation (43) to relate the ultrasound intensity to the calculated C coefficients determined from the measured temperature increase over time, the performance of the calibrated thermoacoustic sensor was compared to measurements made using a radiation force balance.

Six transducers were calibrated as close to 30, 40, 50, 60, 80, and 100 mW/cm^2 as possible using a radiation force balance. The output intensity of the same transducers was then measured using the thermoacoustic sensor. Between each reading the sensor and the transducer were un-coupled, the gel was cleaned, new gel was reapplied, and the sensor and transducer were re-coupled together. This process simulated a situation similar to a new user taking a fresh reading every time, making it practical evaluation of the thermoacoustic sensor's operation.

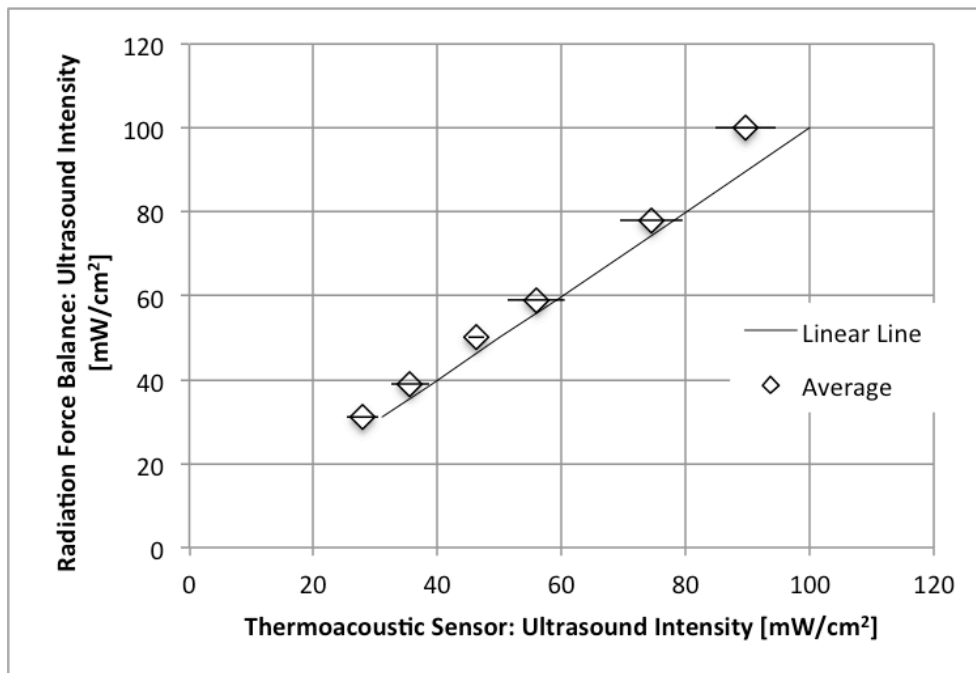


Figure 4-2: Evaluation of the thermoacoustic sensor by comparing measurements made with the thermoacoustic sensor with measurements taken using a radiation force balance. The linear line represents a 1:1 relationship between the Radiation Force Balance and the Thermoacoustic Sensor

Horizontal error bars represent the standard deviation between the three sets of readings taken using the thermoacoustic sensor; a maximum standard deviation of 5.00 mW/cm^2 was calculated. The graph shows a linearity between ultrasound intensity readings taken using a radiation force balance and measurements taken using the thermoacoustic sensor, linear regression of 0.99157.

TABLE XVI
THERMOACOUSTIC SENSOR MEASUREMENTS AT 22 °C

	Target [mW/cm ²]	Measurements			Average [mW/cm ²]
		#1 [mW/cm ²]	#2 [mW/cm ²]	#3 [mW/cm ²]	
1	30.28	25.42	30.41	27.96	27.93
2	40.38	35.39	38.80	32.53	35.57
3	49.14	45.99	47.65	45.05	46.23
4	59.42	53.23	61.19	53.36	55.93
5	80.76	71.39	80.24	71.78	74.47
6	100.71	87.07	95.29	86.54	89.63

TABLE XVII
COMPARISON BETWEEN MEASUREMENTS MADE USING A RADIATION FORCE
BALANCE AND MEASUREMENTS MADE USING A THERMOACOUSTIC SENSOR

	Radiation Force Balance	Thermoacoustic Sensor	Error
1	30.28 mW/cm ²	27.93 mW/cm ²	7.76%
2	40.38 mW/cm ²	35.57 mW/cm ²	11.90%
3	49.14 mW/cm ²	46.23 mW/cm ²	5.92%
4	59.42 mW/cm ²	55.93 mW/cm ²	5.88%
5	80.76 mW/cm ²	74.47 mW/cm ²	7.79%
6	100.71 mW/cm ²	89.63 mW/cm ²	11.00%

Table XVI outlines the measurements taken using the thermoacoustic sensor.

Table XVII compares the two modalities. Evaluated against the radiation force balance, the thermoacoustic sensor had an output with an average error of 8.38% across 18 measurements. Tests were taken in such a way to emulate the practical

operation of the sensor, as it would be used in a laboratory setting. The SonaCell™ system is capable of outputting six different ultrasound intensities at once. At the time this research was done, the SonaCell™ driver boards could reliably output ultrasound up to 100 mW/cm². At higher intensities, components on the driver board began to heat up. The radiation force balance used can dependably measure ultrasound readings above 30 mW/cm². At lower intensities, the background vibrations and noise prevented the device from taking a stable reading. With these two constraints in mind, the thermoacoustic sensor was evaluated between 30 mW/cm² and 100 mW/cm². Possible sources of error include the positioning of the sensor and transducer, error in the fitting model, and the error in the substitution calibration, which will be discussed in the *Thermoacoustic Sensor Error* section of the thesis.

4.2.1. *The Influence of Ambient Temperature*

The thermoacoustic sensor's operation relies on measuring the temperature produced by absorbed ultrasound waves. The influence of various ambient temperatures was measured to determine if the sensor functioned differently at different temperatures. Ultrasound, 80 mW/cm², was measured by the thermoacoustic sensor for 30 seconds at ambient temperatures between 22 °C and 26 °C by placing the sensor in a temperature controlled incubator. Table XVIII outlines the calculated *C* value at different ambient temperatures for the same ultrasound intensity.

TABLE XVIII
CALCULATED C COEFFICIENTS WITH REGARDS TO AMBIENT TEMPERATURE

	22 °C	23 °C	24 °C	25 °C	26 °C
C Value	23.1173	20.3324	18.9962	17.1521	16.5027

For the same ultrasound intensity, the standard deviation between the C values for the different starting temperatures is 2.652 units. The substitution calibration technique used to calibrate the thermoacoustic sensor requires that there is a direct correlation between measured C coefficient values and ultrasound intensity. The difference between the C values at various starting temperatures indicates that the thermoacoustic sensor should be calibrated at different starting temperatures. The final version of the thermoacoustic sensor was calibrated using substitution calibration methods at ten different temperatures, 22 °C to 26.5 °C, as shown in figure 4-3.

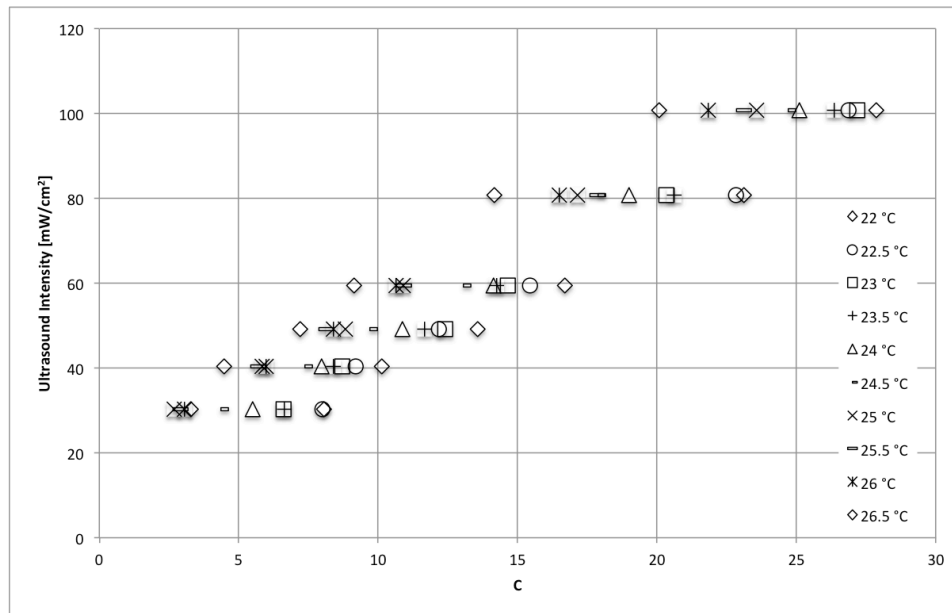


Figure 4-3: Ultrasound Intensity vs. C coefficients calculated from data collected at different ambient temperatures. A clear difference between C values for the same ultrasound intensities can be seen.

The calibration line denoting the relationship between the ultrasound intensity (I) and the calculated C value at each ambient temperature is displayed in Table XIX.

TABLE XIX
CALIBRATION LINE FOR THE RELATIONSHIP BETWEEN ULTRASOUND INTENSITY
AND C VALUES AT AMBIENT TEMPERATURES BETWEEN 22 °C AND 26.5 °C

Ambient Temperature	Calibration Line	R-Squared Value
22 °C	$I = 3.4366 * C + 3.1609$	$R^2 = 0.99585$
22.5 °C	$I = 3.4407 * C + 5.9461$	$R^2 = 0.98865$
23 °C	$I = 3.3552 * C + 9.2404$	$R^2 = 0.99934$
23.5 °C	$I = 3.4013 * C + 9.6891$	$R^2 = 0.99791$
24 °C	$I = 3.5181 * C + 11.077$	$R^2 = 0.99865$
24.5 °C	$I = 3.444 * C + 15.236$	$R^2 = 0.9976$
25 °C	$I = 3.3463 * C + 21.035$	$R^2 = 0.99813$
25.5 °C	$I = 3.3434 * C + 21.232$	$R^2 = 0.99509$
26 °C	$I = 3.6864 * C + 18.691$	$R^2 = 0.99749$
26.5 °C	$I = 4.0335 * C + 20.296$	$R^2 = 0.99618$

TABLE XX
ERROR BETWEEN THERMOACOUSTIC SENSOR MEASUREMENTS AND RADIATION
FORCE BALANCE MEASUREMENTS AT VARIOUS AMBIENT TEMPERATURES

Ambient Temperature	Error
22 °C	7.83%
22.5 °C	7.00%
23 °C	4.44%
23.5 °C	8.25%
24 °C	5.68%
24.5 °C	4.90%
25 °C	4.23%
25.5 °C	8.14%
26 °C	6.70%
26.5 °C	11.65%

After the thermoacoustic sensor was calibrated at each ambient temperature, it was evaluated. 180 readings were taken: 3 readings at 6 ultrasound intensities, for 10 different ambient temperatures. The results compared to readings taken with a radiation force balance are shown in Table XX. Across 180 readings, the

thermoacoustic sensor measured ultrasound intensity with an average error of 6.88% of the target value, and a maximum standard deviation of 5.13 mW/cm².

4.2.2. Thermoacoustic Sensor Evaluation: Response to Duty Cycle

The ultrasound duty cycle is the fraction of time a pulsed ultrasound signal is on during one period, a continuous ultrasound signal has a duty cycle of 100%. The SonaCell™ ultrasound generator typically runs at a 20% duty cycle, with a period of 1 ms; therefore, the signal is on for 200 μs and off for 800 μs. The ultrasound intensity is proportional to the duty cycle, an ultrasound beam with a 40% duty cycle should have double the ultrasound intensity compared to one emitted with a 20% duty cycle. The response of the thermoacoustic sensor to various duty cycles was analyzed. Nine different duty cycles, 10% - 90% with a 10% increment, were measured using the thermoacoustic sensor. The same output parameters were measured using the radiation force balance and the results were compared.

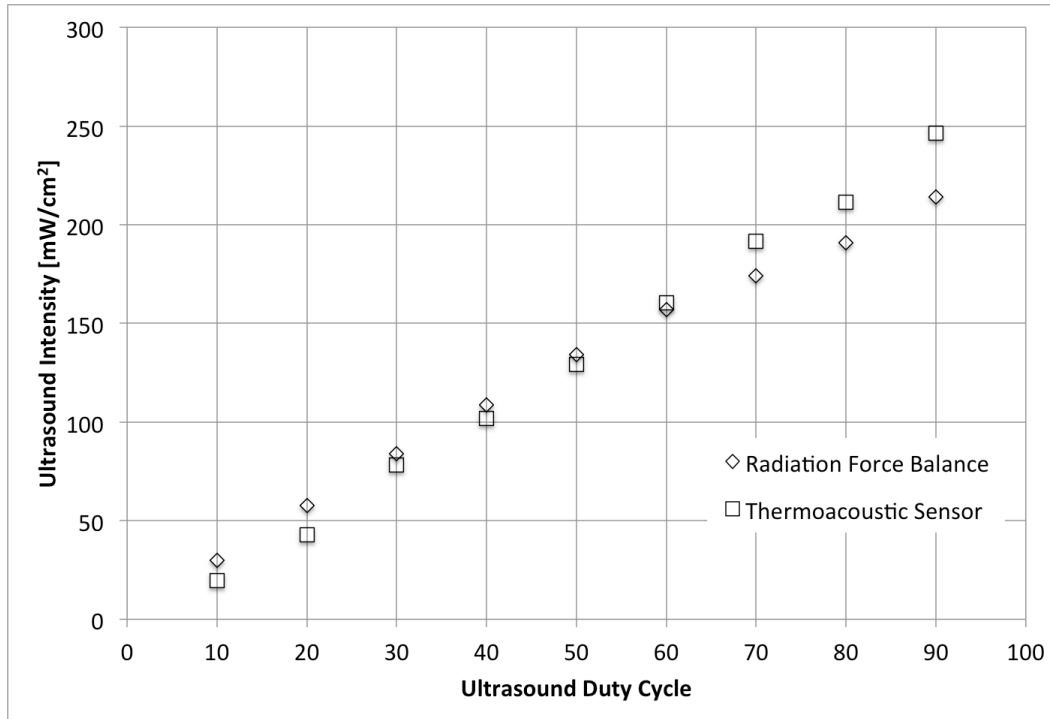


Figure 4-4: Influence of duty cycle on thermoacoustic sensor measurements

Figure 4-4 shows the output intensity of an ultrasound transducer measured using the radiation force balance and a thermoacoustic sensor at various duty cycles. As expected, the thermoacoustic sensor's calculated ultrasound intensity increased proportional to the increased duty cycle, a trend mirrored by the radiation force balance.

4.2.3. *Assessment of a Copper Backed Sensor vs. a Sensor with No Copper Backing*

In order to distribute the heat more quickly along the back face of the sensor, a thin copper sheet, 0.30 mm thick, was attached to the plexiglass material using a thermal paste. The role of the copper sheet is to uniformly distribute the heat across the entire back face. The operation of the thermoacoustic sensor is dependent on the temperature readings taken at the back face of the sensor over a certain duration of time. In this design, the temperature measured at one location

is assumed to be the average temperature across the back face. Ideally, the entire back face's temperature would rise simultaneously. If there were not a uniform change in temperature, the goal would be to quickly distribute the heat from one location across the entire surface. Discrepancy between readings will arise if the ultrasound energy heats an area away from the thermistor on a material with low thermal diffusivity.

The transducer was placed in five different locations on the sensor, on four of the sensor's edges, and on the center of the sensor, and readings were taken, figure 4-5. Three readings were taken in each position when ultrasound was applied at 30 mW/cm^2 at an ambient temperature of $22 \text{ }^\circ\text{C}$, the coefficient C was recorded. The standard deviation was calculated to evaluate the effect of positioning on sensor readings. The objective is to measure the influence of transducer – sensor orientation on the operation of the thermoacoustic sensor and determine if the added copper layer reduces the variation caused by the different orientations.

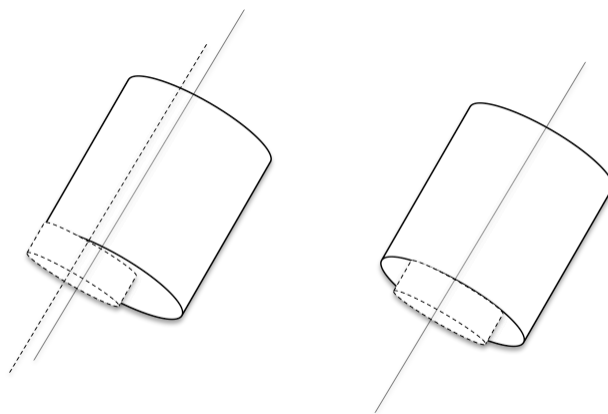


Figure 4-5: Orientation of the transducer (dotted line) and the thermoacoustic sensor (solid line). To evaluate the influence of orientation, the sensor was placed on four of the sensor's edges (left), and in the middle of the sensor (right) and readings were taken.

TABLE XXI
THE IMPACT OF SENSOR – TRANSDUCER ORIENTATION ON THERMOACOUSTIC
SENSOR OPERATION

Copper Backed	Bottom	Left	Middle	Right	Top	STDEV
Set 1	8.2495	8.3120	8.2963	8.1870	8.4057	0.0812
Set 2	8.4760	8.4525	8.6087	8.4603	8.5931	0.0765
Set 3	8.6009	8.6946	8.8196	8.7181	8.5931	0.0929
Avg						0.0836
No Copper	Bottom	Left	Middle	Right	Top	STDEV
Set 1	7.9371	7.9605	8.0308	8.3041	8.7337	0.3358
Set 2	8.7337	8.9914	8.7259	9.0695	8.7337	0.1663
Set 3	9.3663	9.4756	9.4366	9.4444	9.6318	0.0984
Avg						0.2002

Changing the orientation between the sensor and the transducer yielded standard deviations that accounted for less than 1% of the measured C coefficients for the copper backed sensor, and 2.34% for the sensor without the copper layer. The substitution calibration methods that have to be used to calibrate the thermoacoustic sensor require that variations between readings be minimized. A large amount of standard deviation will result in a large amount of error. As seen in Table XXI, the average standard deviation of the copper backed sensor is 58.2% less than the average standard deviation of the sensor with no copper back. This is due to the higher thermal diffusivity of the copper compared to the plexiglass material allowing the temperature to dissipate across the back face more evenly.

The results shown in figure 4-6 clearly show why the sensor without the copper back will not yield accurate results. At the same starting temperature, the calculated C coefficients must be close to the same value every reading. This is especially important because substitution calibration methods are used. Once the sensor is calibrated, the same C coefficient that correlates to a specific ultrasound

intensity should be outputted every time that ultrasound intensity is applied. Conversely, the results shown in figure 4-7 show that the sensor with the copper backing can output much more consistent results. In order to implement an algorithm that requires measurements to be made using the average temperature across the absorbers back face, one or more of the following must be taken into consideration, the ultrasound beam radius must be equal to 100% of the absorber radius, multiple sensors must be implemented, or a high conductivity surface must be used to rapidly distribute heat across the back face [25].

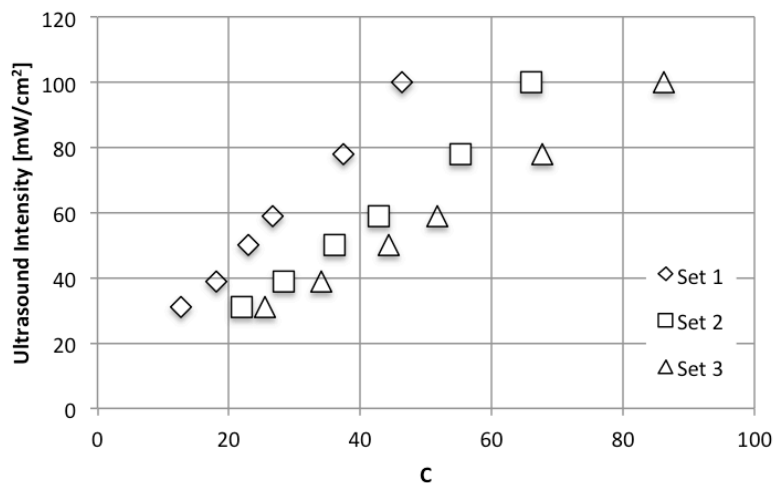


Figure 4-6: Ultrasound Intensity vs. C values using a sensor with no copper back. 3 sets of readings are taken and compared.

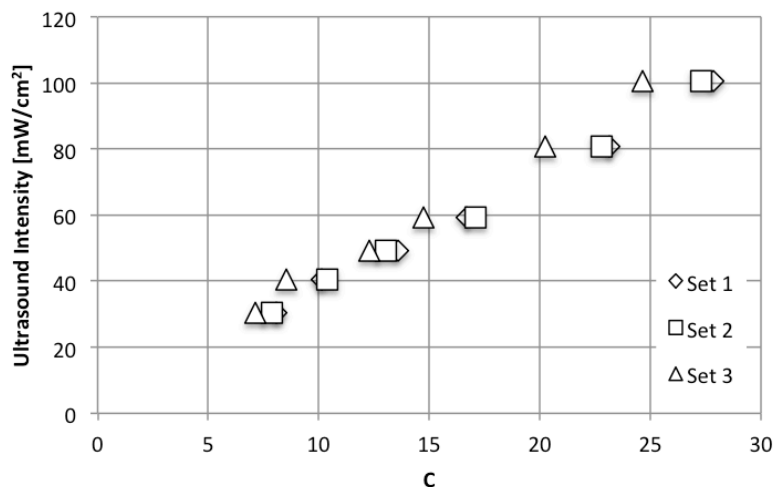


Figure 4-7: Ultrasound Intensity vs. C values using a sensor with a copper back. 3 sets of readings are taken and compared.

4.2.4. Evaluation of Number of Data Points Required For Accurate Readings

After the thermoacoustic sensor was calibrated, the number of data points that the sensor needed during a reading to get an accurate reading was evaluated. The sensor was calibrated at 30 seconds; figure 4-5 shows that when an ultrasound intensity of 30 mW/cm^2 is applied to the sensor, the error between the target value and the thermoacoustic sensor decreases as more data points are used for the curve fitting process. After 15 data points were measured, the error between the target value and the ultrasound intensity calculated by the thermoacoustic sensor dropped below 10%, and after 18 data points the error dropped below 5% and remained below 5%. Therefore, the designed thermoacoustic sensor must have at least 15 temperature readings in order to have enough data for the least squares fitting method to accurately calculate the C coefficient corresponding to the target ultrasound intensity.

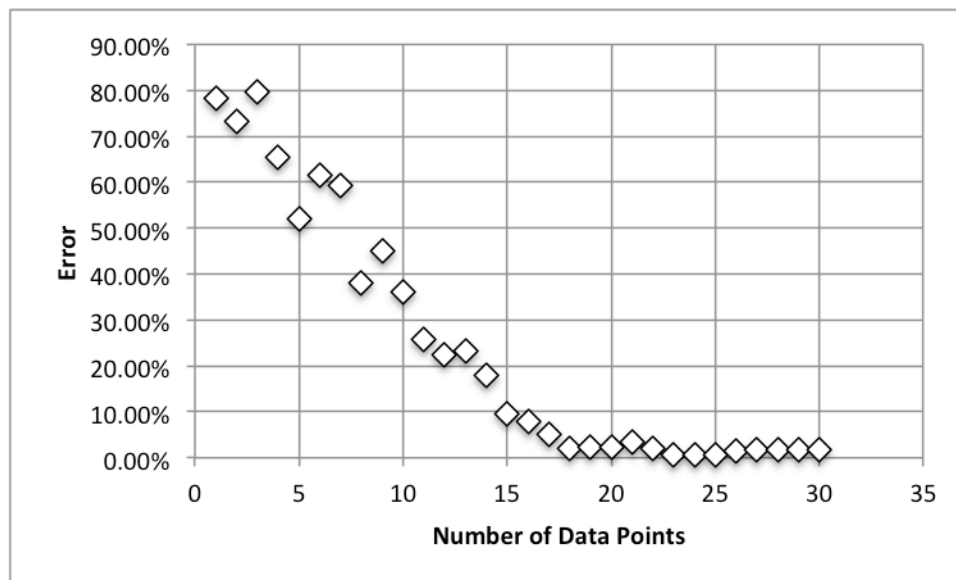


Figure 4-8: The number of data points needed to take an accurate reading using the thermoacoustic sensor. After 15 data points the error between the calculated ultrasound intensity and the target ultrasound intensity falls below 10%.

4.2.5. *Thermoacoustic Sensor Error*

A sensor's error and consistency are two main barriers that must be overcome for it to be a useful and practical tool. When directly compared to the radiation force balance, the average error for the thermoacoustic sensor readings was 8.38% across six different ultrasound intensities measured three times each. When the copper backed sensor was being evaluated at different starting temperatures, the recorded average error was 6.88% across six different ultrasound intensities, measured three times each, at ten different starting temperatures, a total of 180 readings. This error can be contributed to a few factors.

A source of error stems from inaccuracy during the thermistor calibration. Linearity was observed between the change in resistance and the change in temperature, with an R^2 value of 0.98957. Ideally, the change in resistance would be directly proportional to the change in temperature with an R^2 value of 1. One way to reduce calibration error would be to implement a method that measures the change in temperature on back face where the thermistor is located, instead of correlating the change in water temperature to the change in resistance. This would eliminate the error caused by the time needed for the heat to diffuse down the absorber to the thermistor.

The position of the sensor on the transducer is another source of error. Even with the copper layer, there was a 1 – 2% observed difference in readings when the sensor was placed in different orientations compared to the transducer. Implementing a standardization system that aligns the sensor with the transducer

could minimize this error. This would ensure that the ultrasound's focal point is always striking the same place in the sensor.

The transient model chosen to relate measured temperature vs. time data was developed for a system placed in a water bath where the heat from the transducer is not a concern, and part of the heat produced in the absorber is emitted into the water. We showed that the τ value measured experimentally is not equal to the τ proposed in [25] for the developed model. While the model used was able to meet the design goals of the project, this is another source of error for our system. Developing a transient model that factors in the heating process contributed by the transducer would decrease the standard deviation between of the calculated coefficients, and decrease the error of the sensor.

The reflections of the incident ultrasound wave back towards the transducer may contribute to the sensor's error. Standing waves inside the thermoacoustic sensor, or interference with incident waves striking the transducer would contribute to inconsistencies between readings. Improving the physical design of the sensor to minimize the difference in acoustic impedance between the sensor and the transducer, as well as designing the sensor out of a material with a higher acoustic absorbance to minimize the percent of ultrasound waves reflected within the sensor and transmitted back towards the transducer would reduce the sensor's error.

Another source of error can be contributed to the inconsistencies seen in the ultrasound transducers. Due to the manufacturing process, different transducers will have slightly different properties. This may lead to one

transducer producing more heat, which would affect the calibrated sensor. Additionally, if an ultrasound transducer were used that was made from another material, the thermoacoustic sensor would have to be re-calibrated to accommodate for the heating properties of the new transducer. The analysis done in this thesis is based solely on the ultrasound transducers used by the SonaCell™ system.

Finally, like any electrical system, noise will contribute to the thermoacoustic sensor's error. Electrical noise on the ADC input pin will affect the microcontroller's readings. This is mediated using filtering caps and oversampling methods. The overall error of the thermoacoustic sensor will always be linked to the measurement technique chosen during the substitution calibration process, in this case a radiation force balance. Standard radiation force balances measuring low MHz frequency ranges and power ranges in the area of 100 mW are able to take measurements with uncertainties in the range of $\pm 7\%$ [20].

Chapter 5: Implementing the Thermoacoustic Sensor in an Embedded System

After the transient model was validated, the thermoacoustic sensor was implemented in an embedded system. Making the sensor a stand alone device required programming the least squares model into the ATmega324P microcontroller so that the curve fitting process could be carried out in real time, implementing a real time clock, and programming in communication between the thermoacoustic sensor and the SonaCell™ system's LCD screen.

5.1. Programming the Least Squares Model

The iterative least squares algorithm was programmed into an ATmega324P microcontroller to fit measured temperature vs. time data to the curve represented by equation (33), page 57.

$$T_{ave}(t) = C \left(1 - e^{-\frac{t}{\tau}} \right) + T_0$$

This process takes a temperature measurement (T) every second (t), and calculates the residual (R^2) value using the initial conditions provided for the coefficients C . If the R^2 value is greater than a certain value, in this case 0.00001, the coefficients are incremented. After each coefficient is incremented, the R^2 value is calculated again, if the new R^2 value is less than the previous R^2 value the coefficient will continue to be incremented; however, if the new R^2 value is greater than the previous R^2 value, the coefficient will be decremented during the next cycle. This process is repeated until the R^2 value of the entire equation is less than 0.00001. The least squares algorithm flow chart is depicted in figure 5-1, and the code programmed into the ATmega324P microcontroller is shown in Appendix A.

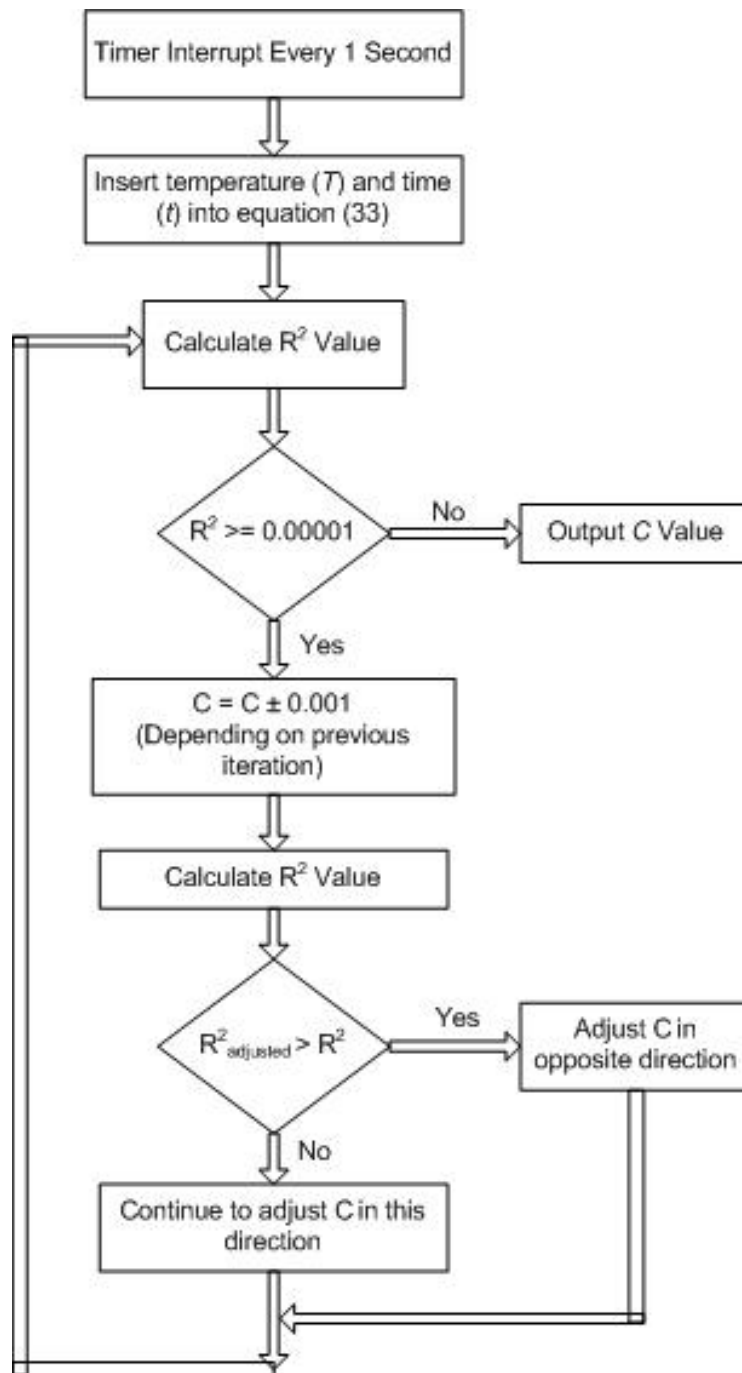


Figure 5-1: Least squares algorithm flow chart

The least squares algorithm requires a limiting R^2 . The R^2 value, or the residual, is the squared difference between the measured value and the value calculated by the model, and determines how close the model needs to fit to the measured data. When choosing an R^2 value there is a trade off between accuracy and computation time, if the R^2 is decreased, the computation time will increase, and the accuracy will increase. Conversely, if the R^2 is increased, the allowed error between the model and the actual measured data is increased and the time required to find the correct coefficients will decrease. The least squares algorithm also requires a coefficient step value. The coefficient step value refers to the amount each coefficient will be increased or decreased each iteration as the least squares program attempts to fit the model to the measured data. A large step value will allow the algorithm to move through a wide range of values; however, if the step value is too big the optimal value may never be achieved. An R^2 value of 0.00001 and step value of 0.001 were experimentally determined.

5.2. The Real Time Clock

A real time clock (RTC) is implemented in the thermoacoustic sensor design in order to take accurate measurements every second. In order to do this, the microcontroller's asynchronous timer, coupled with a 32.768 kHz crystal is used. 32.768 kHz crystals are cheap oscillators that are used in most watches. The value is divisible by 2^{15} , meaning 15 divisions will yield a 1 Hz output, enabling real time keeping with minimal processing. Implementing a real time clock using the ATmega324P's asynchronous timer is a low power, low cost solution. The external crystal clocks the timer by utilizing the microcontroller's

asynchronous Timer Overflow Interrupt routine. The advantages of implementing an RTC in software compared to using an external hardware real time clock are, it is cheaper, requires fewer components, consumes less power, and offers more flexibility [45].

The ATmega324P's RTC utilizes the asynchronous operation of the RTC module. The 32.768 kHz crystal is placed between the two timer oscillator pins (TOSC1 and TOSC2), and a Timer Overflow Interrupt routine is programmed. The amount of time for the Timer/Counter to complete one overflow is always the same; therefore, this interrupt can be used to accurately monitor one-second intervals. The accuracy of this method is connected to the accuracy of the crystal. The asynchronous operation will allow the timer to run without any delays, even when the CPU is under heavy computations. A small negligible discrepancy will occur when the timer variables have to update because this process cannot be carried out in parallel with other processes. The code used to implement the RTC is shown in Appendix A.

5.3. Communication with the SonaCell™ Ultrasound System

Communication with the SonaCell™ system is carried out through a RS-485 bus connected to the microcontroller's universal asynchronous receiver/transmitter (USART) ports. The ATmega324P's USART port was initialized to transmit and receive at a 9600 baud rate. The receiver interrupt was enabled so that operations could be triggered when the sensor received instructions from other microcontrollers in the SonaCell™ system. To remain consistent with the rest of the system, operation was done asynchronously using

8-bit character sizes. The code used to initialize and operate the ATmega324P's USART ports is presented in Appendix A.

The communication flow chart is outlined in the figure 5-2, where the solid line symbolizes operations carried out on the SonaCell™ control printed circuit board, the dashed line equates to functionality done by the thermoacoustic sensor microcontroller, and dotted line refers to the ultrasound generating circuit board.

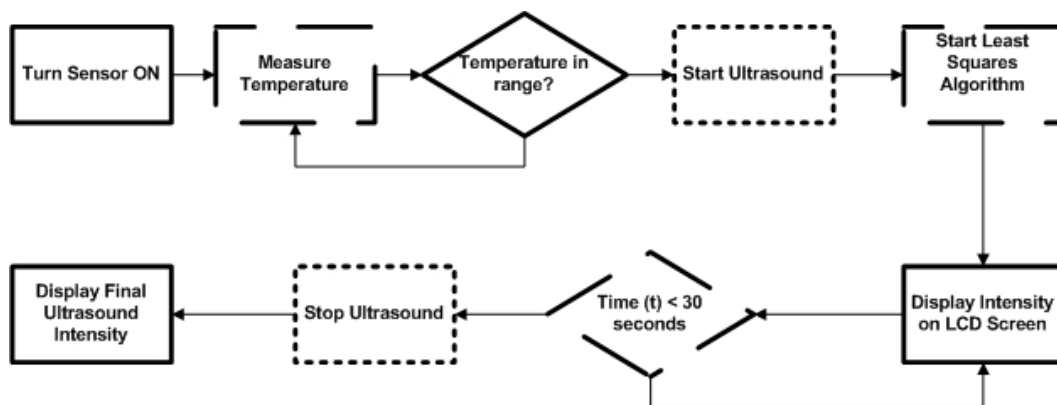


Figure 5-2: Communication flow chart between thermoacoustic sensor and SonaCell™ system. Solid line: operations carried out on the SonaCell™ control board. Dashed line: operations carried out by the thermoacoustic sensor board. Dotted line: Operation carried out on the ultrasound generating board

Chapter 6: Future Studies

The work reported in this thesis describes a functional prototype of a close-proximity thermoacoustic sensor. I have demonstrated that a thermoacoustic sensor method can be used in a close-proximity setup with an embedded system microcontroller design to measure ultrasound intensity in real time. Future study of the thermoacoustic sensor includes improving the physical design of the sensor, investigating the application of the sensor in a biological system, and further integrating the thermoacoustic sensor with the SonaCell™ system.

Physical Design

Further investigation and improvements can be made to the physical design of the sensor. The length of the absorber and the materials used can be optimized to the transducers used by the SonaCell™. Evaluations of the equilibrium model have shown that the dimensions of the absorber length influences the time for the sensor to reach equilibrium [28]; therefore, a similar study can be done to determine the influence of the absorber length on the transient model. Completely absorbing the incident wave inside the absorber may prevent the development of standing waves, and minimize the waves transmitted out of the sensor back towards the transducer. After the fundamental components are optimized, the next stage would involve taking the sensor from a developmental product to a more polished instrument. The overall design could be less bulky. The hollow cylinder's volume can be reduced; the sensor does not need such a large volume of air to thermally isolate the temperature sensing area.

Additionally, a better connector between the sensor and the SonaCell™ can be chosen.

Application of Sensor in Biological Systems

Further study can be done using the thermoacoustic sensor in cross-discipline experiments. One of the initial applications for the thermoacoustic sensor was to implement it in a biological system growing fungi for work done for the biofuel industry. A thermoacoustic sensor is much cheaper and more rugged than a hydrophone and easier to sterilize without damaging the active components [21]. Therefore, the thermoacoustic sensor can be implemented in various biological systems to measure the ultrasound intensity applied into the system. This can yield scores of useful information, including how well the transducer is coupled to the system and how much ultrasound is transmitted through the gel – material boundary. The sensor can measure if the ultrasound is propagating throughout the whole system, and what the distribution of the ultrasound intensity in the system is, for example where the near field is, where the far field is, and if there is a focal point where ultrasound intensity is significantly higher than other areas. Finally, the sensor could be used to measure the correlation between the growth of microorganisms and attenuated or absorbed ultrasound.

Integration with the SonaCell™ System

The thermoacoustic sensor has been partially integrated into the SonaCell™ system. It plugs into the system's motherboard, is powered by the same supply, controlled by the system's controller board and can display results onto the SonaCell's™ LCD screen. However, further integration can be done to

enhance the SonaCell's™ overall function. A working prototype of a completely digital SonaCell™ system has been designed and tested. In this system, the analog potentiometer that controlled a voltage regulator that determined the output intensity of the ultrasound transducer was replaced with a digital to analog converter, an op-amp to amplify the voltage, and a BJT to amplify the current. This digital set up allows the possibility for the sensor to implement feedback loops to the SonaCell™ system. There are two applications where sensor to ultrasound feedback can be useful. If the sensor is implemented in a system that ultrasound is applied to, the sensor can measure the applied ultrasound intensity and communicate with the generator to increase or decrease the applied ultrasound intensity. Or warn the user if there is an abnormal ultrasound reading. The second application is auto-calibration. An accurate sensor system with feedback capabilities can be used to auto-calibrate the ultrasound generator.

Additional Sensor Functionality

The sensor's functionality can be improved upon to make it a more versatile instrument. At the time of development, the thermoacoustic sensor could take readings as high as 100 mW/cm^2 , which corresponded to the maximum output intensity the SonaCell™ device could output. Additional characterization should be carried out at high intensities to ensure the relationship remains linear. The operation of the thermoacoustic sensor with different ultrasound transducers could also be explored. The thermoacoustic sensor designed was calibrated specifically for the transducers used by the SonaCell™ ultrasound generator. A transducer made out of a different material would generate a different amount of

heat; therefore, a set of substitution calibrations using the new transducer would have to be done before using the sensor with this transducer. Over time, ultrasound transducer efficiency can degrade and its heating rates may change, effecting the calibration of our proposed method. Further studies are needed to quantify this. In terms of additional functionality, one group I am working with is implementing a wireless communication between the sensor and the SonaCell™ box. Corresponding XBee wireless modules are being prototyped on the sensor's PCB board and in the SonaCell™ system.

Chapter 7: Conclusion

A close-proximity, real time thermoacoustic sensor was designed and implemented in the SonaCellTM ultrasound generator. In a close-proximity setup, a copper backed plexiglass absorber was used to convert ultrasound energy into heat. A least squares algorithm fit the measured change in temperature to an equation that represented the relationship between the applied ultrasound intensity to the averaged temperature rise at the back of the absorber. The calculated C coefficient is the only variable dependent on the applied ultrasound intensity. Using substitution calibration techniques with a radiation force balance, a linear relationship was found between C and the applied ultrasound. An embedded system was designed to integrate the sensor into the ultrasound generator and full communication between the sensor and the ultrasound generator's control board was implemented. The final prototype was able to measure absorbed ultrasound and display the calculated intensity in real time on the SonaCell'sTM LCD screen.

Compared to thermoacoustic sensor design outlined in literature, and submitted as patents, the design implemented in this thesis has several novel components. The implementation of a thin metal layer to increase the heat conduction at the back of the absorber and reduce the dependence of the ultrasound transducer's focal point was evaluated for the first time. The results show that the copper layer can increase the heat diffusion 1000 fold compared to plexiglass alone. No other sensor described in literature used the sensor in contact with the ultrasound transducer. The heat generated by the transducer complicates the relationship between the absorbed ultrasound and the measured temperature

change. However, this setup is more convenient than previously demonstrated setups that require the sensor and transducer be placed in a water bath. Finally, an embedded system design utilizing a microcontroller running a least squares algorithm was implemented to process the data in real time. An extensive patent search was conducted with the University of Alberta's patent librarian. The United States Patent Database and the International Database were examined. Various ultrasound power sensor patents were uncovered, but during this study no patents using the close-proximity thermoacoustic techniques described in this thesis were found.

Analysis of the transient model used was carried out using the MATLAB curve fitting toolbox. The model was fit to measured data and 95% certainty prediction bounds, residual plots, and goodness of fit parameters were collected. The residual plots were centered around 0 and randomly distributed, showing that the model fit the data well for each ultrasound intensity measured. This was verified by the sum of squares, R-squared, and root mean squared error values that were calculated.

Full characterization of the thermoacoustic sensor was carried out. Thermistor calibration related the change in the thermistor's resistance to the change in temperature, with a linear regression coefficient of 0.98957, and a maximum standard deviation 0.6% across three sets of readings. Substitution calibration was carried out using a radiation force balance to relate the calculated C coefficients with the applied ultrasound intensity. A linear relationship was observed between the C coefficient and the ultrasound intensity, with a linear

regression coefficient of 0.99585 and a 95% certainty of calculating ultrasound intensities within $\pm 7.56 \text{ mW/cm}^2$. The thermoacoustic sensor was evaluated by comparing measurements taken with the sensor with measurements taken with the radiation force balance. Over 18 readings, the average error between the values calculated by the thermoacoustic sensor and the ultrasound intensities measured using the radiation force balance was 8.38%. Across three sets of readings, the thermoacoustic sensor had a maximum standard deviation of 5.00 mW/cm^2 . The influence of the sensor's starting temperature on its operation was examined. As the starting temperature increased, the slope of the linear line fitted to the first 30 seconds of collected temperature vs. time data decreased. The final version of the sensor was calibrated for a wide range of starting temperatures. The sensor had an error of 6.88% after 180 measurements spanning 10 different temperatures. The sensor's response to changes in ultrasound duty cycle was examined. The measured ultrasound intensity increased proportionally with the increase in duty cycle. The same trend was seen using a radiation force balance.

A thermoacoustic sensor will not replace the industry standards for ultrasound calibration; however, the design goals of the project were met and from these results it can be concluded that a close-proximity, real time thermoacoustic sensor can provide a convenient way to quickly verify ultrasound intensity output without any complicated setup procedures.

References

- [1] Cheeke, J. D. N. : Fundamentals and applications of ultrasonic waves. Boca Raton: CRC Press.
- [2] Ensminger, D. (Ed.). (1988). Ultrasonics: Fundamentals, technology, applications (Second ed.) M. Dekker.
- [3] NDT Resource Center. (2011). Piezoelectric transducers. Retrieved 11/10, 2011, from <http://www.ndt-ed.org/EducationResources/CommunityCollege/Ultrasonics/EquipmentTrans/piezotransducers.htm>
- [4] Magnetostrictive Versus Piezoelectric Transducers For Power Ultrasonic Applications, Blackstone~NEY Ultrasonics, Inc., Jamestown, NY.
- [5] Ensminger, D. (Ed.). (2009). Ultrasonics: Data, equations, and their practical uses. CRC Press.
- [6] NDT Resource Center. (2011). Reflection and Transmission Coefficients (Pressure). Retrieved 11/10, 2011, from <http://www.ndt-ed.org/EducationResources/CommunityCollege/Ultrasonics/Physics/reflectiontransmission.htm>
- [7] P. Sprawls, The Physical Principles of Medical Imaging, 2nd ed., Madison, Wisconsin: Medical Physics Publishing, 2000.
- [8] Khanna, A., Nelmes, R. T., Gougoulas, N., Maffulli, N., & Gray, J. (2009). The effects of LIPUS on soft-tissue healing: A review of literature. *British Medical Bulletin*, 89, 169-182.
- [9] Fay, B., & Rinker, M. (1996). The thermoacoustic effect and its use in ultrasonic power determination. *Ultrasonics*, 34(2-5), 563-566.
- [10] Webster, D. F., Harvey, W., Dyson, M., & Pond, J. B. (1980). The role of ultrasound-induced cavitation in the 'in vitro' stimulation of collagen synthesis in human fibroblasts. *Ultrasonics*, 18(1), 33-37.
- [11] Marvel, S., Okrasinski, S., Bernacki, S. H., Loba, E., & Dayton, P. A. (2010). The development and validation of a LIPUS system with preliminary observations of ultrasonic effects on human adult stem cells. *IEEE Transactions on Ultrasonics, Ferroelectrics, and Frequency Control*, 57(9), 1977-1984.
- [12] Hilal Gul, Peng Xu, Woon T. Ang, Min Huang, Xiaoyan Yang, James Xing and Jie Chen, Ultrasound treatment enhances proliferation of hematopoietic stem/progenitor cells: implication for clinical transplantation, gene and cellular therapies, annual conference of International Society for Cellular Therapy, Philadelphia, PA, May 25, 2010
- [13] Doan, N., Reher, P., Meghji, S., & Harris, M. (1999). In vitro effects of therapeutic ultrasound on cell proliferation, protein synthesis, and cytokine production by human fibroblasts, osteoblasts, and monocytes. *Journal of Oral and Maxillofacial Surgery : Official Journal of the American Association of Oral and Maxillofacial Surgeons*, 57(4), 409-19; discussion 420.
- [14] Sinisterra, J. V. (1992). Application of ultrasound to biotechnology: An overview. *Ultrasonics*, 30(3), 180-185.

- [15] Yang, K. H., Parvizi, J., Wang, S. J., Lewallen, D. G., Kinnick, R. R., Greenleaf, J. F., et al. (1996). Exposure to low-intensity ultrasound increases aggrecan gene expression in a rat femur fracture model. *Journal of Orthopaedic Research : Official Publication of the Orthopaedic Research Society*, 14(5), 802-809.
- [16] Gene therapy progress and prospects: Ultrasound for gene transfer Revised and Expanded, Marcel Dekker, Inc., pp4
- [17] P. E. Huber, P. Pfisterer, In vitro and in vivo transfection of plasmid DNA in the Dunning prostate tumor R3327-AT1 is enhanced by focused ultrasound. *Gene Ther* 2000;7:1516 – 1525.
- [18] Shaw, A., & Hodnett, M. (2008). Calibration and measurement issues for therapeutic ultrasound. *Ultrasonics*, 48(4), 234-252.
- [19] S.D. Pye, C. Milford, The performance of ultrasound therapy machines in Lothian region, 1992, *Ultrasound Med. Biol.* 20 (4). (1994) 347–359.
- [20] Ultrasonic Exposimetry (Ziskin, M. and Lewin, P., eds), p. 35, CRC Press., 1993.
- [21] Onda Corporation. (1999). Theory of operation of hydrophones. Retrieved 10/01, 2011, from http://www.ondacorp.com/tecref_tutorialhydrophone_theory.shtml
- [22] Zeqiri, B., Zauhar, G., Hodnett, M., & Barrie, J. (2011). Progress in developing a thermal method for measuring the output power of medical ultrasound transducers that exploits the pyroelectric effect. *Ultrasonics*, 51(4), 420-424.
- [23] Wilkens, B. A thermal technique for local ultrasound intensity measurement: Part 1. sensor concept and prototype calibration. (2010). *Measurement Science and Technology*, 21(11) 115805.
- [24] Wilkens V and, R. H. (2004). Output intensity measurements on a diagnostic ultrasound machine using a calibrated thermoacoustic sensor. *Journal of Physics: Conference Series* 1, 140.
- [25] Myers, M. R., & Herman, B. A. (2002). A theoretical assessment of a thermal technique to measure acoustic power radiated by ultrasound transducers. *IEEE Transactions on Ultrasonics, Ferroelectrics, and Frequency Control*, 49(5), 565-572.
- [26] William J., F., & Ruth Baumann, F. (1954). Determination of Absolute Sound Levels and Acoustic Absorption Coefficients by Thermocouple Probes - Theory. *The Journal of the Acoustical Society of America*, 26(3), 294-310.
- [27] Wilkens, V. (2002). Thermoacoustic ultrasound power measurement using evaluation of transient temperature profiles. *Ultrasonics Symposium, 2002. Proceedings. 2002 IEEE*, , 2 1399-1402 vol.2.
- [28] Fay, B., Rinker, M., & Lewin, P. A. (1994). Thermoacoustic sensor for ultrasound power measurements and ultrasonic equipment calibration. *Ultrasound in Medicine & Biology*, 20(4), 367-373.

- [29] Wilkens, V. A thermal technique for local ultrasound intensity measurement: Part 2. application to exposimetry on a medical diagnostic device. (2010). Measurement Science and Technology, 21(11) 115806.
- [30] Matbase VOF. (2009). MATBASE: Mechanical, physical and environmental properties of materials. Retrieved 11/10, 2011, from <http://www.matbase.com/index.php>
- [31] Onda Corporation. (2003). Table of acoustic properties of materials. Retrieved 11/10, 2011, from http://www.ondacorp.com/tecref_acoustictable.shtml
- [32] A. Sedra, K. Smith, Microelectronic Circuits, 5th ed. New York: Oxford University Press, 2004.
- [33] Thermometrics. (1999). What is a thermistor? Retrieved 12/01, 2011, from <http://www.thermometrics.com/htmldocs/whatis.htm>
- [34] Honeywell Sensing and Control. 111-202CAK-H01 Discrete Thermistor. Retrieved 09/23, 2011, from http://sensing.honeywell.com/index.cfm?ci_id=140301&la_id=1&pr_id=145401
- [35] ATMEL Corporation. (2005). Enhancing ADC resolution by oversampling. Retrieved 09/23, 2011, from http://www.atmel.com/dyn/resources/prod_documents/doc8003.pdf
- [36] MAXIM. (2002). MAX6682 thermistor-to-digital converter. Retrieved 09/23, 2011, from <http://www.maxim-ic.com/datasheet/index.mvp/id/3319>
- [37] ATMEL Corporation. (2010). 8-bit AVR microcontroller with 32KBytes of in-system programmable flash. San Jose, CA: ATMEL Corporation.
- [38] MAXIM. (2003). Low-power, slew-rate-limited RS-485/RS-422 transceivers. Sunnyvale, CA: MAXIM.
- [39] Weisstein, Eric W. Least Squares Fitting. From MathWorld--A Wolfram Web Resource. <http://mathworld.wolfram.com/LeastSquaresFitting.html>
- [40] NIST/SEMATECH. e-Handbook of Statistical Methods. <http://www.itl.nist.gov/div898/handbook/>, 12/12/2011.
- [41] MathWorks. (2011). Least squares (curve fitting): Lsqcurvefit. Retrieved 05/16, 2011, from <http://www.mathworks.com/help/toolbox/optim/ug/lsqcurvefit.html>
- [42] Ohmic Instruments Co. (2005). Ultrasound Power Meter: Model UPM-DT-1AV. Easton, Maryland: Ohmic Instruments Co.
- [43] ATMEL Corporation. (2009). AVR134: Real time clock (RTC) using the asynchronous timer. San Jose, CA: ATMEL Corporation.

Appendix A: Thermoacoustic Sensor ATmega324P Code

```

#include <avr/pgmspace.h>
#include <avr/io.h>
#include <stdio.h>
#include <inttypes.h>
#include <util/delay.h>
#include <string.h>
#include <stdlib.h>
#include <math.h>
#include <avr/interrupt.h>

#define F_CPU 12000000UL;

//Variables for Communication with Sensor Board
volatile int SensorON = 0;
volatile int SensorAlgorithm = 0;

//Variables for calculating temp, C1, and US Intensity
volatile int count = 1;
int count1 = 0; // R2 cycle count
long x;
double v;
double v1;
double v0 = 0;
double US = 0;

//Initial Parameters
volatile double a = 1.0013;
volatile double b = 0.2641;
volatile double c = 0.9863;
volatile double d = 0.2639;
volatile double e = 1.0073;
volatile double f = 0.2641;
volatile double I;

int operation_a = 1;
int operation_b = 1;
int operation_c = 1;
int operation_d = 1;
int operation_e = 1;
int operation_f = 1;

int calculateCurve_count = 0;

double R2;
double R2_temp;

// Function to printf out of UART
int uart_putchar(char c, FILE *stream) {
    loop_until_bit_is_set(UCSR0A, UDRE0);
    UDR0 = c;
    return 0;
}

// Function to send character from UART1

```

```

int uart_putchar1(char c) {
    loop_until_bit_is_set(UCSR1A, UDRE1);
    UDR1 = c;
    return 0;
}

// Function to read character from UART0
int uart_getchar(FILE *stream) {
    char c;
    loop_until_bit_is_set(UCSR0A, RXC0);
    if (UCSR0A & _BV(FE0))
        return _FDEV_EOF;
    if (UCSR0A & _BV(DOR0))
        return _FDEV_ERR;
    c = UDR0;
    // Echo the character.
    uart_putchar(c, stream);
    // Return the character.
    return(c);
}

// Establish File stream for UART communication
FILE uart_str = FDEV_SETUP_STREAM(uart_putchar, uart_getchar,
    _FDEV_SETUP_RW);

// Function to Initialize UART Port0 to transmit
void UartTransmitterInit(void)
{
    UBRR0L = 77; //12 MHz external crystal and baud rate 9600
    // Sets no double speed or multiple coms
    UCSR0A = (0<<U2X0) | (0<<MPCM0);
    UCSR0B =
(0<<RXCIE0) | (0<<TXCIE0) | (0<<UDRIE0) | (0<<RXEN0) | (1<<TXEN0) | (0<<UCSZ
02);
    UCSR0C =
(0<<UMSEL00) | (0<<UMSEL01) | (0<<UPM00) | (0<<UPM01) | (0<<USBS0) | (1<<UCS
Z01) | (1<<UCSZ00) | (0<<UCPOL0);
    return;
}

// Function to Initialize UART1 to transmit and receive
void UartTransmitterInit1(void)
{
    UBRR1L = 77;
    UCSR1A = (0<<U2X1) | (0<<MPCM1);
    UCSR1B =
(1<<RXCIE1) | (0<<TXCIE1) | (0<<UDRIE1) | (1<<RXEN1) | (1<<TXEN1) | (0<<UCSZ
12);
    UCSR1C =
(0<<UMSEL11) | (0<<UMSEL10) | (0<<UPM11) | (0<<UPM10) | (0<<USBS1) | (1<<UCS
Z11) | (1<<UCSZ10) | (0<<UCPOL1);
    return;
}

// Function to Initialize UART Port1 for reception
void UartReceiverInit(void)
{
    UBRR1L = 77;

```

```

        UCSR1A = (0<<U2X1)|(0<<MPCM1);
        UCSR1B =
(0<<RXCIE1)|(0<<TXCIE1)|(0<<UDRIE1)|(1<<RXEN1)|(0<<TXEN1)|(0<<UCSZ
12);
        UCSR1C =
(0<<UMSEL11)|(0<<UMSEL10)|(0<<UPM11)|(0<<UPM10)|(0<<USBS1)|(1<<UCS
Z11)|(1<<UCSZ10)|(0<<UCPOL1);
        return;
    }

//Function to manage clock
void RTCInit (void)
{
    // Disable the Timer2 Interrupts
    TIMSK2 &= ~( (1 << OCIE2B) | (1 << OCIE2A) | (1 << TOIE2));

    TCCR2A = (0<<WGM21)|(0<<WGM20);
    TCCR2B = (0<<WGM22);

    //External 32K clock being used
    //ASSR = (0<<EXCLK)|(1<<AS2);
    ASSR = (1<<AS2);

    // Initialize the timer counter vars
    //OCR2A = 31 yields a 1 second counter
    TCNT2 = 0;  OCR2A = 31; OCR2B = 0x00;

    // Timer Prescale value 1024
    TCCR2B = (0x7 << CS20);

    // Wave form generation mode for the counter
    TCCR2A = (1 << WGM21);

    // Timer Interrupts Compare Reg. A Interrupt Enable
    TIMSK2 = (1 << OCIE2A);

    return;
}

void Oversampling (void)
{
    //long x;
    long y;
    double CH;
    double CL;
    double high;
    double low;

    x = 0;
    y = 0;

    //CS
    PORTB = 0b00000001; //PB0 high
    PORTD = 0x03;

    for (int counter = 0; counter < 256; counter++)
    {

```

```

//Set ADC on
ADCSRA |= (1<<ADSC);

CL = ADCL; // low 8 bits
CH = ADCH; // high 8 bits

//When there is something at the ADC, read the ADC
while(!(ADCSRA & (1<<ADIF)));
ADCSRA|=(1<<ADIF);

high = pow(16, 2) * CH; //Convert high 8 bits
low = CL;

//Put high 8 bits and low 8 bits together
y = high + low;
x = x + y; //Add oversampled data together

}

PORTB = 0x00;
PORTD = 0x01;

//Shift for oversampling procedure
x = x >> 4;

//Temperature
//Slope from thermistor-thermometer calibration (Nov 15, 2011)
v = (x) * -0.0182 + 94.456;

PORTD = 0x00; // Max chip CS Off

}

void calcR2 (void)
{
    R2 = (v - (a*((1 - exp(-count/b)) - c*(1 - exp(-count/d)) +
e*(1 - exp(-count/f)))));
    R2 = pow(R2, 2);

    printf("\n\r");
    printf("%f", a);
    printf(", ");

    return;
}

//Check R2s
int checkR2 (int current_operation)
{
    int operation;
    double R2_adjusted;
    double R2_diff;

    R2_adjusted = (v - (a*((1 - exp(-count/b)) - c*(1 - exp(-
count/d)) + e*(1 - exp(-count/f)))));
    R2_adjusted = pow(R2_adjusted, 2);
    R2_diff = R2_adjusted - R2;

```

```
if (R2_diff < 0) {
    if (current_operation == 1) {
        operation = 1;
    }
    if (current_operation == 2) {
        operation = 2;
    }
}

if (R2_diff > 0) {
    if (current_operation == 1) {
        operation = 2;
    }
    if (current_operation == 2) {
        operation = 1;
    }
}
return operation;
}

void func_operation_f (void) {
    if (operation_f == 1) {
        calcR2();
        f = f + 0.000001;
        operation_f = checkR2(operation_f);
    }

    if (operation_f == 2) {
        calcR2();
        f = f - 0.000001;
        operation_f = checkR2(operation_f);
    }

    return;
}

void func_operation_e (void) {
    if (operation_e == 1) {
        calcR2();
        e = e + 0.000001;
        operation_e = checkR2(operation_e);
        func_operation_f();
    }

    if (operation_e == 2) {
        calcR2();
        e = e - 0.000001;
        operation_e = checkR2(operation_e);
        func_operation_f();
    }
    return;
}

void func_operation_d (void) {
```

```
    if (operation_d == 1) {
        calcR2();
        d = d + 0.000001;
        operation_d = checkR2(operation_d);
        func_operation_e();
    }

    if (operation_d == 2) {
        calcR2();
        d = d - 0.000001;
        operation_d = checkR2(operation_d);
        func_operation_e();
    }

    return;
}

void func_operation_c (void) {

    if (operation_c == 1) {
        calcR2();
        c = c + 0.000001;
        operation_c = checkR2(operation_c);
        func_operation_d();
    }

    if (operation_c == 2) {
        calcR2();
        c = c - 0.000001;
        operation_c = checkR2(operation_c);
        func_operation_d();
    }

    return;
}

void func_operation_b (void) {

    if (operation_b == 1) {
        calcR2();
        b = b + 0.000001;
        operation_b = checkR2(operation_b);
        func_operation_c();
    }

    if (operation_b == 2) {
        calcR2();
        b = b - 0.000001;
        operation_b = checkR2(operation_b);
        func_operation_c();
    }

    return;
}

void func_operation_a(void) {

    if (operation_a == 1) {
```

```

        calcR2();

        a = a + 0.00001;
        operation_a = checkR2(operation_a);
        func_operation_b();
    }

    if (operation_a == 2) {
        calcR2();
        a = a - 0.00001;
        operation_a = checkR2(operation_a);
        func_operation_b();
    }
    return;
}

void calculateCurve(void) {
    calcR2();
    R2_temp = R2;

    //R2 = 0.00001 is what is used in the MATLAB program
    while (R2 >= 0.00001) {
        func_operation_a();
        count1 = count1 + 1;
    }

    return;
}

//OCIE2A compare interupt
ISR(TIMER2_COMPA_vect)
{

    if (SensorAlgorithm == 0)
    {
        //Always poll for temperatures
        Oversampling();

        //Send temp to controller board and PUTTY
        int m = (v-(int)v)*100; //Split temperature into two
parts

        printf ("\n\r");
        printf ("%f", v); //Temperature value

        _delay_us(100);
        uart_putchar1(v); //Char1 sent to controller board
(int of temp)
        _delay_us(100);
        uart_putchar1(m); //Char2 sent to controller board
(hundreth value of temp)
        printf (" , ");
        printf ("%d", count);
    }

    if (SensorAlgorithm == 1)
    {

```

```

if (count < 3)
{
    //Always poll for temperatures
    Oversampling();

    //Send temp to controller board and PUTTY
    int m = (v-(int)v)*100; //Split temperature into
two parts

    printf ("\n\r");
    printf ("%f", v); //Normalized Temperature value

    _delay_us(100);
    //Char1 sent to controller board (int of temp)
    uart_putchar1(v);
    _delay_us(100);
    //Char2 sent to controller board (hundreth value of temp)
    uart_putchar1(m);
    printf (", ");
    printf ("%d", count);
}

if (count == 3) {
    Oversampling();
    v0 = v;
}

if (count > 3) {
    Oversampling();

    v = v/v0;
    calculateCurve ();

    //Calculate US using 23 C calibration curve
    US = 3915.6*a - 3881.6;

    //Send temp to controller board and PUTTY
    //Split US into two parts
    int m = (US-(int)US)*100;

    printf ("\n\r");
    printf ("%f", v); //US value
    printf (", ");
    printf ("%f", v1); //Normalized Temperature value

    _delay_us(100);
    //Char1 sent to controller board (int of temp)
    uart_putchar1(US);
    _delay_us(100);
    //Char2 sent to controller board (hundreth value of temp)
    uart_putchar1(m);

    printf (", ");
    printf ("%d", count);

    printf (", ");
    printf ("%f", a);
}

```

```

    }
}

    count++;
    count1 = 0;
// Disable the timer interrupt
TIMSK2 &= ~(1 << OCIE2A);

//printf("\n\r %d", TCNT2);
//PORTA = 0x00;

/* Re-initialize the timer */
TCNT2 = 0;

}

void ADCinit (void)
{
    ADMUX |=
(0<<REFS1)|(0<<REFS0)|(0<<ADLAR)|(0<<MUX4)|(0<<MUX3)|(0<<MUX2)|(0<<
<MUX1)|(0<<MUX0);
    ADCSRA |= (1<<ADEN)|(1<<ADPS2)|(1<<ADPS1)|(1<<ADPS0);
    ADCSRB &= (0<<ADTS2)&(0<<ADTS1)&(0<<ADTS0);
    //ADCSRA |= (1<<ADSC)|(1<<ADSCF);
}

//UART Interrupt
ISR(USART1_RX_vect)
{
    char ReceivedByte;
    ReceivedByte = UDR1; // Fetch the recieved byte value into
the variable "ByteReceived"

    if (ReceivedByte == 0x43)
    {
        SensorON = 1;
    }
    if (ReceivedByte == 0x44)
    {
        SensorON = 0;
    }
    if (ReceivedByte == 0x45)
    {
        SensorAlgorithm = 1;
        count = 0;
        a = 1.0013;
        b = 0.2641;
        c = 0.9863;
        d = 0.2639;
        e = 1.0073;
        f = 0.2641;
    }
    if (ReceivedByte == 0x46)
    {
        SensorAlgorithm = 0;
    }
}
}

```

```
int main(void)
{
    /* Enable Global Interrupts */
    sei();
    DDRB = 0xFF;
    DDRC = 0xFF;
    DDRD = 0xFF;
    //DDRA = 0xFF;
    //Call function to initialize UART Transmitter
    UartTransmitterInit();
    UartTransmitterInit1();
    ADCinit();
    RTCInit();
    //Establish the default streams to use the uart.
    stdout = &uart_str;
    stdin = &uart_str;
    stderr = &uart_str;

    PORTC = 0xFF;
    while(1)
    {
        if (SensorON == 1)
        {
            // Enable the Timer Interrupt
            TIMSK2 |= (1 << OCIE2A);
        }
        if (SensorON == 0)
        {
            printf("Sensor OFF");
            //uart_putchar1(0x44); // Sensor OFF
            //uart_putchar1(0x44);
            //Disable the timer interrupt
            TIMSK2 &= ~(1 << OCIE2A);

            SensorON = 2;
        }
    }
    return 0;
}
```

Appendix B: MATLAB *lsqcurvefit* function

```

close all;

%configure the optimset for use with lsqcurvefit
options = optimset('lsqcurvefit');

%increase the number of function evaluations for more accuracy
options.MaxFunEvals = 5000000;
options.MaxIter = 5000000;

initialConditions0 = [1,1,22];

[newParameters4, error4] = lsqcurvefit(@myPolyCurve0,
initialConditions0, x, y, [], [], options);

y5 = myPolyCurve0(newParameters4, x);

newParameters4'
error4
.....

function output = myPolyCurve0 (param,input)
a1 = param(1);
b1 = param(2);
c1 = param(3);

output = a1.*(1 - exp(-input./b1)) + c1;

```